THEORETICAL CALCULATIONS ON THE PERFORMANCE OF PHOTOVOLTAIC SOLAR CELLS

A THESIS
SUBMITTED TO
THE UNIVERSITY OF POONA

FOR THE DEGREE OF
DOCTOR OF PHILOSOPHY
IN PHYSICS

BY

G. S.R. KRISHNA MURTHY

SOLID STATE MATERIALS GROUP
NATIONAL CHEMICAL LABORATORY
POONA - 411 008 (INDIA)

APRIL 1980

C O N T E N T S

Chapter			Page
		Acknowledgement	i
		List of symbols	ii
I		General Introduction	
	1.1	Current-voltage relation	2
	1.2	Optical effects in semiconductors	16
	1.3	Photovoltaic cells	22
		References	30
II		Theoretical study on the behaviour of Metal-p-n Schottky barrier solar cells.	
	2.1	Introduction	34
	2.2	Homojunction Metal-p-n photovoltaic cells	39
	2.3	Heterojunction solar cells	53
		References	69
III		Theoretical performance of back-illuminated thin film MIS Schottky barrier solar cells.	
	3.1	Introduction	72
	3.2	Back-illuminated solar cell	76
	3.3	Results and conclusion	84
		References	89

IV		Theoretical calculations on the performance of Amorphous-Si/low grade single crystal Si solar cells	
	4.1	Introduction	92
	4.2	J-V characteristics under illumination.	96
	4.3	Results and Discussion	104
		Reference	107
		SUMMARY	110

ACKNOWLEDGEMENT

I am deeply indebted to Dr. A.P.B. Sinha, FNA, for his keen interest, inspiring guidance and constant encouragement during the course of this work.

I wish to express, in particular, my gratitude to Dr. V.J. Rao for his helpful suggestions and stimulating discussions. It is a pleasure for me to thank Dr.(Miss) N.R. Pavaskar and Dr.(Mrs) A. Mitra for their invaluable assistance. I am thankful to the Council of Scientific and Industrial Research, New Delhi, for the award of research fellowship.

Finally, I thank the Director, National Chemical Laboratory, Poona for allowing me to submit this work in the form of a thesis.

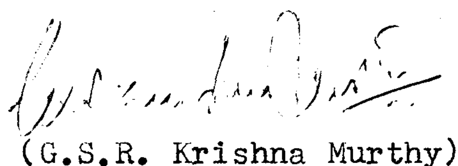

Poona -8
April 1980.

(G.S.R. Krishna Murthy)

CHAPTER I

GENERAL INTRODUCTION

The use of photovoltaic cells for direct energy conversion has so far been largely confined to space applications[1-7]. However, the increasing need for alternate terresterial energy sources and ecological considerations have made solar energy and photovoltaic conversion an active area of research. The problems involved in these two cases differ to some extent. For space applications, the cells should be light, have a high conversion efficiency and be capable of withstanding radiation and possible severe temperature cycling. For terresterial applications,[8-15] cells must be inexpensive and may have to be protected from the ambient atmosphere.

In this chapter, we review the principles underlying the operation of photovoltaic solar cells in general. The subsequent chapters would deal with relevant specific aspects of the respective photovoltaic cells more fully.

For a photovoltage to develop, the light generated electrons and holes must be separated by some built-in internal field in the system[16-22]. This can be due to (1) a junction between two regions of a semiconductor having different types of conductivity such as a p-n junction, or (2) a junction between a metal and a semiconductor (Schottky).

The p-n junction can be a homojunction which has the same semiconductor on both sides of the junction[23-25], or a

heterojunction composed of two different semiconductors[26-28]. Our treatment includes p-n junctions of both the homo- and hetero-type and the metal-semiconductor Schottky diodes.

When solar radiation is absorbed by a material, electrons and holes are generated[16,17]. The minimum energy that a photon must have in order to create an electron-hole pair is the band gap energy, E_g of the absorbing material[23]. The absorption coefficient rises more steeply with increasing photon energy for a direct gap material than for an indirect gap material, since the latter requires an additional scattering event accompanying the photon absorption[29-31]. The magnitude of the absorption coefficient determines the thickness of material needed to absorb light. Once generated, the electrons and holes would simply recombine in the absence of a junction which separates them and allows the minority carriers (electrons in a p-type material, and holes in an n-type material) to reach a region in which they are in majority. Then they proceed to the electrodes and contribute to the photo-generated current.

1.1 Current-voltage relation

Homo-junctions

The energy band diagrams of a p-type and an n-type semiconductor are given in Figs. 1-1 (a) and 1-1 (b)

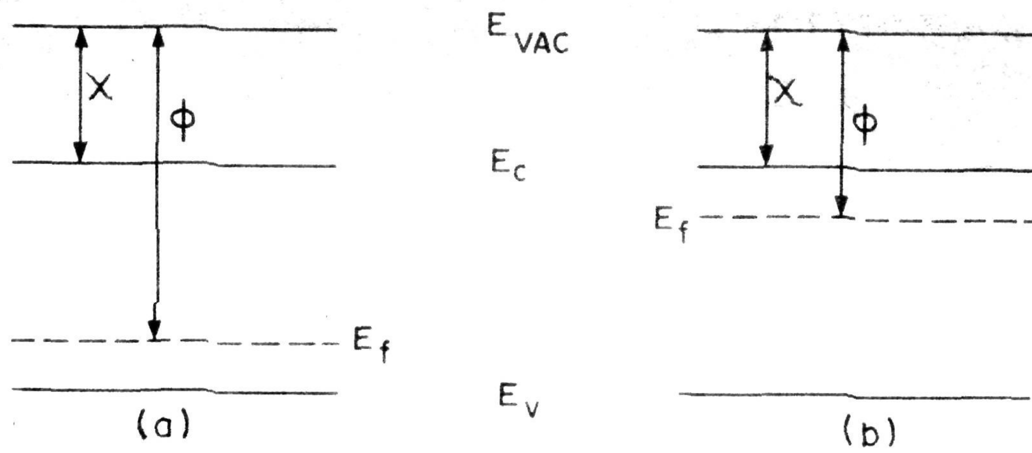

FIG. 1·1. ENERGY DIAGRAMS FOR BANDS IN (a) p–TYPE (b) n–SEMICONDUCTORS.

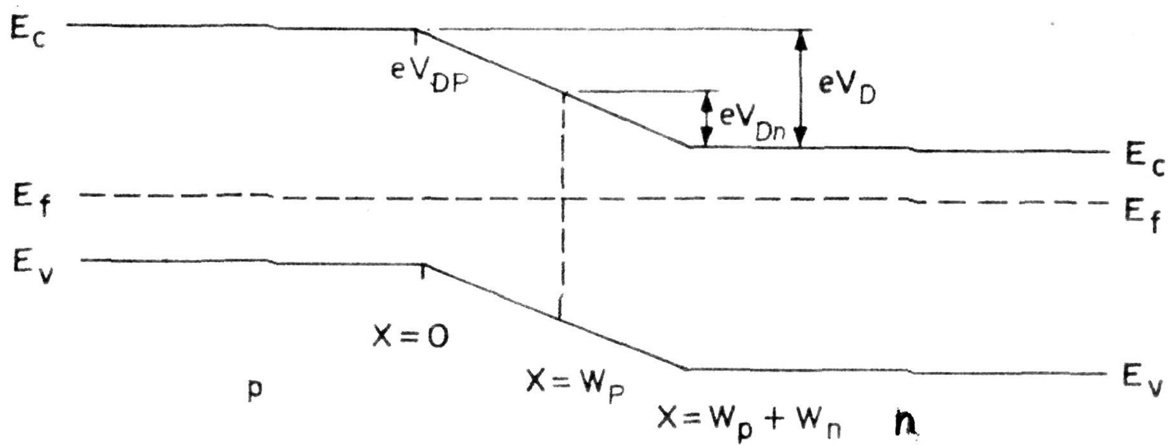

FIG. 1·2. ENERGY DIAGRAM FOR BANDS IN p–n JUNCTION

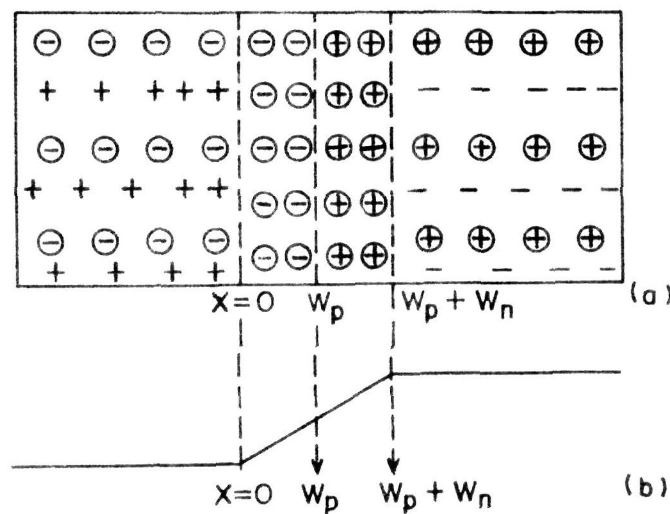

FIG. 1·3. (a) BLOCK DIAGRAM OF p/n JUNCTION

(b) ENERGY DIAGRAM FOR HOLES

respectively. When a junction is made, holes from the p-type material and electrons from the n-type material go over to the other side. This creates a space charge at the junction and causes a band bending[32-35]. The charge separation goes on to the extent necessary to equalise the fermi levels on the two sides (Fig. 1-2). In equilibrium, there is a continuous flow of majority and minority carriers from both materials, but the sum of currents due to these charge carriers is zero. Fig. 1-2 gives the band diagram of a p-n junction.

Fig. 1-3 shows the space charge layer adjacent to the p-n junction (also known as the depletion region). Let w_p be the thickness of the space charge layer in the p-type material and w_n in the n-type material. Space charge exists only in the depletion region and the rest of the bulk semiconductor is neutral.

The space charge layer gives rise to a potential barrier, which can be determined by solving the Poisson's equation for the two regions[32,35-39]. The charge density is eN_A on the 'p' side and eN_D on the 'n' side of the depletion region. It is assumed that all acceptors and donors are ionised.

Thus if $V_1(x)$ is the potential at any distance x in the p-region, the Poisson's equation gives

$$\frac{d^2V_1(x)}{dx^2} = \frac{eN_A}{\epsilon_0 \epsilon} \quad .. \quad 1\text{-}1$$

Similarly if $V_2(x)$ is the potential at any distance x in the n-region

$$\frac{d^2V_2(x)}{dx^2} = - \frac{eN_D}{\epsilon_0 \epsilon} \quad .. \quad 1\text{-}2$$

The solution of the above equations with the following boundary conditions determine the potential profile in the depletion region.

$$V_1(0) = 0, \qquad \left.\frac{dV_1(x)}{dx}\right|_{x=w_p} = \left.\frac{dV_2(x)}{dx}\right|_{x=w_p},$$

$$\left.\frac{dV_1(x)}{dx}\right|_{x=0} = 0 \quad \text{and} \quad \left.\frac{dV_2(x)}{dx}\right|_{x=w_p+w_n} = 0 .$$

From these boundary conditions,

$$V_1(x) = \frac{eN_A x^2}{2\epsilon_0\epsilon}$$

$$V_2(x) = -\frac{eN_D x^2}{2\epsilon_0\epsilon} + \frac{ew_p}{\epsilon_0\epsilon}(N_A+N_D)\,x - \frac{ew_p^2}{2\epsilon_0\epsilon}(N_A+N_D)$$

The potential at $x = w_p + w_n$ is known as the contact potential or diffusion potential and is given by

$$V_D\Big|_{w_p+w_n} = \frac{e}{2\,\epsilon_0\epsilon}\,\frac{N_A N_D}{(N_A+N_D)}\,(w_p+w_n)^2 \qquad .. \quad 1\text{-}3$$

and the thickness of the depletion region

$$w_p + w_n = \left(\frac{2\,\epsilon_0\epsilon\,V_D}{e}\right)^{1/2} \cdot \left(\frac{N_A+N_D}{N_A N_D}\right)^{1/2} \qquad .. \quad 1\text{-}4$$

The junction gets narrower as the impurity concentration is increased.

If $N_A >> N_D$

$$w_p + w_n = \left(\frac{2\epsilon_0 \epsilon V_D}{e}\right)^{1/2} \cdot \left(\frac{1}{N_D}\right)^{1/2} \qquad .. \quad 1\text{-}5$$

In such a case, the junction is confined almost entirely to the 'n' region.

Under equilibrium, in the absence of any applied voltage, the following relations hold[33,36].

$$p(w_p+w_n) = N_A \quad \exp\left(-\frac{eV_D}{kT}\right) = p_n$$

and $$p(0) = N_A ,$$

$$n(w_p+w_n) = N_D$$

$$n(0) = N_D \quad \exp -\left(\frac{eV_D}{kT}\right) = n_p \qquad .. \quad 1\text{-}6$$

If the junction is biased in the forward direction by connecting the p side to a positive potential and the n side to a negative potential, the potential barrier for the majority charge carriers is reduced to V_D-V and hence

$$n(0) = n_p \cdot \exp \frac{eV}{kT} \qquad .. \quad 1\text{-}7$$

Similarly

$$p\,(w_p+w_n) = p_n \,.\, \exp \frac{eV}{kT} \,. \qquad \text{.. 1-8}$$

The width of the depletion region is also reduced by forward biasing as V_D is replaced by V_D-V.

The continuity equation for minority carriers in the p-type material is given by[32,36]

$$\frac{dn}{dt} = \frac{n_p - n}{\tau_n} + D_n \frac{d^2n}{dx^2} = 0 \qquad \text{.. 1-9}$$

and $$J_n = eD_n \left.\frac{dn}{dx}\right|_{x=0} \qquad \text{.. 1-10}$$

where the effect of any external field or voltage is taken to increase the minority carrier concentration as per the equation given above.

A solution of the minority carrier continuity equations can be obtained for any applied voltage, V by using the boundary conditions given below.

$$n(0) = n_p \,.\, \exp \frac{eV}{kT}$$

and

$$n(-\infty) = n_p$$

The solution is given as,

$$n(x) = n_p + n_p \left(\exp \frac{eV}{kT} - 1\right)\left(\exp + \frac{x}{L_n}\right) \quad .. \ 1\text{-}11$$

and

$$\frac{dn(x)}{dx} = \frac{n_p}{L_n} \left(\exp \frac{eV}{kT} - 1\right)\left(\exp + \frac{x}{L_n}\right) \quad .. \ 1\text{-}12$$

Therefore,

$$J_n = eD_n \left.\frac{dn}{dx}\right|_{x=0} = \frac{eD_n n_p}{L_n} \left(\exp \frac{eV}{kT} - 1\right) \quad .. \ 1\text{-}13$$

Similarly, it can be shown that

$$J_p = \frac{eD_p p_n}{L_p} \left(\exp \frac{eV}{kT} - 1\right) \quad .. \ 1\text{-}14$$

Hence

$$J = J_n + J_p = \left(\frac{eD_p n_p}{L_n} + \frac{eD_p p_n}{L_p}\right)\left(\exp \frac{eV}{kT} - 1\right)$$

or

$$J = J_o \ (\exp \frac{eV}{kT} - 1) \quad .. \ 1\text{-}15$$

where

$$J_o = \frac{eD_n n_p}{L_n} + \frac{eD_p\, p_n}{L_p}$$

is the reverse saturation current density.

If $N_A \gg N_D$, (heavily doped p type in junction with lightly doped n type).

$$n_p \ll p_n$$

then

$$J_o = \frac{eD_p\, p_n}{L_p}$$

In order to estimate the value of J_o and its dependence on temperature and on the resistivity of the base layer of the semiconductor, we use the law of mass action,

$$p_n = \frac{n_i^2}{N_D} \quad \text{and} \quad \rho_n = \frac{1}{N_D\, e\mu_n}$$

or

$$p_n = n_i^2 \cdot \rho_n \cdot e\mu_n$$

and

$$J_o = \frac{D_p}{L_p} \cdot n_i^2 \cdot \rho_n\, e^2\mu_n$$

Incorporating the value of n_i^2

$$J_o = \frac{D_p}{L_p} \times 2.23 \times 10^{31} . \; T^3 \; \exp(-E_g/kT) \; \rho_n e^2 \mu_n$$

Since

$$L_p = \sqrt{D_p \tau_p}$$

$$J_o = 2.23 \times 10^{31} \; T^3 \left(\frac{D_p}{\tau_p}\right)^{1/2} e^2 \rho_n \mu_n \times \exp(-E_g/kT) \quad .. \; 1\text{-}16$$

The equation 1-16 shows that higher the resistivity of the base material, higher is the value of the reverse saturation current density J_o. Further a decrease in the mobility of carriers or an increase in the minority carrier life time decreases J_o.

The essential prerequisites for a low J_o, therefore, are low mobility of charge carriers and high minority carrier life time. Furthermore, as is well-known[39,40]

$$D_n = \frac{kT}{e} \mu_n \quad \text{and}$$

$$\tau_n = \frac{1}{(N_A + n_p) \, r}$$

where r is the constant of proportionality called recombination coefficient.

If $n_p \ll N_A$,

$$\tau_n = \frac{1}{r\,N_A} .$$

The minority carrier life time depends on N_A the impurity doping level and decreases with increasing impurity concentration. Recently Fossum[41] has given an analysis for the life time of minority carriers in silicon. The equation for the life time of minority carriers in silicon is,

$$\tau_n = \frac{\tau_o}{1 + \frac{N_A}{N_0}} \qquad \text{.. 1-17}$$

where $\tau_o = 3.95 \times 10^{-4}$ sec.,

$N_0 = 7.1 \times 10^{15}\ cm^{-3}$.

Heterojunctions

A heterojunction is defined as a junction between two different semiconductor materials[42-45]. The materials may be single crystal, polycrystalline or amorphous and

may also be abrupt or graded. The heterojunctions may be isotype having the same type conductivity on both sides or anisotype having different types of conductivity e.g. p and n on the two sides of the heterojunction. We shall only consider single crystal anisotype heterojunctions.

A typical equilibrium energy band profile of an abrupt p-n heterojunction formed by bringing two semiconductors of different band gaps into intimate contact is shown in Fig.1-4.

The subscript 1 and 2 refer to p and n type semiconductors respectively. It can be seen that the discontinuity in the conduction band edges, ΔE_c is equal to the difference in the electron affinities of the two semiconductors and the discontinuity in the valence band edge, ΔE_v is equal to $(E_{g_2} - E_{g_1} - \Delta E_c)$. In this type of heterojunction a depletion layer is formed on either side of the interface and just as in case of a homojunction,

$$N_D w_n = N_A w_p .$$

The total built-in voltage V_D is due to the difference in the work functions and is equal to sum of the built-in voltages on both sides.

$$V_D = V_{D_1} + V_{D_2} \qquad .. \ 1\text{-}18$$

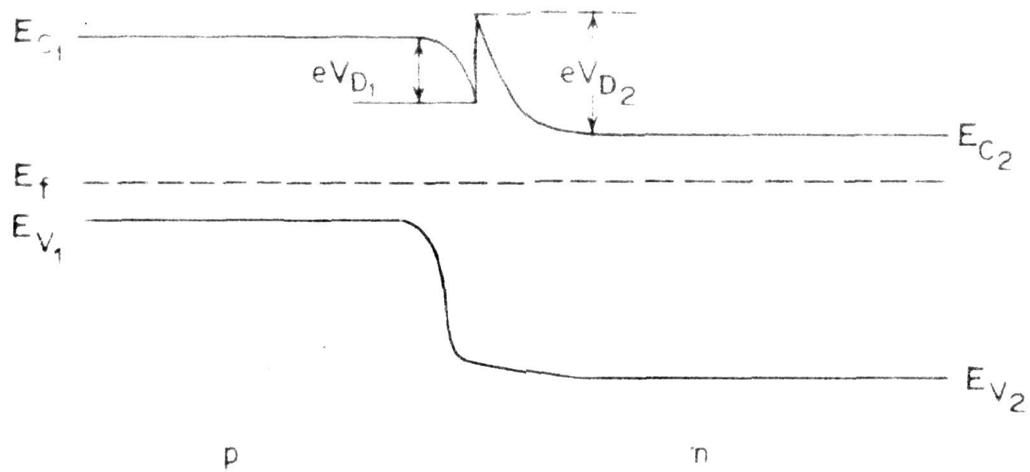

FIG. 1·4

ENERGY DIAGRAM FOR p/n HETERO JUNCTION

The energy band profile near the interface plays an important role in controlling the current transport in a heterojunction. In the absence of interface states, the energy band profile depends upon the electron affinities, energy band gaps and the work functions of the two semiconductors forming the junction. For a heterojunction with

$$\chi_1 > \chi_2,$$

$$\phi_1 > \phi_2,$$

and $$E_{g_1} < E_{g_2}$$

the dark current-voltage relationship has been derived as[42,45]

$$J = J_o \left[\exp \frac{eV}{kT} - 1\right].$$

On assuming transmission coefficient to be equal to unity,

$$J_o = eN_{D2} \left(\frac{D_{n_1}}{\tau_{n_1}}\right)^{1/2} \exp \left(- \frac{eV_D - \Delta E_c}{kT}\right)$$

If $\chi_1 = \chi_2$ and $E_{g_1} = E_{g_2}$, the above equation for J_o reduces to that of the homopolar junction.

Metal-Schottky diodes

The contact between a metal and a semiconductor can produce a barrier under certain conditions. For a metal of an n-type semiconductor a barrier is produced when the condition $\phi_m > \phi_s$ is satisfied[36,43,47].

Energy level diagrams for metal and n-type semiconductor have been shown in Fig. 1-5(a) and 1-5(b). The metal-semiconductor contact acts as a rectifier, since a barrier $(\phi_m - \phi_s)$ exists in the conduction band of the semiconductor. For a forward bias the semiconductor is to be made negative with respect to the metal when the electrons flow from the semiconductor into the metal. If $\phi_m < \phi_s$, there is virtually no barrier and the contact is ohmic. The simplified equations for the depletion region, built-in voltage and the capacitance of a Schottky barrier diode are similar to those for a p-n junction. For a metal- n-type semiconductor Schottky diode, one has[36,43].

$$w = \left[\frac{2\epsilon\epsilon_0}{eN_D}\left(V_D - V - \frac{kT}{e}\right)\right]^{1/2} \quad .. \quad 1\text{-}19$$

where w is the width of the space charge region in the semiconductor.

For the Schottky metal-semiconductor diode the J-V dependence is similar to that got for the p-n diode.

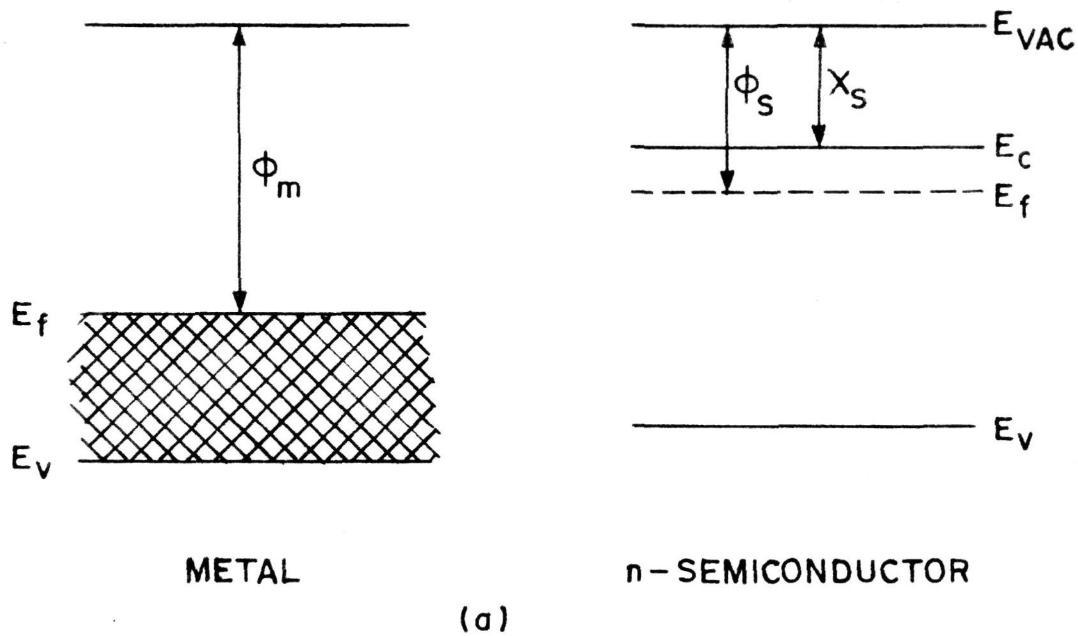

(a)

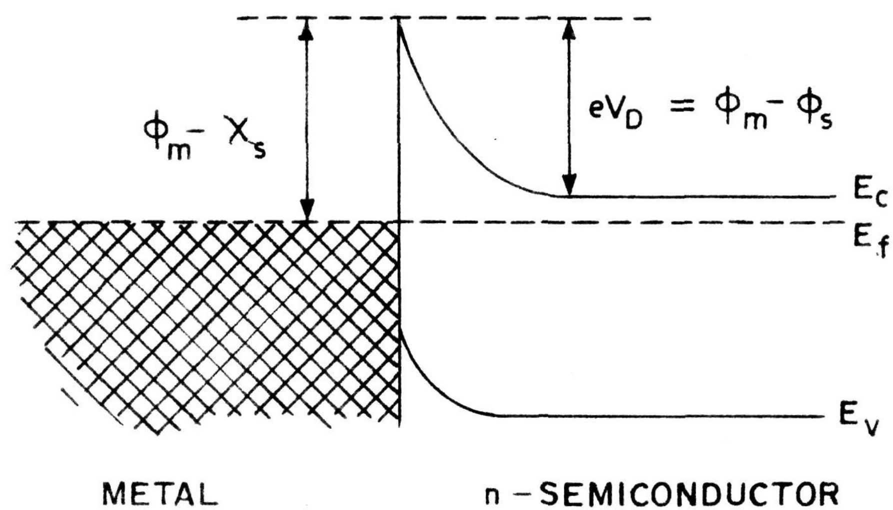

(b)

FIG. 1·5

ENERGY LEVEL DIAGRAM OF METAL CONTACT TO n-TYPE SEMICONDUCTOR

[(a) WITH $\phi_m > \phi_s$, CONTACT (b) RECTIFIER JUNCTION BETWEEN METAL | n-TYPE SEMICONDUCTOR]

The dark current is controlled by diffusion or by thermionic emission, depending on whether the space charge region is thicker or thinner than the diffusion length. For thermionic emission, the current[36]

$$J = A^* T^2 \exp\left(- \frac{e\phi_B}{kT}\right) [\exp \left(\frac{eV}{kT}\right) - 1] \qquad .. \; 1\text{-}20$$

where A^* is the modified Richardson constant for thermionic emission into the semiconductor, the modification being the use of an effective mass

$$A^* = \frac{4\pi \; em^* k^2}{h^3} = 120 \; \frac{m^*c}{m_o} \; amp/cm^2 \; {}^oK^2 .$$

For wider space charge regions the diffusion theory must be applied instead of this thermionic emission process. When space charge regions are comparable in thickness to the diffusion length, a combined approach may be used.

In summary one can write

$$J = J_o \; [\exp \frac{eV}{kT} - 1] \qquad .. \; 1\text{-}21$$

where J_o is the saturation current.

1.2 Optical effects in semiconductors

We shall consider the effect of incident radiation on a p-n junction. When light of wave length λ is incident on the surface of a semiconductor, the generation rate of hole-electron pairs, as a function of distance x from the surface, is [16,24,25,48].

$$g(x) = N(\lambda) \cdot \alpha(\lambda) [1-r(\lambda)] \exp[-\alpha(\lambda) x] \quad .. \quad 1\text{-}22$$

The photocurrent that these carriers produce and the spectral response (the number of carriers generated per incident photon at each wave length) can be determined for the low injection level conditions using the minority carrier continuity equations[49]

$$\frac{dp}{dt} = \frac{\Delta p_n}{\tau_p} + D_p \frac{d^2 \Delta p}{dx^2} - g(x) \quad .. \quad 1\text{-}23$$

for holes in the n-type material and

$$\frac{dn}{dt} = -\frac{\Delta p_n}{\tau_n} + D_n \frac{d^2 \Delta n}{dx^2} + g(x) \quad .. \quad 1\text{-}24$$

for electron in the p-type material. The hole and electron currents are

$$J_p = e D_p \frac{d\Delta p}{dx}$$

$$J_n = e D_n \frac{d\Delta n}{dx}$$

For the case of p/n junction where the base is n-type and the top side p-type, the photogenerated current continuity equation for hole in the 'n' layer at equilibrium

$$\frac{d\Delta p}{dt} = - \frac{\Delta p}{\tau_p} + D_p \frac{d^2\Delta p}{dx^2} + g(x) = 0$$

i.e. $$\frac{d\Delta p}{dt} = D_p \frac{d^2\Delta p}{dx^2} + g(x) - \frac{\Delta p}{\tau_p} = 0 \qquad .. \quad 1\text{-}25$$

In order to solve this, the boundary conditions are[35,49]

$$\Delta p = 0 \quad \text{at} \quad x = d_1 + w$$

and $$S_p \, \Delta p = D_p \frac{d\Delta p}{dx} \quad \text{at } x = d \, .$$

As the back contact is ohmic, S_p, the surface recombination velocity at the back, can be taken as infinite. Hence the second condition would become

$$\Delta p = 0 \quad \text{at } x = d$$

By using this boundary conditions, the hole distribution in the n-type base layer is given as

$$\Delta p = \frac{\alpha N(1-r)\,\mathcal{T}_p}{\alpha^2 L_p^2 - 1}\left\{\exp\ [-\alpha(d_1+w)]\right\} \times$$

$$\left[\cosh\left(\frac{x-d_1-w}{L_p}\right) - \exp\ [-\alpha(x-d_1-w)]\right.$$

$$\left.\frac{\cosh\dfrac{d-d_1-w}{L_p} - \exp\ [-\alpha(d-d_1-w)]}{\sinh\dfrac{d-d_1-w}{L_p}}\ \sinh\frac{x-d_1-w}{L_p}\right] \quad .. \ 1\text{-}26$$

and the photocurrent per unit band width due to holes collected at the base is[49]

$$J_p = \frac{eN(1-r)\,\alpha\,L_p}{(\alpha^2 L_p^{\,2}-1)}\left\{\exp\ [-d(d_1+w)]\right\} \times$$

$$\left[\alpha L_p - \frac{\cosh\dfrac{d-d_1-w}{L_p} - \exp\ (-\alpha(d-d_1-w))}{\sinh\dfrac{d-d_1-w}{L_p}}\right] \quad .. \ 1\text{-}27$$

Similarly, using the continuity equation for electrons

in the p-type top layer, the number of photogenerated electrons in the top layer can be calculated with the following boundary conditions.

$$D_n \left. \frac{d\Delta n}{dx} \right|_{x=0} = S_n \, \Delta n$$

and $\Delta n = 0$ at $x = d_1$

Then the electron density in the top layer is given as

$$\Delta n = \frac{\alpha N(1-r)\tau_n}{(\alpha^2 L_n^2 - 1)} \times$$

$$\left[\frac{\left(\frac{S_n L_n}{D_n} + \alpha L_n\right) \sinh \frac{d_1 - x}{L_n} + \exp(-\alpha d_1)\left(\frac{S_n L_n}{D_n} \sinh \frac{x}{L_n} + \cosh \frac{x}{L_n}\right)}{\frac{S_n L_n}{D_n} \sinh \frac{d_1}{L_n} + \cosh \frac{x_n}{L_p}} - \exp(-\alpha x) \right] \quad .. \quad 1\text{-}28$$

and the resulting electron photocurrent density at the junction edge is

$$J_n = \frac{eN(1-r)\alpha L_n}{(\alpha^2 L_n^2 - 1)}$$

$$\left[\frac{\left(\frac{S_n L_n}{D_n} + \alpha L_n\right) - \exp(-\alpha d_1)\left(\frac{S_n L_n}{D_n}\cosh\frac{d_1}{L_n} + \sinh\frac{d_1}{L_n}\right)}{\frac{S_n L_n}{D_n}\sinh\frac{d_1}{L_n} + \cosh\frac{d_1}{L_n}} - \alpha L_n \exp(-\alpha d_1) \right] \quad .. \quad 1\text{-}29$$

Some photocurrent collection takes place from the depletion region as well. The electric field in this region can be considered high enough so that the photogenerated carriers are accelerated out of the depletion region before they can recombine so the photocurrent density is equal to the number of photons absorbed[50].

$$J_{dr} = eN(1-r) \,.\, \exp(-\alpha d) \; [1 - \exp(-\alpha w)] \quad .. \quad 1\text{-}30$$

Thus the total short-circuit photocurrent at a given wave length is the sum of J_p, J_n and J_{dr}.

Therefore

$$J_l(\lambda) = J_p + J_n + J_{dr} \qquad .. \qquad 1\text{-}31$$

Under complete solar illumination (i.e. either under AMO or AMI)[51,52], the total photogenerated current would be obtained by integrating over the entire spectrum

$$J_L = \int_{\lambda_o = 0.3\mu}^{\lambda_g = hc/E_g} J_l(\lambda)\, d\lambda \qquad .. \qquad 1\text{-}32$$

Similarly if the Schottky barrier has been made on an n-type semiconductor, the photogenerated current and its spectral response come from the depletion region as well as from the bulk of the semiconductor. The collection from the depletion region is qualitatively the same as in a p-n junction. It is assumed that the high field in the depletion region sweeps carriers out before they can recombine, leading to a current equal to[49]

$$J_{dr} = eN\,[1-\exp(-\alpha w)]$$

The collection from the base of the Schottky barrier

is also qualitatively the same as from the base of p-n junction. This equation can be simplified if the device thickness is much greater than the diffusion length. In that case,

$$J_p = \frac{eN\alpha L_p}{1 + \alpha L_p} \exp(-\alpha w) \quad .. \quad 1\text{-}33$$

and the total photocurrent is the sum of J_p and J_{dr}.

1.3 Photovoltaic cells

The minority carriers generated due to the incident radiation cross the junction by diffusion due to the energy gradient (Fig.1-6). The carriers which cross junction cause a potential to develop which forward-biases the junction. In case a load is connected, the current density through the load resistance R_L is given as

$$J = J_o \left\{ \exp \frac{e(V-JR_s)}{kT} - 1 \right\} - J_L \quad .. \quad 1\text{-}34$$

The output of the cell can be obtained experimentally by varying the load resistance and the variation in J is shown in Fig.1-7. The maximum power is determined from the J-V curve by finding the rectangle with the largest area under J-V curve in the fourth quadrant.

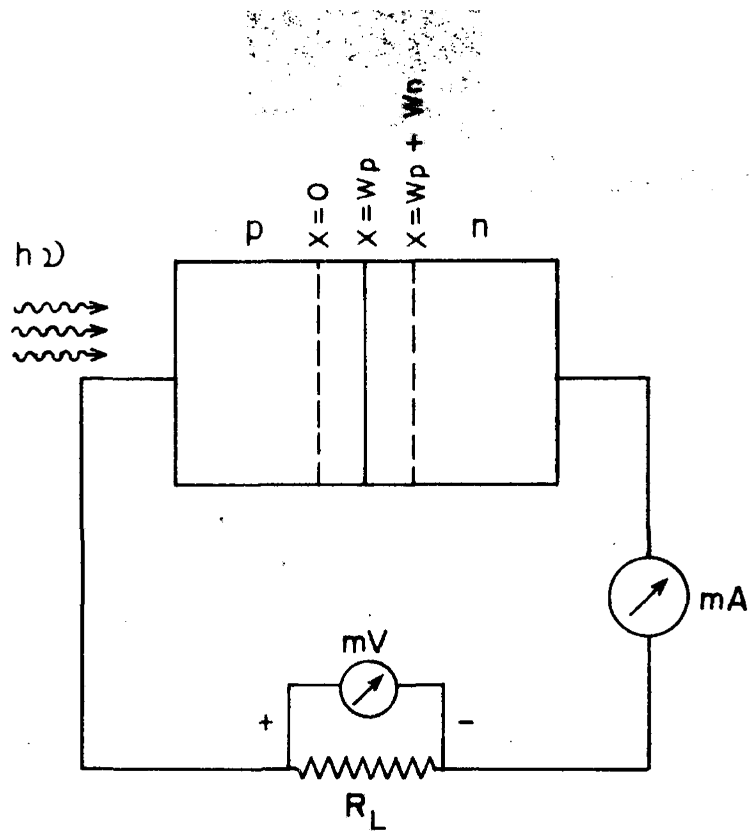

FIG. 1·6

CIRCUIT DIAGRAM FOR A PHOTO VOLTAIC CELL

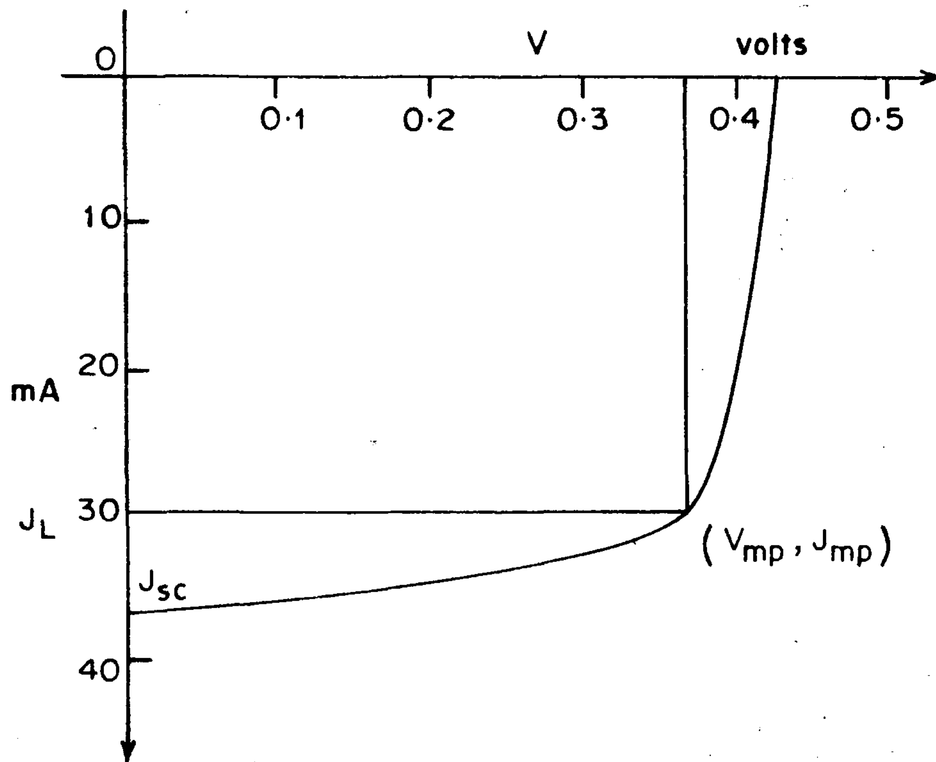

FIG. 1·7

J-V CHARCTERSTICS UNDER ILLUMINATION

The voltage at maximum power V_{mp} and the current J_{mp} give the maximum power output

$$P_{out} = V_{mp} \cdot J_{mp} \qquad .. \quad 1\text{-}35$$

The efficiency of the solar cell is defined as the ratio of the maximum power output to the incident power

$$\eta = \frac{P_{out}}{P_{in}} \times 100\% \qquad .. \quad 1\text{-}36$$

The incident power depends upon the type of illumination. The incident radiation can be either (1) AM0 or (2) AM1 or AM2 whose intensity is 135, 100, 90 mw/cm^2 respectively[51,52].

<u>Open circuit voltage</u>

The open circuit voltage is defined as the voltage at the point J = 0 on the J-V curve under illumination. Therefore,

$$V_{oc} = \frac{kT}{e} \ln \left\{ \frac{J_L}{J_0} + 1 \right\} \qquad .. \quad 1\text{-}37$$

Since $J_L >> J_o$,

$$V_{oc} = \frac{kT}{e} \ln \frac{J_L}{J_0}$$

Therefore, V_{oc} can be maximized by minimizing J_o. The dark saturation current for p/n junction can be written as

$$J_o = \frac{eD_p p_n}{L_n} + \frac{eD_n n_p}{L_p}$$

Considering a heavily doped 'p' region in contact with a moderately doped 'n' region,

$$J_o = e p_n \left[\frac{D_p}{\tau_p} \right]^{1/2}$$

since $$L_p = \sqrt{D_p \tau_p}$$

Thus in order to get high open circuit voltage, one should use a material having low resistivity, high minority carrier life time and low mobility of both electrons and holes.

<u>Short-circuit current</u>

The short-circuit current density in ideal case is equal to the photogenerated current

$$J_{sc} = J_L$$

However, in a practical case, the cell may have shunt resistance R_{sh} as well as a series resistance R_s. The

equivalent circuit for such a system is shown in Fig. 1-8.

For a non-ideal diode, with all these factors, the J-V characteristic is given as

$$J = J_o \left[\exp \frac{e(V-J_L R_s)}{kT} - 1 \right] + \frac{V-JR_s}{R_{sh}} - J_L \quad \text{.. 1-38}$$

As the shunt resistance is in parallel and its value is generally high, its effect can be neglected. However, the effect of the series resistance is more harmful. A series resistance of just $5\,\Omega$ reduces the available power to less than 30% of the optimum power obtainable with $R_s = 0$. Assuming $R_{sh} \to \infty$, the J-V characteristics become

$$J = J_o \left\{ \exp \frac{e(V-JR_s)}{kT} - 1 \right\} - J_L$$

i.e. $$V_L = \frac{kT}{e} \ln \left\{ \frac{J_L + J}{J_o} + 1 \right\} + JR_s$$

and the power that can be obtained from such a device is

$$P = J \, . \, V$$

$$= J \left[\frac{kT}{e} \ln \left(\frac{J_L + J}{J_o} + 1 \right) + JR_s \right]$$

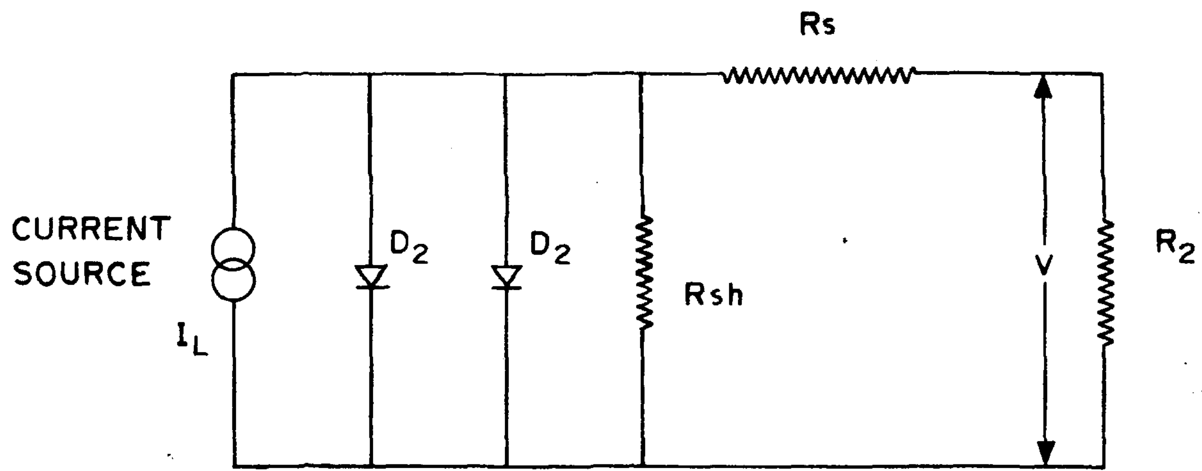

FIG. 1·8

EQUIVALENT DIAGRAM FOR A SOLAR CELL

If 'd' is the thickness of cell, it should be made as small as possible such that the resistance in the base layer of the device is minimum. Th is not a critical parameter since it is easy to keep this resistance to a value of less than one ohm.

As most of the solar radiation is absorbed within a few microns from the surface, the excess minority carriers produced by the photon absorption should cross the junction before they recombine. Hence the thickness of top layer should be small to avoid recombination.

The surface layer resistance is given as

$$R_{diff.} = \frac{w}{4\ t_1 L} \qquad \text{.. 1-39}$$

where L is the length of the cell, t_1 is the thickness of surface. If the thickness of top layer is small, the resistance increases. Hence the thickness of surface layer, t_1 has to be properly chosen. Series resistance can also be decreased by choosing a proper grid contact[52]

Reflection losses

To estimate the reflection losses, the relation between reflection coefficient (r) and refraction coefficient (n_1) has to be considered.

$$r = \frac{(n_1-1)^2}{(n_1+1)^2} \quad .. \quad 1\text{-}40$$

A relationship between 'n_1' and 'E_g' i.e.

$$E_g.n_1^4 = 173$$

given by Moss[31] is approximately true for materials of the zinc blende and diamond type structure which shows that for Si, E_g = 1.1 ev, n_1 = 3.54 and r = 0.31 and for GaAs, E_g = 1.45 ev, n_1 = 3.33 and r = 0.29.

Thus there is not much difference in 'r' in the range of E_g which is available for the photovoltaic cells. The reflection losses which form about 30% should be eliminated in order to improve the efficiency of the cell. Antireflection coatings are provided to achieve this.

Fill factor

Generally, the maximum power output (P_{mp}) is represented as the fraction of the product of the open circuit voltage (V_{oc}) and the short-circuit current (J_{sc}). This fraction is known as fill factor (FF) or curve factor[54].

$$P_{mp} = FF \cdot V_{oc} \cdot J_{sc}$$

Hence the efficiency can be represented as

$$\eta = \frac{FF.V_{oc}.J_{sc}}{P_{in}} \times 100\% .$$

In general, the factors affecting the performance of the solar cell can be written as follows:

The efficiency of the solar cell, defined as the ratio of the maximum power delivered to the power input, is maximized by maximizing the short-circuit current, J_{sc}, the open circuit voltage, V_{oc} and the fill factor. To maximize the J_{sc}, the absorption of the incident light should be as large as possible. The thickness of the absorbing layer needed to do this is determined by the absorption coefficient. Additionally, the maximum number of the minority carriers generated should cross the junction. The number of minority carriers which reach the junction increases with increase in their diffusion length. The diffusion length increases as the square root of the product of the mobility of the carriers and their recombination life time. The recombination life time depends on the recombination cross section and the density of defects. The mobility of the carriers, in turn, depends on the scattering mechanisms present. The open circuit voltage depends on the magnitude of the barrier height. The width

of the region over which the barrier exists is dependent on the density of impurities.

With this introduction and a general review of the principles and operation of photovoltaic cells, we now present an account of our theoretical work on some aspects of solar cells in the subsequent chapters. Chapter 2 will deal with the theory and calculations on the performance of homo and hetero type M-p-n Schottky barrier solar cells. Chapter 3 will cover the performance of the back illuminated MIS solar cells. In chapter 4, theoretical calculations on the efficiency of p/n heterojunction of a-Si and low grade single crystal silicon will be presented.

References

1. H.A. Zahl, Chemical and Engineering News, 37, 96 (1959).

2. K.A. Ray, AIEE Summer General Meeting, Denver Co., June 17-22,(1962).

3. B. Ross, Aviation and Space, Hydraulic and Gas Turbine Conference, Los Angles, C.A., March 3,(1963).

4. J.V. Foster, 5th IEEE Photovoltaic Specialists Conference, 3 Greenbelt, MD, Oct.18-20, P. E-5 (1965).

5. G. Wolff, 9th Photovoltaic Specialists Conference, Silver Spring, MD, p.240,(1972).

6. H. Eder, J. Spacecraft and Rockets, 10, 196 (1973).

7. J.P. Thornton and L.W. Crabtree, 9th Intersociety Energy Conversion Engineering Conference, San Francisco, CA; August 26-30 (1974).

8. J.A. Baicker and B.W. Faughnam, J.Appl.Phys., 33, 3271 (1962).

9. P. Rapport and J.J. Wysocki, Acta Electron, 5, 364 (1961).

10. J. Lindmayer and J.F. Allison, COMSAT Tech.Rev., 3, 1 (1973).

11. J. Haynos, J. Allison, R. Arudt and A. Meulenberg, Int.Conf. on Photovoltaic Power Generation, Hamburg, p. 487 (1974) (unpublished).

12. E.J. Charlson and J.C. Lieu, J.Appl.Phys., 46, 3982 (1975).

13. R.J. Stirn and Y.C.M. Yeh, Appl.Phys. Lett., 27, 95 (1975).

14. W.A. Anderson, A.E. Delahoy and R.A. Milano, J.Appl.Phys., 45, 3913 (1974).

15. M.B. Prince, Sharing the Sun, Solar Technology in the seventies, A Joint Conference of the American Section of the International Solar Energy Soc., and the Solar Energy Soc. of Canada, August, p.186 (1946).

16. E. Becquerel, Compt.Rend. 9, 561 (1839).

17. W.G. Adams and R.E. Day, Proc.Roy.Soc., A25, 113 (1977).

18. B. Lange, Zeil.Phys. 31, 139 (1930).

19. L.O. Grondahl, Rev.Mod.Phys., 5, 141 (1933).

20. W. Schottky, Zeil.Phys., 31, 913 (1930).

21. D.M. Chapin, C.S. Fuller and G.L. Pearson, J.Appl.Phys., 25, 676 (1954).

22. J.J. Wysocki, P. Rapport, E. Davidson and J.J. Loferski, IEEE Trans. Ele. Dev. ED-13, 420 (1966).

23. M. Wolf, Proc. IRE, 48, 1246 (1960).

24. J.J. Loferski, J.Appl.Phys., 27, 777 (1956).

25. M.B. Prince, J.Appl.Phys., 26, 534 (1955).

26. E.R. Hill and B.G. Keramida, IEEE Trans.Electron.Dev., ED-14, 22 (1967).

27. A. Kunioka and Y. Sakai, Solid State Electron., 8, 961 (1965).

28. R.L. Anderson, Proc.Int.Conf. Semicond.Prague,(1960) (Czech.Acad.Sci.), p.563.

29. W.C. Dash and R. Newman, Phys.Rev., 99, 1151 (1955).

30. J.I. Pankove, Optical Processes in Semiconductors,
31*. (Prentice-Hall, Inc., New Jersey, 1971).

32. W. Shockley, Bell. Syst.Tech. J., 28, 435 (1949).

33. W. Shockley, Electrons and holes in semiconductors (Van Nostrand Book Co., 1950).

34. C.T. Sah, R.N. Noyce and W. Shockley, Proc.IRE, 45, 1228 (1957).

35. A.S. Grove, Physics and Technology of Semiconductor Devices, (John-Wiley and Sons, Inc., New York, 1967).

31*. T.S. Moss, Optical Properties of Semiconductors, (Butterworths Scientific Publication, London, 1959).

36. S.M. Sze, Physics of Semiconductor Devices, (John-Wiley and Sons, New York, 1969).

37. C. Kittel, Introduction to Solid State Physics, (John-Wiley and Sons, New York, 1953).

38. J.L. Moll, Physics of Semiconductors, (McGraw-Hill, N.Y. 1964).

39. R.A. Smith , Semiconductors (Cambridge at University Press, 1959).

40. D. Kondall, Conf. on the Physics and Application of Lithium diffused Silicon (1969).

41. J.G. Fossum, Solid State Electronics, 19, 269 (1976).

42. R.L. Anderson, IBM.J.Res.Develop., 4, 283 (1960).

43. A.G. Milnes and D.L. Feucht, Heterojunctions and Metal-Semiconductor Junctions (Academic Press, New York, 1972).

44. R.K. Purohit and B.L. Sharma, Semiconductor Heterojunctions, (Pergamon Press, Oxford, 1974).

45. R.L. Anderson, Solid State Electron., 5, 341 (1962).

46. L.L. Chang, Solid State Electron., 8, 721 (1965).

47. H.K. Henisch, Rectifying Semiconductor Contacts, (Claredon Press, Oxford, 1957).

48. P. Rapport, Phys.Rev., 93, 246 (1954).

49. H.J. Hovel, Semiconductor and Semimetals, Vol.11, Solar Cells, (Edited by A.K. Willardson, A.C. Beer, Academic Press, 1975).

50. W.W. Gartner, Phys.Rev., 116, 84 (1959).

51. P. Moon, J. Franklin Inst., 230, 586 (1940).

52. M.P. Thekaekara, Opt.Spectra, 6, 32 (1972).

53. R.J. Handy, Solid State Electron., 10, 765 (1967).

54. J. Lindmayer, COMSAT. Tech.Rev., 2, 105 (1972).

CHAPTER II

THEORETICAL STUDY ON THE BEHAVIOUR OF Metal-p-n SCHOTTKY BARRIER SOLAR CELLS

2.1 Introduction

Schottky barrier solar (SBS) cells appear suitable for large scale terrestrial applications because of their low cost of fabrication[1-6]. Furthermore, they are prepared at lower temperatures, hence the degradation in the bulk properties of the semiconductor is negligible. However, as is well-known, the open circuit voltage in SBS cells is less than that in the p-n junction solar cells[7-11]. Calculations by Pulfrey and McOuat[12] indicated a theoretical efficiency of 22-24% for silicon SBS cells, however, in practical cases, it is difficult to achieve an efficiency of more than 10%. This difference is due to the fact that Pulfrey and McOuat assumed a quantum efficiency of unity and the barrier height equal to the energy gap. By using a more realistic value for the barrier height in n-type silicon[13], the efficiencies of 11% and 17.8% have been calculated for Schottky cells with gold and platinum respectively[14,15]. In actual practice however, platinum gives considerably lower efficiency than gold due to the higher sheet resistance.

Recent theoretical[16-21] and experimental[22-27] work has shown that the presence of a thin interfacial insulating layer between the metal and the semiconductor (MIS) can considerably increase the photovoltaic conversion efficiency

of such solar cells. The thickness of this insulating layer is of the order of 30 Å.

The open circuit voltage V_{oc} for the MIS solar cell increases as the thickness of the oxide layer increases, but at the same time, the short circuit current decreases and the overall efficiency of the cell increases upto a certain thickness of the oxide layer, beyond which, it decreases. Hence there is an optimum value of the oxide layer thickness which is around 30 Å.

The height of a Schottky barrier depends upon the metal work function, the electron affinity of the semiconductor[28], the distribution of interface states, the nature of interfacial layer if present, and the electric field at the semiconductor surface. Shannon[29] has proposed to use this dependence on the surface electric field as a convenient means to control the barrier height.

The J-V characteristics of a Schottky barrier is[28]

$$J = A^{*} T^{2} \exp\left(-\frac{\phi'_{B}}{kT}\right) \left[\exp \frac{eV}{nkT} - 1\right] . \quad .. \qquad 2\text{-}1$$

The barrier height ϕ'_B is dependent upon the surface field and it can be written as

$$\phi'_{B} = (\phi_{m} - \chi_{s}) - (e\,\mathcal{E}/4\pi \epsilon_{o})^{1/2} \quad .. \qquad 2\text{-}2$$

where the second term is the lowering of barrier height due to the surface field. The change of the barrier height is thus dependent upon the sign and magnitude of the electric field at the surface of semiconductor. Furthermore, since the surface field,

$$\mathcal{E} = [2e\, N_D\, (V_d - V)/\, \epsilon\epsilon_o]^{1/2}, \qquad .. \quad 2\text{-}3$$

a low saturation current should be obtained for lightly doped substrates. A highly doped substrate will reduce the barrier height in the forward direction. In agreement with this, Shannon observed that a thin highly doped layer at the surface of the semiconductor causes the electric field to increase and hence the barrier height to decrease.

Later, he has considered a situation where the surface layer is oppositely doped to the substrate, as this was expected to lead to an increase in the barrier height on the basis of equations 2-2 and 2-3[30].

The space charge due to the Gaussian donor profile in the implanted layer modifies the band bending at the surface of the semiconductor. In an ideal system the barrier height between the metal and the semiconductor is equal to the difference between the electron affinity of the metal and that of the semiconductor. Thus for a given concentration

in the base layer, the barrier height is fixed. This can be explained with the help of Fig. 2-1. In Fig. 2-1, curve 1 corresponds to a zero surface field and the doping concentration in the layer is minimum below which there is no increase in the effective barrier height. For a thin layer of lightly doped substrate, the surface field is zero for a certain concentration of implanted atoms.

The effect of increase in the number of implanted atoms is shown by curve 2. It can be seen that at a certain doping a potential maximum for holes is obtained across the implanted layer. If $N_A >> N_D$ and the concentration of the implanted atoms is much higher than the zero field concentration, then using the Poisson's equation, it can be shown that the potential maximum will occur close to the layer-substrate boundary.

Clearly as the doping concentration in the layer increases, the effective barrier height increases until the fermi level comes to within a few kT from the conduction band edge beyond which the p-layer is not fully depleted of holes and a sort of n-p junction is formed. This situation is represented by curve 3.

Shannon reported a device made of Ni-Si Schottky diode with ion implanted antimony[31]. The theoretically predicted reduction of barrier height in a n-type substrate,

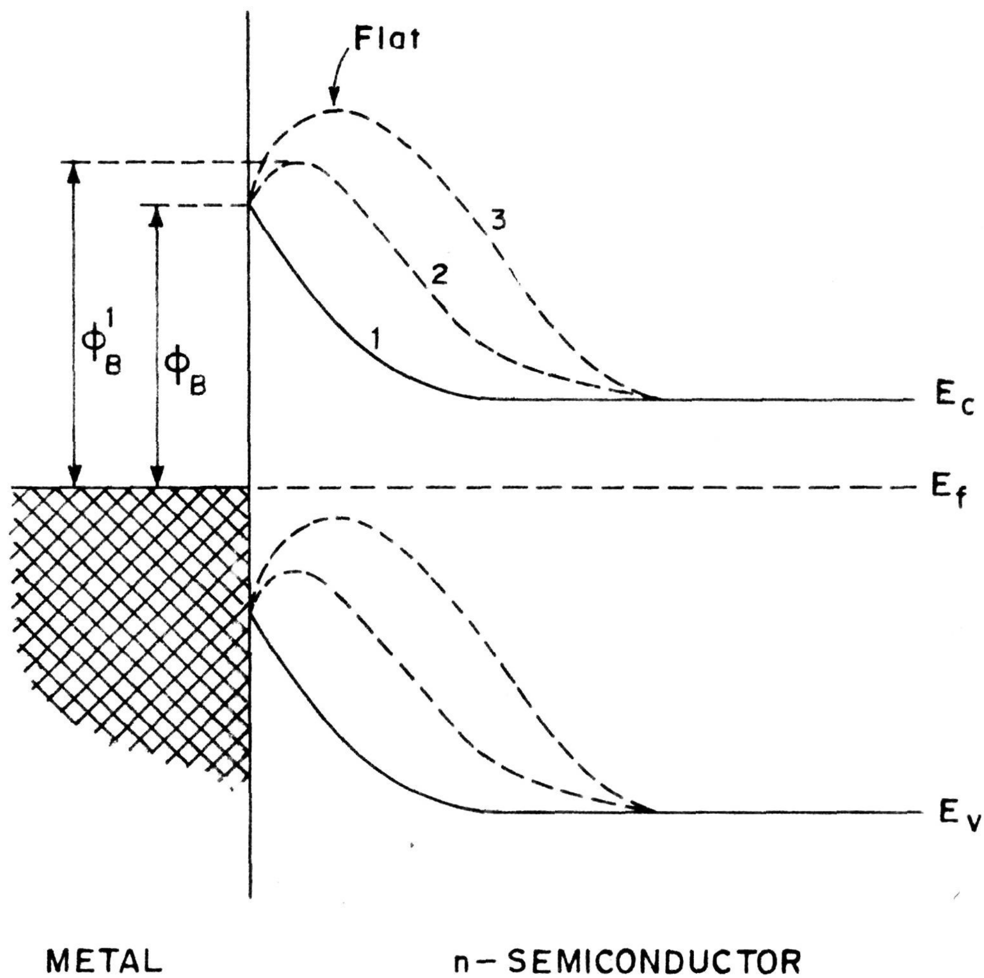

FIG. 2·1.

SCHEMATIC DIAGRAM OF ENERGY BANDS IN SCHOTTKY BARRIER ON n-TYPE MATERIAL WITH THE VARIATION OF p-TYPE SURFACE LAYER

assuming all the implanted antimony to be electrically active, was compared with that found experimentally. The measurements on Ni-Si barrier having a built-in potential of 0.3 V showed that the barrier height could be lowered by 0.15 eV without any degradation of the reverse characteristic using a 5 KeV antimony source. Similarly the increase in the barrier height of p-type silicon was measured following a 5 KeV antimony implantation. But considerable discrepancy between the calculated increase in barrier height and that measured was found, particularly at higher concentration of implanted atoms. This could be accounted for by the activity of the implantation. This has been confirmed by Pai et al[32].

Van der Ziel[33] has considered the M-p-n silicon Schottky barrier diode and shown that the barrier height depends upon the thickness and the dopant density of the 'p' layer.

Later, Li[34] has extended Van der Ziel's calculations for a GaAs Schottky barrier solar cell. He has shown that the barrier height of this diode is equal to the band gap of the semiconductor. The present work however, shows that in a system like this, the barrier height can not approach the energy gap of the semiconductor but it would be less than the band gap of the semiconductor by a few kT's[35].

2.2 Homojunction Metal-p-n photovoltaic cells

In this thesis, we have considered a metal-p-n-Si Schottky barrier whose band structure is shown in Fig. 2-2. Let us consider an n-type material on which a Schottky barrier has been made. A thin layer of p-type material is inserted in between the metal and the semiconductor.

The effective barrier height for this system follows the relation,

$$\phi_{Bn} = \phi_m - \chi_s + eV_m \qquad .. \quad 2\text{-}4$$

where eV_m is the increase of barrier height. In order to find out a relation between the increased potential barrier, V_m and the donor and acceptor concentrations, the following Poisson's equations are considered:

$$\frac{d^2\psi_1}{dx^2} = \frac{eN_A}{\epsilon_s \epsilon_o} ; \quad 0 < x < w_p \qquad .. \quad 2\text{-}5$$

$$\frac{d^2\psi_2}{dx^2} = - \frac{eN_D}{\epsilon_s \epsilon_o} ; \quad w_p < x < w_p + w_n \qquad .. \quad 2\text{-}6$$

The prevailing boundary conditions are

(a) $\psi(0) = 0$

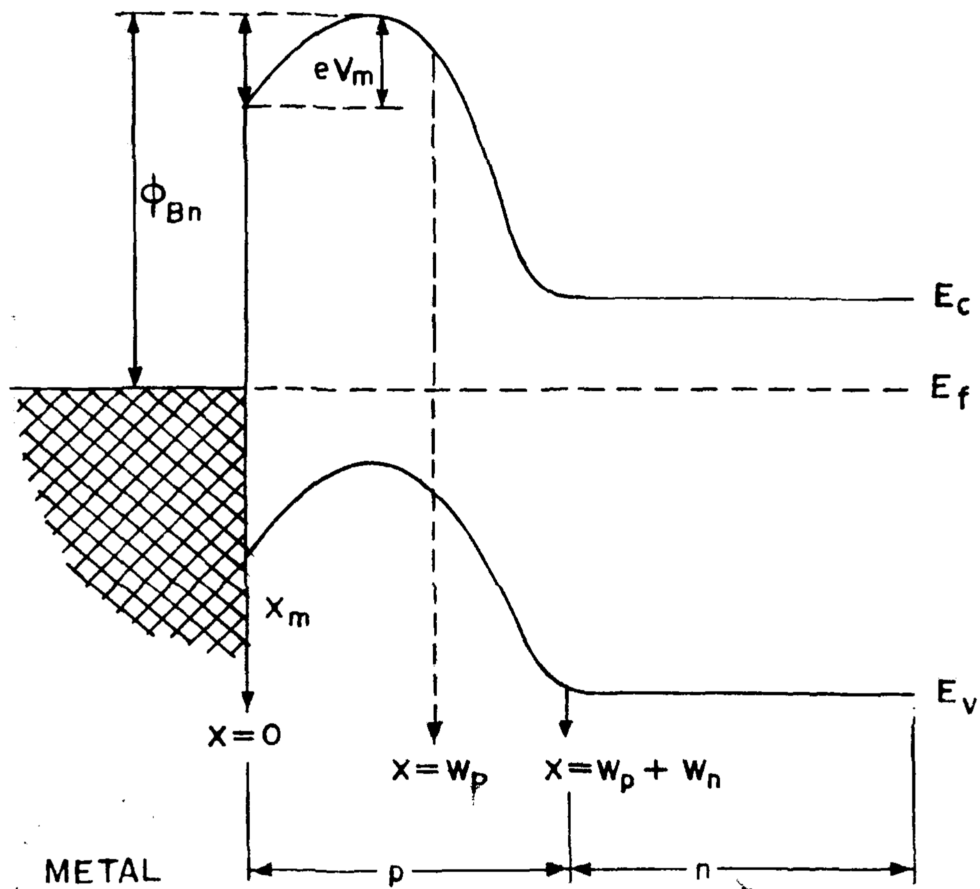

FIG. 2·2.

SCHEMATIC ENERGY BAND DIAGRAM OF METAL-p-n SCHOTTKY BARRIER SOLAR CELL

(b) $\psi(w_p+w_n) = \phi_m - \phi_n - V$

(c) $\frac{d\psi(x)}{dx}$ is continuous

(d) $\psi_1(x)\Big|_{w_p} = \psi_2(x)\Big|_{w_p}$

(e) $\frac{d\psi}{dx}\Big|_{x=0} = \frac{eN_D w_n - eN_A w_p}{\epsilon_s \epsilon_o}$ and

(f) $\frac{d\psi}{dx}\Big|_{w_p+w_n} = 0$.

Th. 6645

After integrating equation 2-5,

$$\psi(x) = \psi_1(x) = \frac{eN_A}{\epsilon_o \epsilon_s} \frac{x^2}{2} + A_1 x + B_1, \quad 0 < x < w_p \qquad .. \text{ 2-7}$$

At $x = 0$, $\psi(0) = 0$, therefore $B_1 = 0$.

In order to evaluate the other parameter A_1, the condition (c) is used.

Th. 6645

$$\left.\frac{d_1 \psi(x)}{dx}\right|_{x=0} = \frac{eN_D w_n - eN_A w_p}{\epsilon_s \epsilon_o} = A_1$$

After substitution for A_1 and B_1 in equation 2-7

$$\psi_1(x) = \frac{eN_A}{\epsilon_s \epsilon_o}\left[\frac{x^2}{2} - w_p x\right] + \frac{eN_D w_n}{\epsilon_s \epsilon_o} x \qquad \cdot\cdot \quad 2\text{-}8$$

Similarly the other Poisson's equation gives

$$\psi_2(x) = -\frac{eN_D}{\epsilon_s \epsilon_o} \frac{x^2}{2} + A_2 x + B_2 \qquad \cdot\cdot \quad 2\text{-}9$$

$$w_p < x < w_p + w_n$$

By using the boundary condition (f),

$$\left.\frac{d\,\psi_2(x)}{dx}\right|_{w_p+w_n} = 0 = -\frac{eN_D}{\epsilon_s \epsilon_o}(w_p + w_n) + A_2$$

one gets

$$A_2 = \frac{eN_D}{\epsilon_s \epsilon_o}(w_p + w_n)$$

and the boundary condition (d) gives

$$\frac{eN_A}{\epsilon_s \epsilon_o}\left\{\frac{w_p^2}{2} - w_p^2\right\} + \frac{eN_D w_n w_p}{\epsilon_s \epsilon_o}$$

$$= -\frac{eN_D}{\epsilon_s \epsilon_o}\frac{w_p^2}{2} + \frac{eN_D}{\epsilon_s \epsilon_o}(w_p+w_n)w_p + B_2.$$

Hence

$$B_2 = -\frac{e}{\epsilon_s \epsilon_o}(N_A+N_D)\cdot\frac{w_p^2}{2}$$

and by substituting the value of A_2 and B_2 in equation 2-9

$$\psi_2(x) = -\frac{eN_D}{\epsilon_s \epsilon_o}\frac{x^2}{2} + \frac{eN_D}{\epsilon_s \epsilon_o}(w_p+w_n)x$$

$$-\frac{e}{\epsilon_s \epsilon_o}(N_A+N_D)\cdot\frac{w_p^2}{2} \qquad .. \quad 2\text{-}10$$

In order to find the relation between w_p and w_n, the boundary condition (b) is used.

$$\psi(w_p+w_n) = \frac{\phi_m-\phi_n}{e}$$

i.e.

$$-\frac{eN_D}{\epsilon_s \epsilon_o} \frac{(w_p+w_n)^2}{2} + \frac{2N_D}{\epsilon_s \epsilon_o} (w_p+w_n)^2 - \frac{e}{\epsilon_o \epsilon_s} (N_A+N_D) \frac{w_p^2}{2}$$

$$= \frac{\phi_m - \phi_n}{e}$$

i.e.

$$\frac{eN_D}{\epsilon_o \epsilon_s} (w_p+w_n)^2 = \frac{(\phi_m-\phi_n)}{e} + \frac{e}{\epsilon_s \epsilon_o} (N_A+N_D) \frac{w_p^2}{2} ,$$

$$w_p+w_n = \left[\frac{w_p^2 \quad (N_A+N_D)}{N_D} + \frac{2 \epsilon_s \epsilon_o}{eN_D} \frac{(\phi_m-\phi_n)}{e} \right]^{1/2}$$

$$w_n = -w_p + \left[\frac{w_p^2 \; (N_A+N_D)}{N_D} + \frac{2 \epsilon_s \epsilon_o}{eN_D} \frac{(\phi_m-\phi_n)}{e} \right]^{1/2} \quad .. \text{ 2-11.}$$

Thus, equation 2-11 gives a relationship between w_p and w_n. Due to the insertion of the thin layer, the potential would increase. At the maximum potential

$$\frac{d \, \psi(x)}{dx} = 0$$

Therefore, from equation 2-8, one gets,

$$\frac{eN_A}{\epsilon_s \epsilon_o}(x_m - w_p) + \frac{eN_D w_n}{\epsilon_s \epsilon_o} = 0$$

$$x_m = w_p - \frac{N_D}{N_A} w_n \qquad .. \quad 2\text{-}12$$

This implies that the maximum potential would occur in the 'p' layer itself at a distance x_m from the metal-semiconductor junction and would be given by

$$V_m = \Psi_1(x_m)$$

$$= \frac{eN_A}{\epsilon_s \epsilon_o}\left[\frac{(N_A w_p - N_D w_n)^2}{2N_A^2} - \frac{w_p (N_A w_p - N_D w_n)}{N_A}\right] + \frac{eN_D w_n}{\epsilon_s \epsilon_o}[N_A w_p - N_D w_n]$$

i.e.

$$V_m = -\frac{e}{2\epsilon_s \epsilon_o}\frac{1}{N_A}(N_A w_p - N_D w_n)^2 \qquad .. \quad 2\text{-}13$$

For a Schottky barrier with p-type substrate, the width of the depletion region is[36]

$$x_o = \left[\frac{2\epsilon_s \epsilon_o}{e}\frac{(\phi_p - \phi_m)}{eN_A}\right]^{1/2} \qquad .. \quad 2\text{-}14$$

As we have assumed that the 'p' layer is completely ionized, the maximum potential would occur where the depletion region created due to metal meets that due to the 'n' type layer. In other words, the width of the depletion region due to the metal equals the distance where the maximum potential occurs, i.e.

$$x_m = x_o$$

i.e.,

$$\left[\frac{2\,\epsilon_s \epsilon_o}{e} \; \frac{(\phi_p - \phi_m)}{eN_A}\right]^{1/2} = w_p - \frac{N_D}{N_A} w_n,$$

$$\frac{(N_A w_p - N_D w_n)^2}{N_A} = \frac{2\,\epsilon_s\,\epsilon_o}{e} \; \frac{(\phi_p - \phi_m)}{e}$$

Substituting this value in equation 2-13, one gets

$$V_m = \frac{(\phi_p - \phi_m)}{e}$$

The increase in the height of a metal-Schottky barrier by inserting a thin layer of oppositely conducting semiconductor is therefore equal to eV_m. The maximum effective barrier

$$\phi_B = \phi_m - \chi_s + (\phi_p - \phi_m)$$

$$= E_g - kT \ln \frac{N_v}{N_A} \qquad .. \quad 2\text{-}15$$

Thus ϕ_B would be controlled by the acceptor concentration. By taking higher acceptor concentration, ϕ_B can be increased.

In order to see the photovoltaic performance of the cell, the current-voltage equation has to be considered. Under illumination, the diode equation is given by

$$J = J_o \left[\exp \frac{e(V-JR_s)}{kT} - 1 \right] - J_L \qquad .. \quad 2\text{-}16$$

where R_s is the series resistance of the cell including the grid effect.

$$R_s = R_b + R_{diff.} + R_{front} + R_{back}$$

where R_b = resistance of the base material

$R_{diff.}$ = resistance due to the diffused layer

R_{front} = resistance due to the front grid electrode including the Schottky metal effect

R_{back} = resistance due to the back electrode.

Further

$$R_b = (t_1/A)$$

$$R_{diff.} = \bar{\rho} . d$$

and $$R_{back} = \bar{\rho}_{met} . (t_2/A)$$

where ρ is the resistivity of the base material, t_1 the thickness of the cell, d the thickness of the diffused layer, t_2 the thickness of back contact, $\bar{\rho}_{met}$ the resistivity of the metal used for back ohmic contact, $\bar{\rho}$ the resistivity of the diffused layer and A the area of the cell. Handy's formulae[37] have been used in the calculations of series resistance for a finger type grid pattern (Fig. 2-7), taking the numerical values of 0.35 cm for the spacing between the grid lines and 0.01 cm for their width.

In order to calculate the photogenerated current, the spectral response of the cell is considered. In the region $x = 0$ to $x = x_m$, there would be an accumulation of photogenerated holes which would cause a lowering in the barrier height. In order to simplify the calculations, this effect is assumed to be negligible.

The generation of electron-hole pair is given as

$$g(x) = \alpha N \exp(-\alpha x)$$

The current generated in the depletion region

$$J_{dr} = \int_{x_m}^{w_p+w_n-x_m} e\alpha N \exp(-\alpha x)dx$$

$$= eN [\exp(-\alpha x_m) - \exp\{-\alpha (w_p+w_n-x_m)\}]$$

Photocurrent due to diffusion in bulk region

The continuity equation outside the depletion region at equilibrium is given by[38]

$$\frac{dp}{dt} = D_1 \cdot \frac{d^2\Delta p}{dx^2} + \alpha N \exp(-\alpha x) - \frac{\Delta p}{\tau_1} = 0 \quad .. \text{ 2-17}$$

with the boundary conditions

$$\Delta p = 0 \text{ at } x = w_p + w_n - x_m \text{ and}$$

$$\Delta p = 0 \text{ at } x \to \infty$$

By solving this equation with the boundary conditions

$$\Delta p = \frac{\alpha N \tau_p}{1-\alpha^2 L_p^2} \left[\left(e^{(w_p+w_n-x_m)(-\alpha+\frac{1}{L_p})} \cdot e^{-x/L_p} \right) - e^{-\alpha x} \right] \quad \text{... 2-18}$$

The diffusion current is given by

$$J_{p(diff)} = D_1 \left. \frac{d\Delta p}{dx} \right|_{x = w_p+w_n-x_m}$$

After substituting

$$w = w_p+w_n-x_m$$

the diffusion current is modified because of the assumption of a dead layer in the depletion region and is written as

$$J_{p(diff)} = \frac{e\alpha N L_p}{1+\alpha L_p} \exp(-\alpha w)$$

The current got by the combination of the current due to diffusion and that due to the depletion region,

$$J_1(\lambda) = eN \left\{ \exp(-\alpha x_m) - \frac{\exp(-\alpha w)}{1+\alpha L_p} \right\} \quad .. \ 2\text{-}19$$

The total photogenerated current can be obtained by integrating the above equation over the entire AMO spectrum

$$J_L = \int_{0.3\mu}^{hc/E_g} J_1(\lambda)\, d\lambda \quad .. \ 2\text{-}20$$

The dark current can be calculated by using

$$J_o = A^* T^2 \cdot \exp\left(-\frac{e\phi_B}{kT}\right) \quad .. \ 2\text{-}21$$

Results and Discussion

In order to study the variation of the barrier height as a function of the acceptor and donor concentrations, we have considered a model by taking gold as the Schottky metal over a n-type base material.

The values of various constants used for silicon[39] are $\epsilon_s = 11.7$, $\chi_s = 4.01$ eV, $E_g = 1.1$ eV, $N_v = 1.82 \times 10^{19}$ cm^{-3} and ϕ_m of Au is 4.8 eV. Similarly, for GaAs the values are: $\epsilon_s = 11.1$, $\chi_s = 4.07$, $E_g = 1.47$ eV and $N_v = 1 \times 10^{19}$ cm^{-3}. The photon absorption coefficient $\alpha(\lambda)$ for GaAs was determined from the data presented by Loferski[40].

The values of N_A, N_D and w_p are systematically varied and the corresponding values of w_n and the effective barrier height found by using the equations 2-11, 2-12, 2-13 and 2-14. The variation of the barrier height as a function of the thickness of the 'p' layer has also been seen by varying the donor concentration at various fixed values of the acceptor concentration. The effective barrier height increases as the thickness of 'p' layer increases upto a certain thickness and it attains a maximum which is less than the band gap of base material. This has been shown in Figs. 2-3 and 2-4 for Si and GaAs respectively.

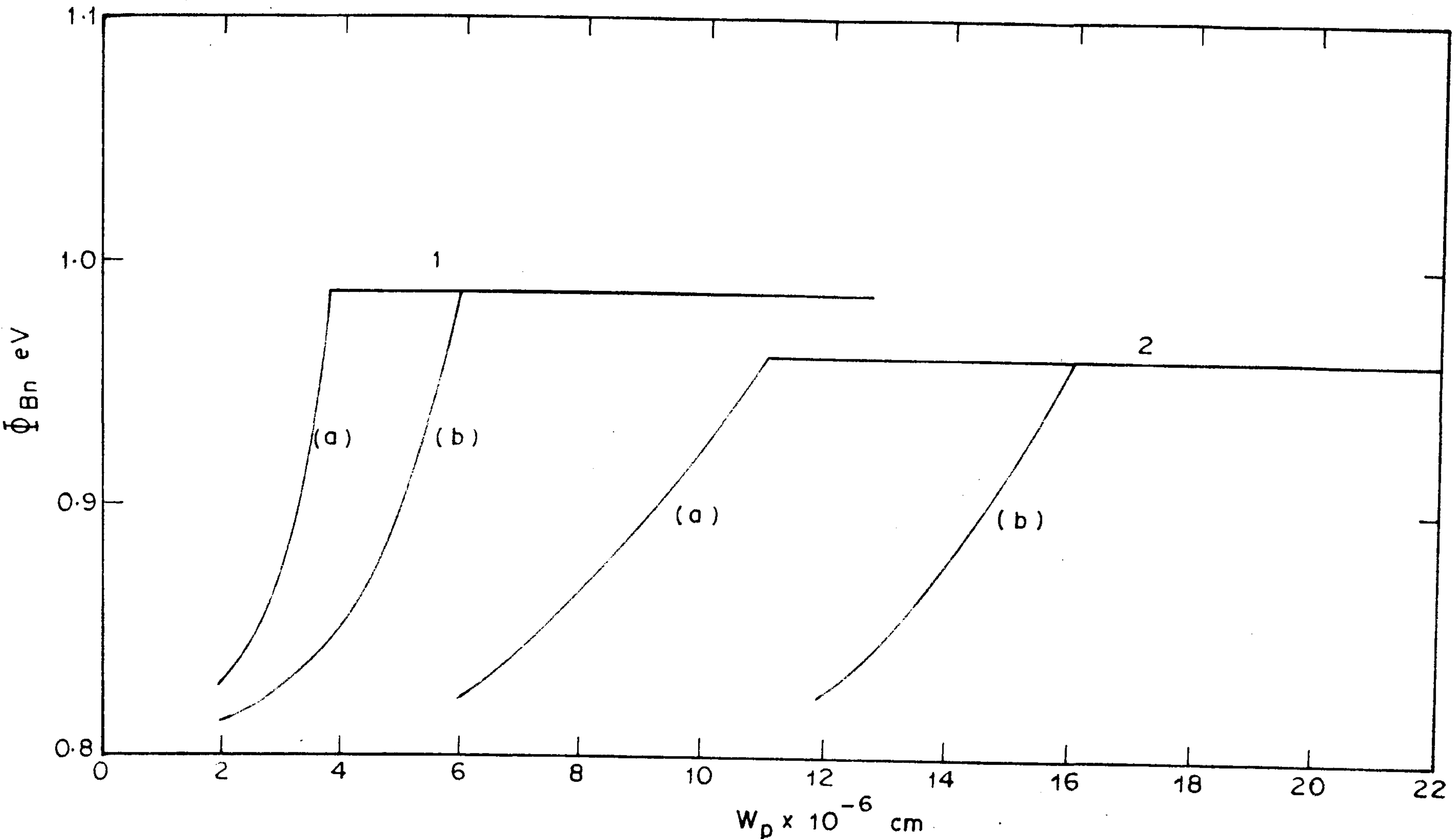

FIG. 2.3. BARRIER HEIGHT Φ_{Bn} AS A FUNCTION OF P-LAYER THICKNESS (W_P) IN A HOMOJUNCTION Si SOLAR CELL

1) (a) $N_A = 2.75 \times 10^{17}\ cm^{-3}$, $N_D = 1 \times 10^{17}\ cm^{-3}$ (b) $N_A = 2.75 \times 10^{17}\ cm^{-3}$, $N_D = 1 \times 10^{16}\ cm^{-3}$

2) (a) $N_A = 5 \times 10^{16}\ cm^{-3}$ $N_D = 1 \times 10^{17}\ cm^{-3}$ (b) $N_A = 5 \times 10^{16}\ cm^{-3}$, $N_D = 1 \times 10^{16}\ cm^{-3}$

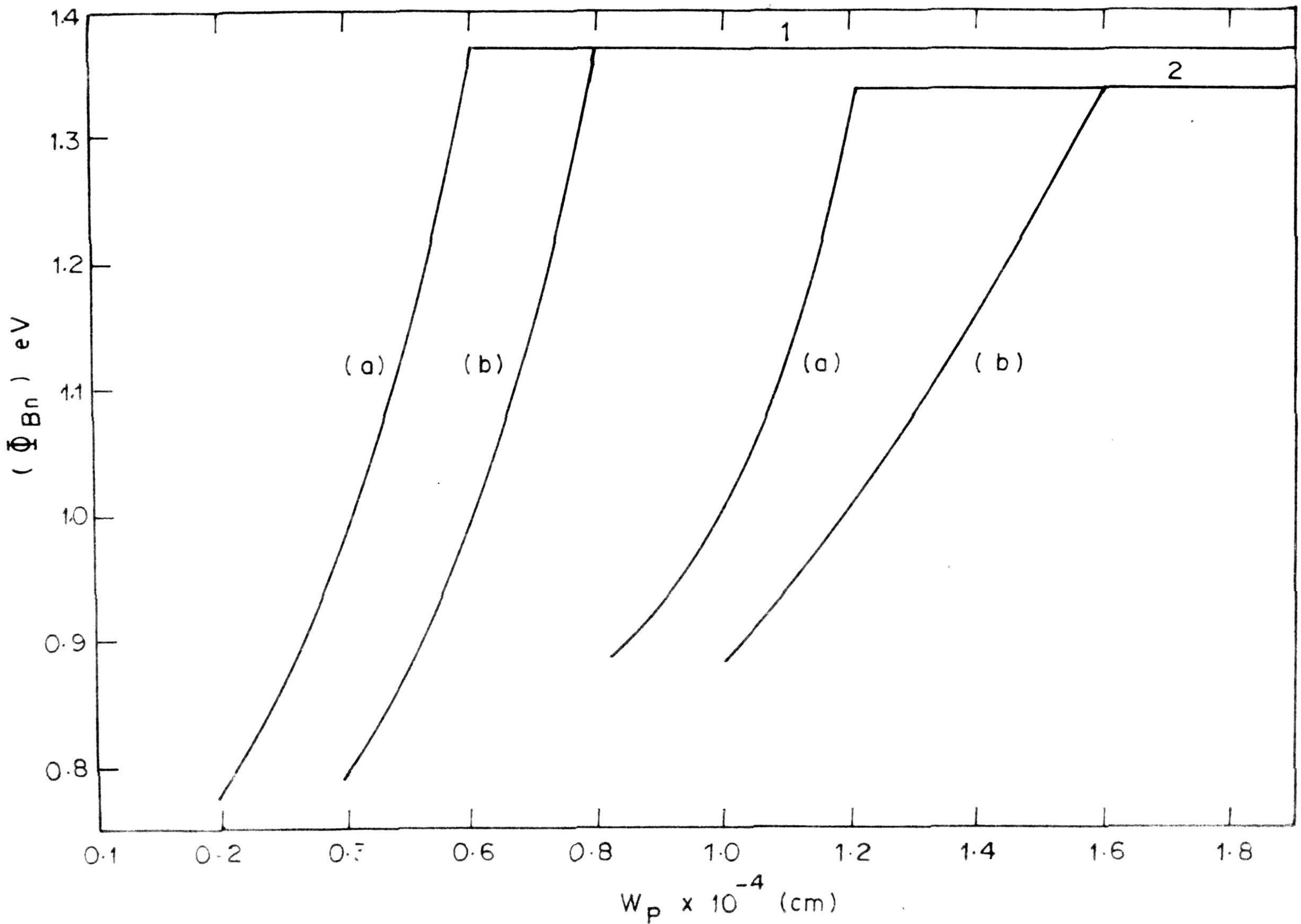

FIG. 2.4. BARRIER HEIGHT AS A FUNCTION OF 'P' LAYER THICKNESS (W_p) AT 1) a) $N_A = 3.25 \times 10^{17}$ cm^{-3}, $N_D = 1 \times 10^{16} cm^{-3}$ b) $N_A = 3.25 \times 10^{17}$ cm^{-3}, $N_D = 1 \times 10^{17}$ cm^{-3} AND 2) a) $N_A = 1.06 \times 10^{17}$ cm^{-3}, $N_D = 1 \times 10^{16}$ cm^{-3} b) $N_A = 1.06 \times 10^{17}$ cm^{-3}, $N_D = 8 \times 10^{16}$ cm^{-3}

Once the maximum barrier height is obtained, if the thickness of the 'p' layer is further increased, the configuration is no more of a diode type, it would be M-p-n transistor, because of the appearance of the flat band at the p/n junction.

The minimum value of w_p at which this maximum barrier height is obtained is called $(w_p)_{opt.}$ The $(\phi_{Bn})_{max.}$ and the corresponding $(w_p)_{opt.}$ values for different N_A and N_D are depicted in Figs. 2-5 and 2-6 for Si and GaAs respectively. To obtain a point corresponding to a given set of values of N_A and N_D the values of $(w_p)_{opt.}$ and $(\phi_{Bn})_{max.}$ are recorded and contours connecting constant values of $(w_p)_{opt.}$ and $(\phi_{Bn})_{max.}$ are drawn. The constant $(\phi_{Bn})_{max.}$ line is horizontal because it is a function of N_A but not of N_D. From these graphs, one can readily find out the optimum values of N_A and w_p to use for any selected N_D and read out the $(\phi_{Bn})_{max.}$ that one would expect for this set of values. It is clear from Figs. 2-5 and 2-6 that for reasonable values of N_A and N_D (i.e. 10^{16} - 10^{18} cm^{-3}) high $(\phi_{Bn})_{max.}$ (approaching E_g) can be obtained only for sufficiently small values of w_p i.e. thin 'p' layer region of ~ 200 Å.

It was claimed by Li[34] that the maximum effective barrier height is equal to the band gap. Our calculations

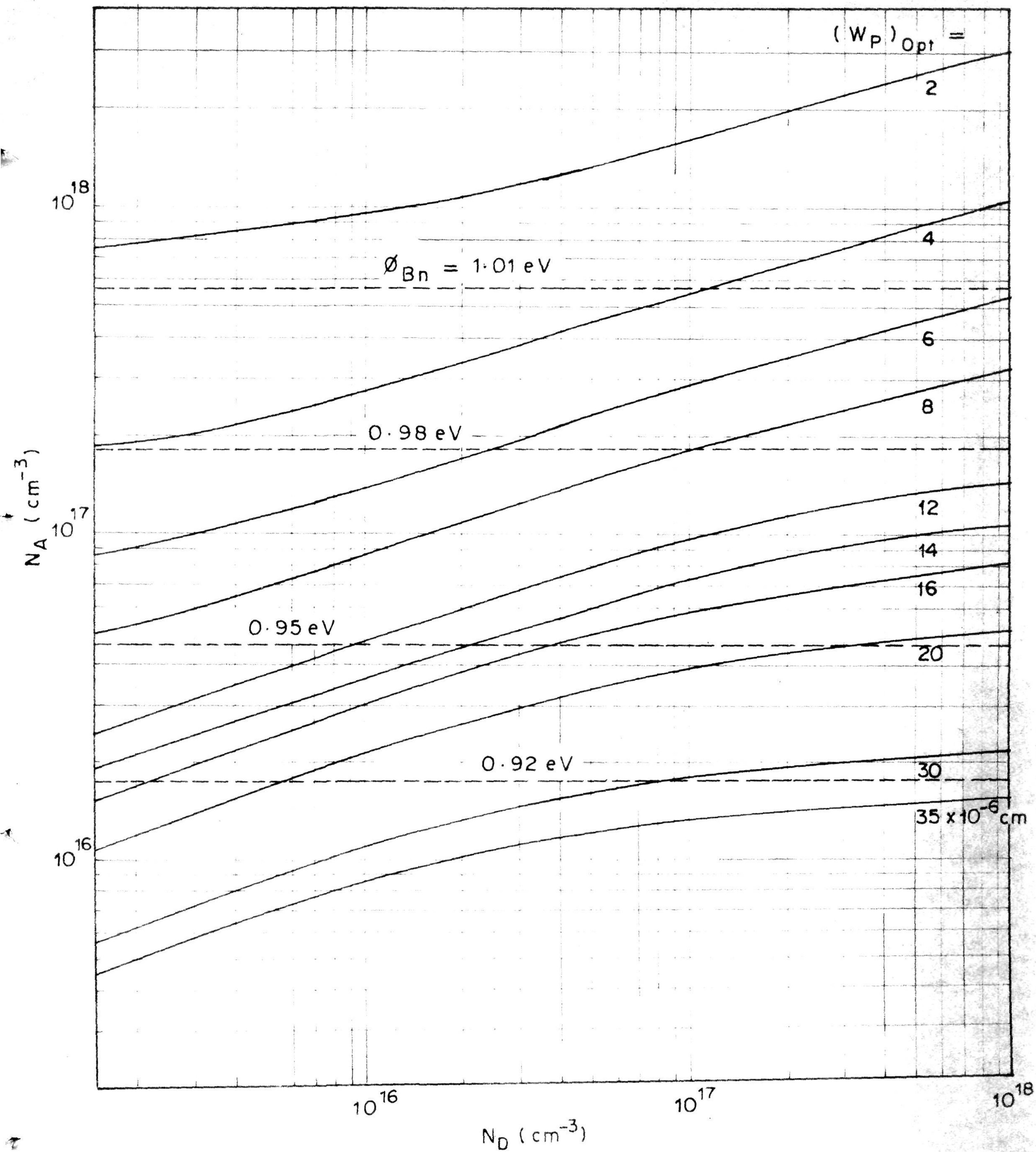

FIG. 2·5. CHANGE OF ACCEPTOR DENSITY WITH RESPECT TO DONOR DENSITY AT DIFFERENT $(W_P)_{opt.}$ FOR SILICON HOMOJUNCTION

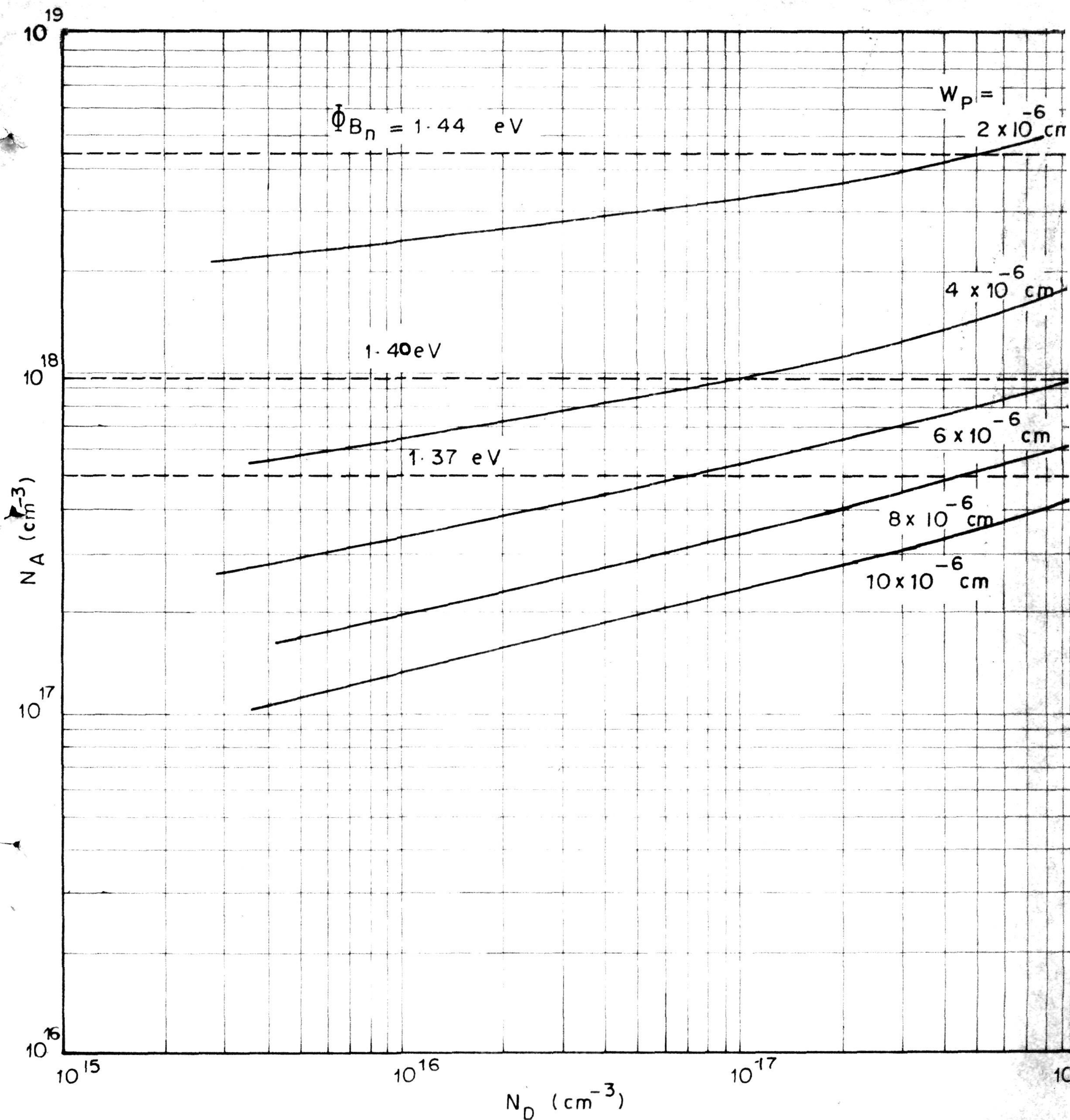

FIG. 2·6. Φ_{B_n} AND $(W_P)_{Opt}$ AS A FUNCTION OF DONOR AND ACCEPTOR DENSITIES (N_D, N_A) IN GaAS HOMOJUNCTION

do not support this conclusion. The maximum effective barrier height turns out to be a function of N_A. This conclusion is significant in the optimisation of solar cell parameters. Thus for a fixed value of N_A, the maximum effective barrier height is fixed but depending upon the donor density, w_p has to be appropriately chosen. Figure 2 in Li's publication gives an erroneous impression because he has arbitrarily extended the ϕ_{Bn} - N_A plots upto a maximum value equal to the energy gap.

After seeing the barrier height behaviour, the calculations of the photovoltaic performance has been done by using the equations 2-19, 2-20, 2-21 and 2-16. In order to calculate the series resistance, we have considered a finger type grid pattern as shown in Fig. 2-7.

Thus by considering the series resistance effect, the open circuit voltage, short circuit current and the complete J-V characteristics have been obtained. The data of photon intensity spectra, $N(\lambda)$ at the AMO have been taken from Thekaekara[41]. As shown in Fig. 2-8, the J-V characteristics for different values of Si homojunction have been drawn from which the fill factor was found out. Thus the maximum power obtained from the cell and hence the maximum efficiency have been calculated for an optimum set of N_A, N_D and $(w_p)_{opt}$. For a given value of $(w_p)_{opt}$.

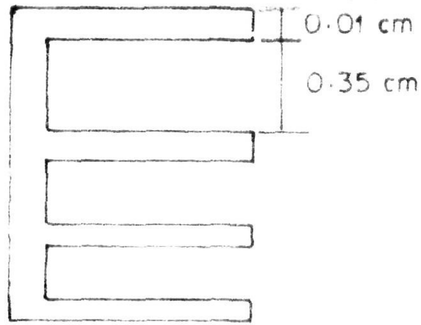

FIG 2·7 GRID PATTERN

VOLTS

0 0·1 0·2 0·3 0·4 0·5 0·6 0·7

J (ma / cm^2)

4 12 20 28 36 44 52

FF = 0·83

(0·585 , 44·0)

J_{SC}

FIG. 2·8. J-V CHARACTERSTICS FOR Si HOMOJUNCTION UNDER ILLUMINATION

(say, 2500, 2000, 1600, 1200, 800, or 200 Å) a set of points on the corresponding contours (Fig. 2-3) are chosen. The values of N_A, N_D and $(\phi_{Bn})_{max.}$ at those points are read out and the $P_{max.}$ has been calculated following the above-mentioned procedure.

The results are tabulated in the Table 1 and 2 and $P_{max.}$ is plotted as a function of N_D for different values of w_p in Fig. 2-9 and 2-10 for Si and GaAs respectively.

From these graphs, it is clear that for a given N_D, the maximum power obtained increases with decreasing w_p (increasing N_A).

As this configuration appears potentially capable of improving the performance of a Schottky barrier solar cell, it was considered desirable to extend the calculations to heterojunction solar cells.

2.3 Heterojunction solar cells

Heterojunction solar cells have already been used to enhance short wave length response, and are potentially as efficient as conventional cells under optimum conditions[42-44]. Fabrication of heterojunction cells is also sometimes simpler because it does not necessarily involve the dopant diffusion. Heterojunction solar cells have many similarities with Schottky barrier solar cells[45]. The most important

Table 1

Au-p-n-Si (homo) Schottky barrier solar cell calculated under AMO illumination

N_D $\times 10^{16}$ cm^{-3}	w_p $\times 10^{-6}$ cm	N_A $\times 10^{16}$ cm^{-3}	w_n $\times 10^{-5}$ cm	x_m $\times 10^{-6}$ cm	$(\phi_{Bn})_{max.}$ ev	J_{sc} mA/cm^2	V_{oc} Volts	P_{max} mW/cm^2	η %
0.14	2	74.4	8.13	1.85	1.018	46.33	0.671	26.14	19.36
0.2	2	76.9	6.85	1.82	1.019	46.48	0.672	26.20	19.450
1.0	2	93.7	3.14	1.66	1.023	45.02	0.675	25.58	18.95
10.0	2	153.0	1.04	1.34	1.036	39.73	0.685	22.92	16.98
100.0	2	296.9	0.297	0.999	1.053	31.57	0.696	18.53	13.73
0.14	8	3.31	7.64	5.82	0.946	44.81	0.598	22.12	16.39
0.2	8	5.38	6.32	5.61	0.949	44.70	0.601	22.23	16.70
1.0	8	8.55	2.87	4.04	0.961	43.70	0.612	22.21	16.45
10.0	8	17.6	0.805	3.43	0.980	38.96	0.627	20.30	15.04
100.0	8	30.4	0.161	1.82	0.994	30.76	0.637	16.33	12.10
0.2	12	2.70	6.23	7.39	0.931	44.01	0.582	21.05	15.59
1.0	12	4.53	2.71	6.01	0.944	43.15	0.595	21.19	15.70
10.0	12	9.20	0.69	4.50	0.963	38.31	0.611	19.39	14.36
100.0	12	14.0	0.115	3.77	0.974	30.36	0.616	15.52	11.50

...

Table 1 (contd.)

0.2	16	1.69	6.05	8.85	0.919	43.50	0.571	20.36	15.08
1.0	16	2.91	2.57	7.17	0.933	42.72	0.584	20.54	15.21
10.0	16	5.66	0.595	5.49	0.950	38.13	0.594	18.80	13.93
100.0	16	7.86	0.088	4.80	0.959	30.00	0.601	14.88	11.02
0.2	20	1.19	5.87	10.1	0.909	43.08	0.560	19.70	14.59
1.0	20	2.06	2.43	8.2	0.924	42.35	0.575	19.96	14.80
10.0	20	3.81	0.52	6.43	0.939	37.79	0.586	18.22	13.50
100.0	20	4.95	0.07	5.80	0.947	29.61	0.598	14.34	10.62
0.2	25	0.84	5.67	11.46	0.900	42.66	0.551	19.17	14.20
1.0	25	1.45	2.26	9.14	0.915	41.94	0.565	19.39	14.36
10.0	25	2.52	0.44	7.62	0.929	37.40	0.576	17.69	13.10
100.0	25	3.09	0.056	6.97	0.936	29.50	0.578	13.99	10.36

Table 2

Au-p-n-GaAs (homo) Schottky **barrier solar cell calculated**
under AMO illumination

N_D $\times 10^{16}$ cm^{-3}	w_p $\times 10^{-6}$cm	N_A $\times 10^{17}$ cm^{-3}	w_n $\times 10^{-5}$cm	x_m $\times 10^{-6}$cm	$(\phi_{Bn})_{max.}$ ev	J_{sc} mA/cm^2	V_{oc} volt	$P_{max.}$ mW/cm^2	η %
0.5	2	23.4	5.446	1.88	1.423	27.98	0.994	24.30	18.15
1.0	2	24.4	3.876	1.84	1.424	27.69	0.996	24.36	18.04
5.0	2	29.0	1.750	1.70	1.431	26.91	1.002	23.75	17.59
10.0	2	32.1	1.24	1.61	1.434	25.91	1.007	22.87	16.94
50.0	2	44.3	0.545	1.38	1.442	25.40	1.011	22.67	16.79
0.5	4	6.17	5.349	3.56	1.388	26.42	0.958	22.26	16.49
1.0	4	6.68	3.80	3.43	1.389	26.21	0.959	22.07	16.35
5.0	4	9.71	1.699	3.02	1.397	25.67	0.966	21.84	16.18
10.0	4	10.0	1.180	2.82	1.401	24.77	0.970	21.68	15.74
50.0	4	14.8	0.492	2.34	1.412	24.50	0.980	21.13	15.65
100.0	4	17.5	0.323	2.15	1.418	23.51	0.977	20.21	14.97

contd...

Table 2 (contd.)

0.5	8	1.75	5.219	6.51	1.355	24.04	0.922	19.37	14.35
1.0	8	1.98	3.685	6.14	1.357	24.00	0.925	19.41	14.38
5.0	8	2.82	1.590	5.18	1.366	23.86	0.934	19.55	14.49
10.0	8	3.35	1.080	4.77	1.371	23.14	0.938	19.00	14.08
50.0	8	4.92	0.396	3.97	1.382	23.13	0.948	19.23	14.25
100.0	8	5.63	0.241	3.72	1.386	22.21	0.951	18.55	13.74
0.5	12	0.875	5.100	9.08	1.336	22.28	0.901	17.50	12.97
1.0	12	1.01	3.576	8.47	1.340	22.37	0.906	17.69	13.10
5.0	12	1.49	1.480	7.03	1.350	22.50	0.916	17.99	13.33
10.0	12	1.77	0.978	6.47	1.354	21.68	0.919	17.40	12.89
50.0	12	2.48	0.321	5.51	1.363	21.47	0.928	17.40	12.89
100.0	12	2.73	0.184	5.26	1.366	21.02	0.930	17.04	12.62
1.0	16	0.637	3.460	10.56	1.328	21.08	0.892	16.41	12.16
5.0	16	0.950	1.380	8.73	1.340	21.38	0.902	16.82	12.46
10.0	16	1.11	0.884	8.08	1.342	20.81	0.908	16.44	12.18
50.0	16	1.48	0.265	7.05	1.350	20.93	0.914	16.71	12.38
100.0	16	1.59	0.147	6.00	1.352	20.01	0.915	16.04	11.88

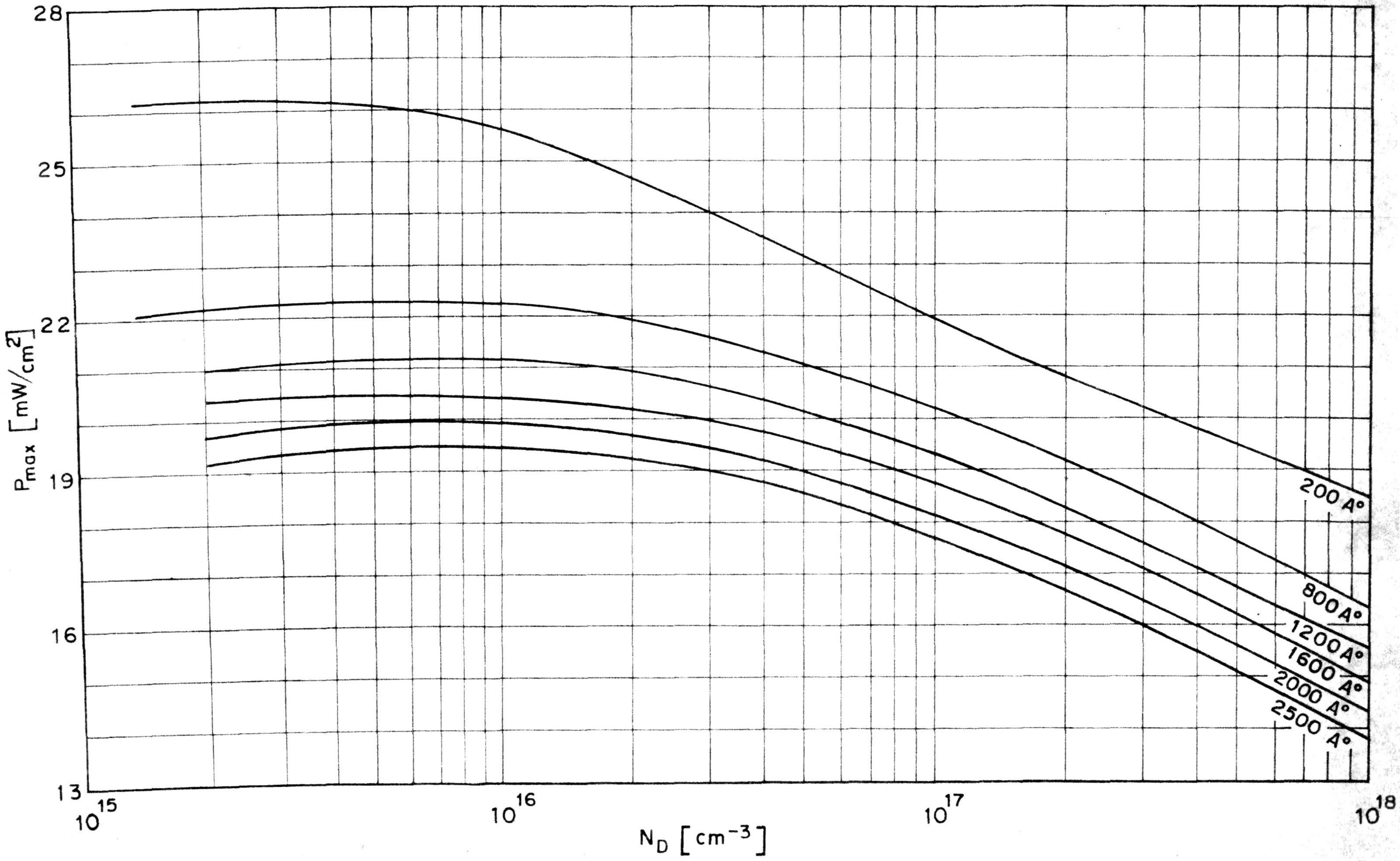

FIG. 2·9. MAXIMUM POWER AS A FUNCTION OF DONOR DENSITY AT DIFFERENT $W_{p(opt)}$ FOR SILICON SOLAR CELL

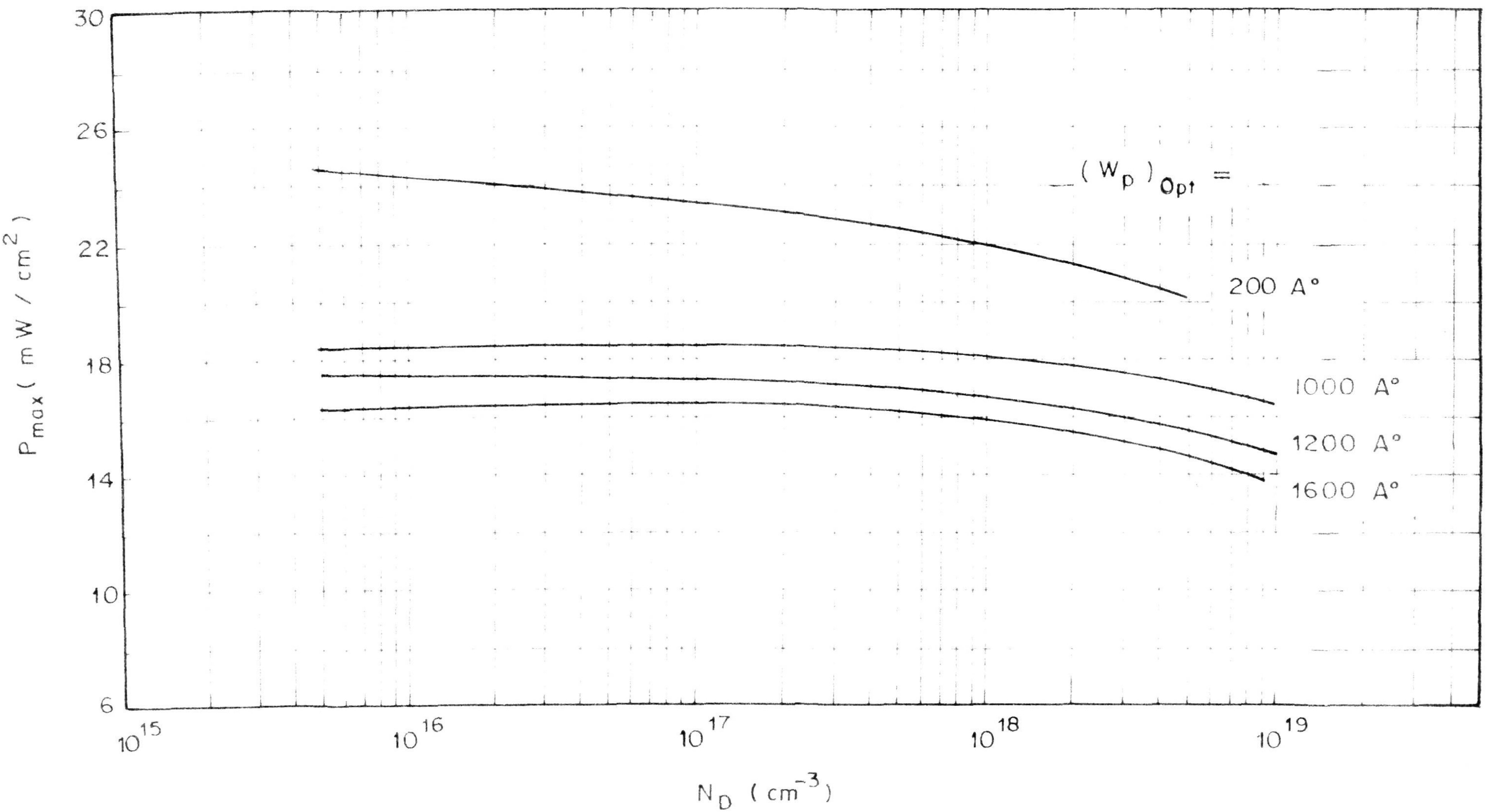

FIG. 2·10. MAXIMUM POWER OUTPUT AS A FUNCTION OF DONOR DENSITY AT DIFFERENT $(W_p)_{Opt}$ FOR GaAs HOMO-JUNCTION SOLAR CELL

similarity is that the short wave length photons can generally be absorbed within or very near the depletion region of the device and this gives a good photoresponse[46,47]. At the same time, the open circuit voltage can be quite high as in a p-n junction without the need to use a carefully controlled interfacial layer.

In order to construct a good heterojunction solar cell, the two materials should have a close lattice match and reasonably close coefficients of thermal expansion. On these considerations, the pairs of materials that can form good cells are given in Table 3[45].

Let us consider two semiconductor materials having the energy gaps E_{g1}, E_{g2}, the electron affinities χ_1 and χ_2, the work functions ϕ_1, ϕ_2 and the dielectric constants ϵ_1 and ϵ_2 respectively. The heterojunction between these materials is shown in Fig. 2-11(a) and 2-11(b).

The difference in energy of the conduction band edges in the two materials is represented by ΔE_c and that in the valence band edges by ΔE_v. In Fig. 2-11(a) the fermi level E_{f_1} is higher than E_{f_2}. When the materials are brought together to form a junction, the fermi levels must attain the same energy by transfer of electrons from semiconductor-1 to semiconductor-2. Due to this transfer

Table 3

Semiconductor Heterojunction pairs with good lattice match conditions

Semiconductor	Preferred doping	Energy gap ev	Electron affinity ev	Dielectric constant (relative)
ZnSe	n	2.67	4.07	9.1
GaAs	p	1.47	4.07	11.1
$Ge_{0.9}$ $Si_{0.1}$	n	0.77	4.11	
Ge	p	0.66	4.13	16.0
GaAs	n	1.47	4.07	11.1
Ge	p	0.66	4.13	16.0
ZnSe	n	2.67	4.07	9.1
Ge	p	0.66	4.13	16.0
AlAs	p	2.15	3.5	10.1
GaAs	n	1.47	4.07	11.1
ZnTe	p	2.26	3.5	10.1
CdSe	n	1.7	4.95	10.0
GaP	n	2.25	4.3	8.4
Si	p	1.11	4.01	11.7
GaSb	n	0.68	4.06	14.8
InAs	p	0.36	4.9	12.5
CdS	n	2.4	4.55	6.7
Cu_2S	p	1.2	4.30	9.0

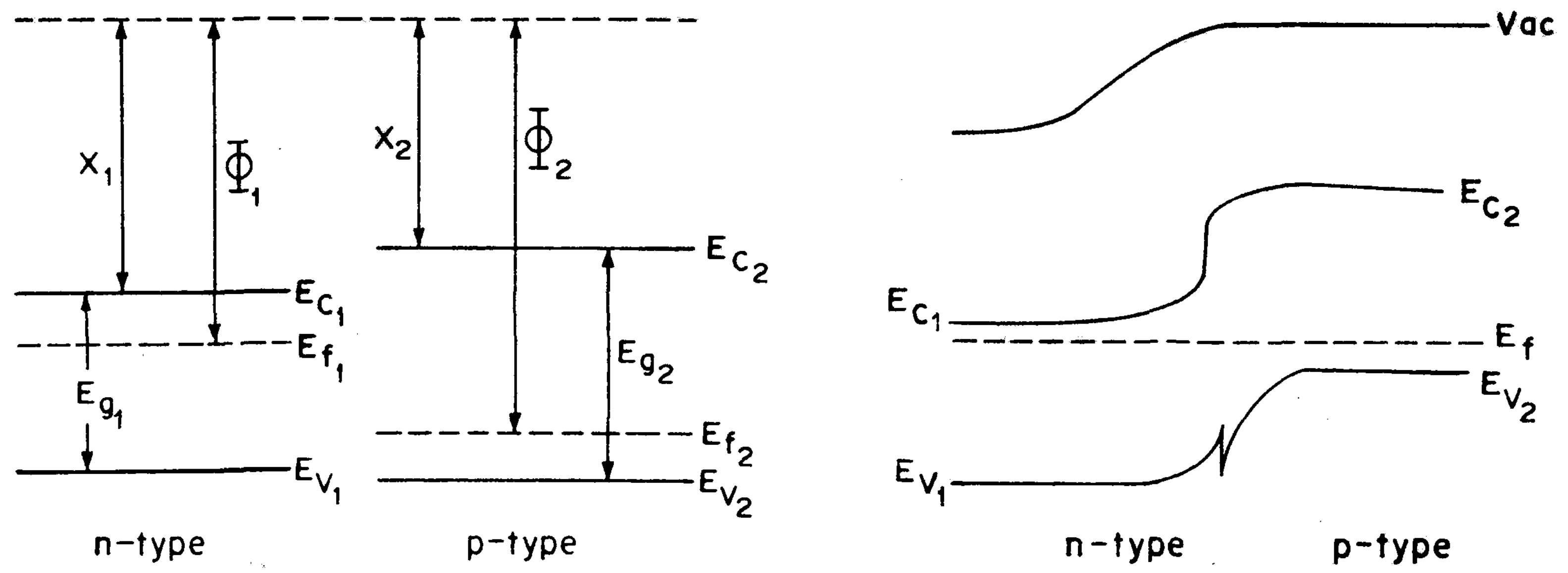

FIG. 2·11. ENERGY BAND DIAGRAM FOR HETEROJUNCTION
(a) n AND p TYPE SEMICONDUCTORS
(b) n/p HETROJUNCTION AFTER EQUILIBRIUM IS ESTABLISHED

of carriers, the band edge in semiconductor-1 bends upward and that in the semiconductor-2 bends downwards[45].

The electrostatic potential difference between any points within any single semiconductor can be represented by the vertical displacement of the band edges between these two points and the electrostatic field can be represented by the slope of the band edges.

The difference in the work functions of the two materials therefore, is the total built-in-voltage, V_D. This is equal to $V_{D_1} + V_{D_2}$ (the sum of the partial built-in voltages), where V_{D_1} and V_{D_2} are the electrostatic potentials supported by semiconductors 1 and 2 respectively.

Thus

$$\phi_2 - \phi_1 = V_{D_1} + V_{D_2} = (\chi_2 + E_{g_2} - \Delta E_2) - (\chi_1 + \Delta E_1) \quad .. \quad 2\text{-}22$$

because

$$\phi_2 = \chi_2 + E_{g_2} - \Delta E_2$$

and $$\phi_1 = \chi_1 + \Delta E_1$$

as can be seen from Fig. 2-11. The electrostatic field is discontinuous at the interface because of the difference in dielectric constants in the two materials[48-50].

As in homojunction, the transition regions are assumed to be completely depleted over the distance w_n and w_p where $w_n/w_p = N_A/N_D$.

Similarly, the expression for ΔE_c and ΔE_v are

$$\Delta E_c = \chi_1 - \chi_2 \quad .. \quad 2\text{-}23$$

$$\Delta E_v = (E_{g_2} - E_{g_1}) - (\chi_1 - \chi_2) \quad .. \quad 2\text{-}24$$

ΔE_v creates a substantial energy spike between the valence bands of junction. Such energy spikes, if large, may limit the hole injection and allow recombination at the interface to dominate the current flow. For most heterojunction pairs, ΔE_c is considerably less than ΔE_v.

In general, in heterojunction solar cells, the smaller of the two energy gaps determine the voltage output that can be achieved from the photocell.

Fig. 2-12(a) and 2-12(b) show a p-n junction under illumination. The short circuit current that can be collected corresponds to the number of photons in the energy range $E_{g_2} - E_{g_1}$. The open circuit voltage is less than the energy gap of the small gap material. The principal advantage of a heterojunction photocell is not basically in the voltage or current performance, but rather in the extent to which the surface recombination losses and sheet resistance losses are reduced because the window effect allows the junction to be placed deeper from the surface than in a homojunction cell.

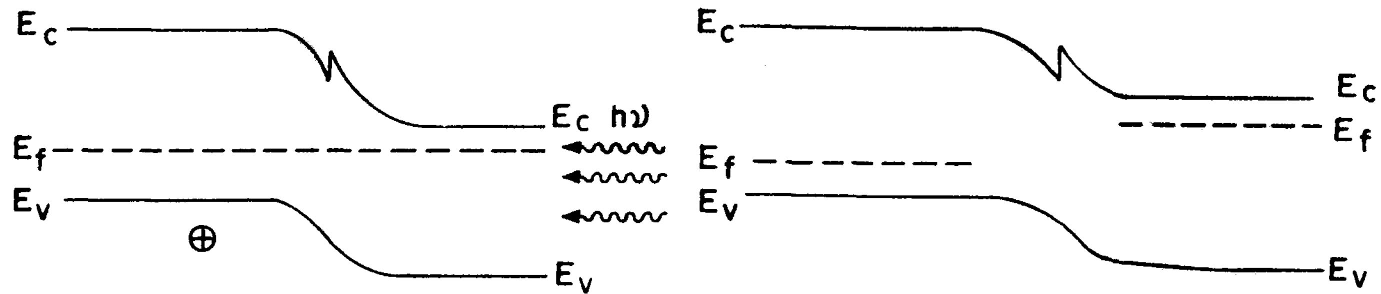

FIG. 2·12. ENERGY BAND DIAGRAM FOR p/n HETEROJUNCTION
(a) BEFORE (b) AFTER ILLUMINATION

The window effect creates a band pass region of sensitivity to photons of energy between E_{g_2} and E_{g_1}. A special feature of a heterojunction is that it allows the formation of junction between semiconductor materials that cannot be doped both 'p' type and 'n' type.

The band structure for a general system of M-p-n heterojunction is shown in Fig. 2-13. Either of the two semiconductors can be selected as p or n depending upon the material properties. This figure shows a large gap n-type over a small gap p-type semiconductor. In view of the kinks in the valence and conduction bands, some assumption have to be imposed in order to make the calculations simpler. The assumptions are $\Delta E_c = 0$ or $\Delta E_v = 0$. The condition $\Delta E_c = 0$ implies that the electron affinities of the semiconductors are equal. The condition $\Delta E_v = 0$ implies that the difference in the electron affinities is equal to the difference in energy gaps of the two semiconductors.

By considering this assumption, there are eight possible combinations. They are (1) high energy gap 'p'/ low energy gap 'n'/metal (2) high energy gap 'n'/low energy gap 'p'/metal (3) low energy gap 'p'/high energy gap 'n'/metal (4) low energy gap 'n'/high energy 'p'/metal, with each assumptions. These possible structures are shown in Figs. 2-14(a) to 2-14(h).

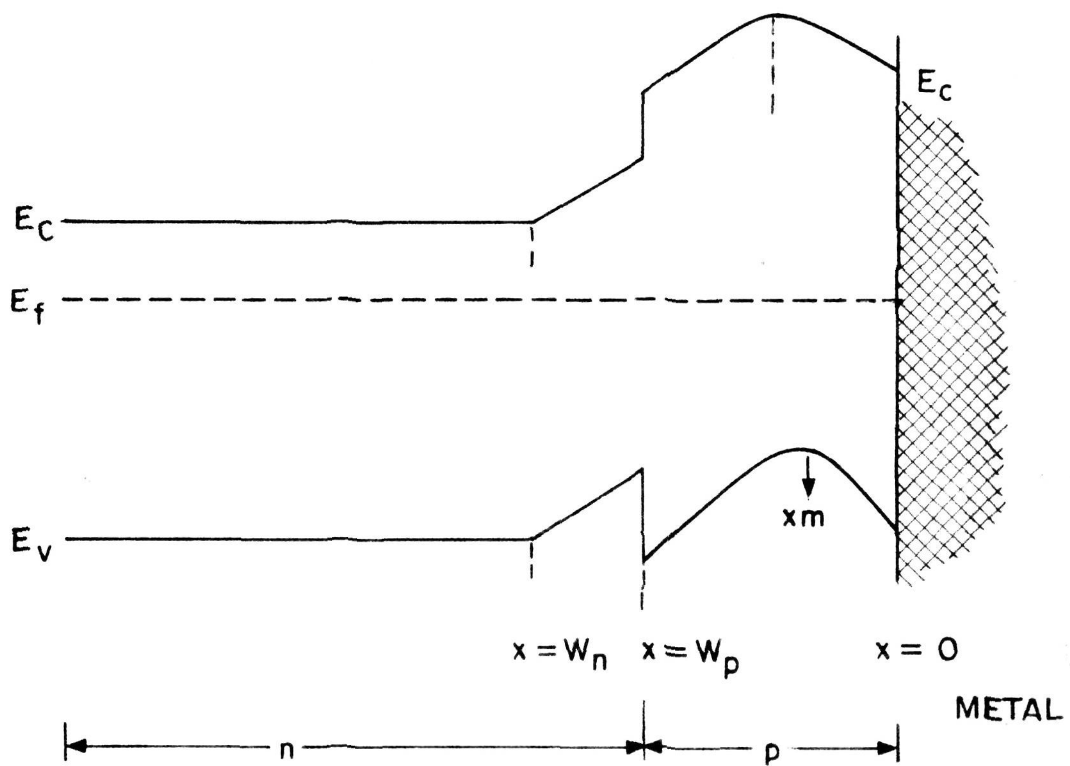

FIG. 2·13. SCHEMATIC ENERGY BAND DIAGRAM OF METAL–p–n–HETEROJUNCTION PHOTO VOLTAIC CELL

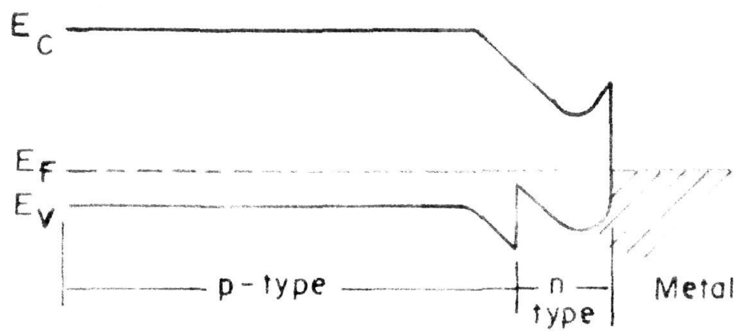

(a) HIGH ENERGY GAP p / LOW ENERGY GAP n / METAL

$\chi_1 = \chi_2$

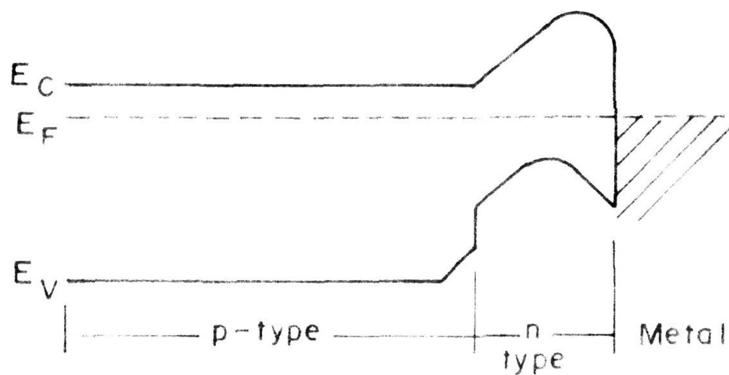

(b) HIGH ENERGY GAP p / LOW ENERGY GAP p / METAL

$\chi_1 = \chi_2$

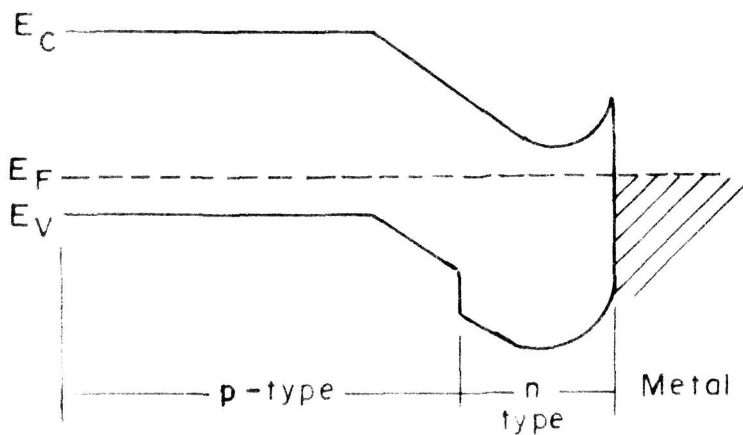

(c) LOW ENERGY GAP p / HIGH ENERGY GAP n / METAL

$\chi_1 = \chi_2$

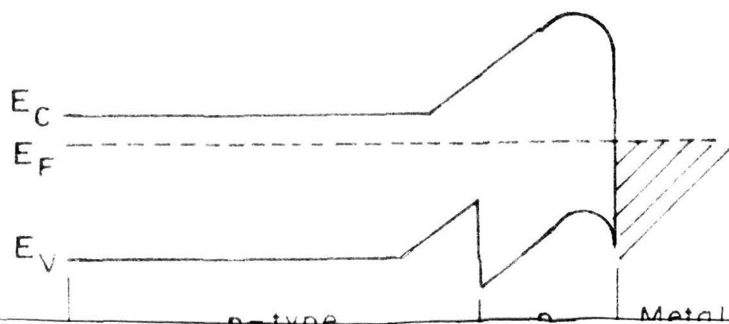

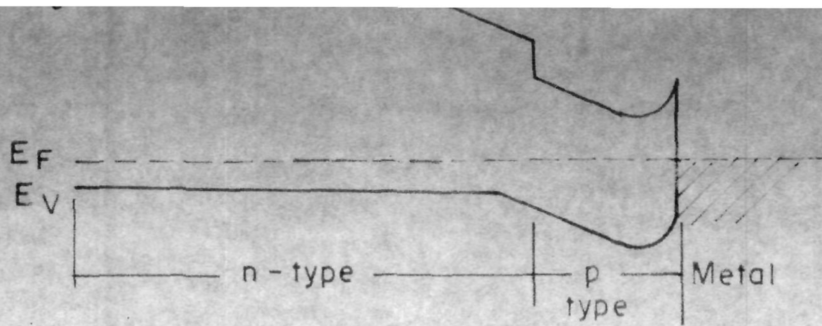

(e) HIGH ENERGY GAP p / LOW ENERGY GAP n / METAL

$\Delta E_V = 0$

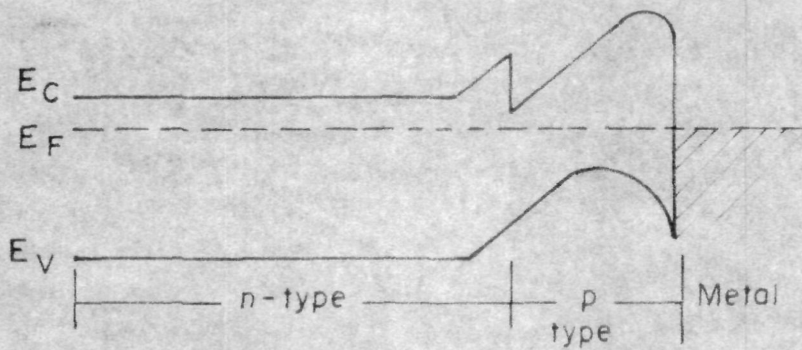

(f) HIGH ENERGY GAP n / LOW ENERGY GAP p / METAL

$\Delta E_V = 0$

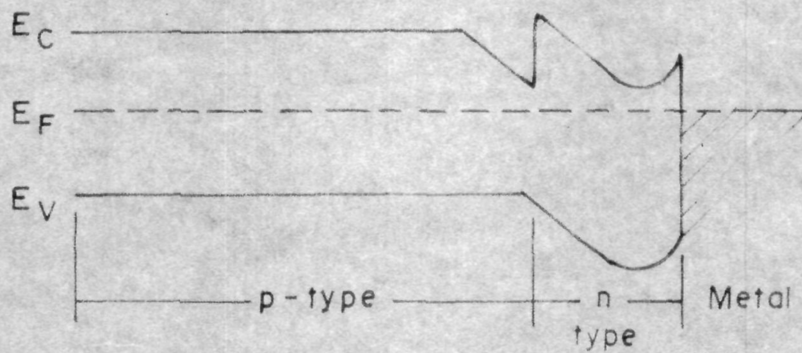

(g) LOW ENERGY GAP p / HIGH ENERGY GAP n / METAL

$\Delta E_V = 0$

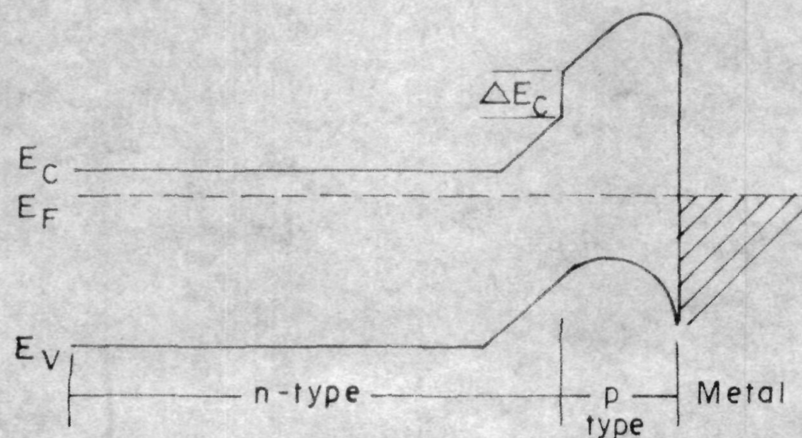

(h) LOW ENERGY GAP n / HIGH ENERGY GAP p / METAL $\Delta E_V = 0$

FIG. 2·14. ENERGY BAND DIAGRAMS OF POSSIBLE M-p-n HETEROJUNCTIONS

For most heterojunction pairs ΔE_c is considerably less than ΔE_v. By selecting n-large/p-small heterojunction, we have the advantage that the electrons which flow into the n-region from the p-base, where a larger part of the photon absorption takes place, are not seriously impeded by the relatively small ΔE_c spike. In case of 'p' large/ 'n' small junction, the relevant spike is ΔE_c and is large, and there would be a more interface recombination.

The second reason for the n-large/p-small choice is that most of the current is caused by the electrons collected as minority carriers from the narrow band gap semiconductors, and the diffusion length of electrons tends to be appreciably more than that of holes.

By considering all these factors, it was decided to examine theoretically the performance of (a) metal-n (large)- p(small) and (b) metal-p (small) -n(large) systems. The band structures for such systems have been shown in Figs. 2-15(a) and 2-15(b) respectively.

The configuration p-GaAs/n-ZnSe/Al is considered as an example for (a) and n-CdS/p-Cu_2S/Au as an example for (b). In either case the higher energy gap material is n-type (CdS or ZnSe). On lines similar to homojunction with necessary modifications in the boundary conditions, the equations for the increase in barrier

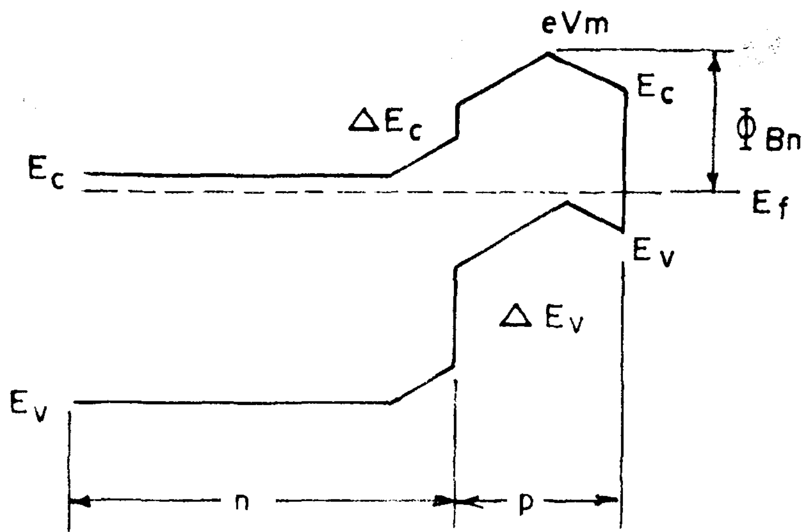

(b)

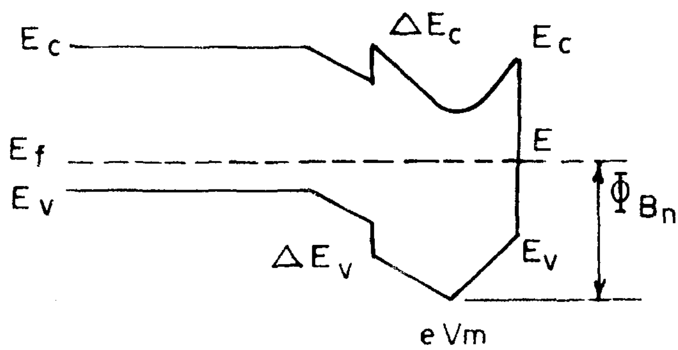

(a)

FIG. 2.15. SCHEMATIC ENERGY BAND DIAGRAM OF
(a) METAL – n (LARGE) – p (SMALL) AND
(b) METAL – p (SMALL) – n (LARGE)
SCHOTTKY BARRIER DIODES

height has been found out as given below. The p-type semiconductor of energy gap E_{g_2} and electron affinity χ_2 has been made to form the Schottky barrier with a metal of work function ϕ_m. In between these two, another n-type semiconductor of energy gap E_{g_1} and electron affinity χ_1 is inserted as shown in Fig. 2-15(a).

As in the case of homojunctions, the layer with doping opposite to the base material is assumed to be completely ionized. The effective barrier height can be written as

$$\phi_{Bp} = (\chi_2 + E_{g_2} - \phi_m) + eV_m \qquad .. \quad 2\text{-}25$$

where V_m is the increase in barrier height. Exactly as in the case of homojunction, the Poisson's equations would be given as

$$\frac{d^2\psi_1}{dx^2} = -\frac{eN_D}{\epsilon_1\epsilon_0} ; \; 0 < x < w_n \qquad .. \quad 2\text{-}26$$

$$\frac{d^2\psi_2}{dx^2} = \frac{eN_A}{\epsilon_0\epsilon_2} ; \; w_n < x < w_p + w_n \qquad .. \quad 2\text{-}27$$

However, here some of the boundary conditions are modified and they are

$$\psi(0) = 0 \quad (a), \quad \psi(w_n+w_p) = \frac{\phi_p-\phi_m}{e} \quad (b),$$

$$\left.\frac{d\psi}{dx}\right|_{w_n+w_p} = 0 \quad (c), \quad \left.\frac{d\psi}{dx}\right|_{x=0} = \frac{eN_D w_n - eN_A w_p}{\epsilon_1 \epsilon_o}.$$

Since the vacuum level is parallel to the band edges, the electrostatic potential difference between any two points, represented by the vertical displacement of the vacuum level between these two points, is continuous. The electrostatic field is discontinuous at the interface due to the difference in dielectric constants in the two materials.

Hence

$$\epsilon_1 \left.\frac{d\psi_1}{dx}\right|_{x=w_n} = \epsilon_2 \left.\frac{d\psi_2}{dx}\right|_{x=w_n} \quad (e).$$

Using these boundary conditions, the relation between w_p and w_n can be obtained by solving the Poisson's equation. By integrating the Poisson's equations,

$$\psi_1(x) = -\frac{eN_D}{\epsilon_1 \epsilon_o}\frac{x^2}{2} + A_1 x + B_1 \quad .. \quad 2\text{-}28$$

$$0 < x < w_n$$

$$\psi_2(x) = \frac{eN_A}{\epsilon_2 \epsilon_o} \frac{x^2}{2} + A_2 x + B_2, \quad w_n < x < w_p + w_n \quad .. \ 2\text{-}29$$

The boundary condition 'a' gives

$$\psi_1(0) = 0 = B_1$$

$$\left.\frac{d\psi(x)}{dx}\right|_{x=0} = A_1 = \frac{eN_D w_n - eN_A w_p}{\epsilon_1 \epsilon_o}$$

In the region $0 < x < w_n$, the potential would be

$$\psi_1(x) = -\frac{eN_D}{\epsilon_1 \epsilon_o} \frac{x^2}{2} + \frac{eN_D w_n - eN_A w_p}{\epsilon_1 \epsilon_o} x \quad .. \ 2\text{-}30$$

In the base region, using the boundary conditions 'c' and 'e'

$$\epsilon_1 \left.\frac{d\psi_1(x)}{dx}\right|_{x=w_n} = \epsilon_2 \left.\frac{d\psi_2}{dx}\right|_{x=w_n}$$

i.e. $$-\frac{eN_D}{\epsilon_o} w_n + \frac{eN_D w_n - eN_A w_p}{\epsilon_o}$$

$$= \frac{eN_A}{\epsilon_o} w_n + A_2 \epsilon_2$$

Therefore $$A_2 = -\frac{eN_A}{\epsilon_2 \epsilon_o} (w_p + w_n)$$

As the potential is continuous

$$\Psi_1(x)\Big|_{x=w_n} = \Psi_2(x)\Big|_{x=w_n}$$

i.e. $$-\frac{eN_D}{\epsilon_1\epsilon_o}\frac{w_n^2}{2} + \frac{eN_D w_n - eN_A w_p}{\epsilon_1\epsilon_o}\, w_n$$

$$= \frac{eN_A}{\epsilon_2\epsilon_o}\frac{w_n^2}{2} - \frac{eN_A}{\epsilon_2\epsilon_o}(w_p+w_n)\, w_n + B_2$$

$$\frac{eN_D}{\epsilon_1\epsilon_o}\frac{w_n^2}{2} - \frac{eN_A}{\epsilon_1\epsilon_o} w_n w_p + \frac{eN_A}{\epsilon_2\epsilon_o}\frac{w_n^2}{2} + \frac{eN_A}{\epsilon_2\epsilon_o} w_n w_p = B_2$$

Hence

$$B_2 = \frac{e}{\epsilon_o}\left\{\frac{N_D}{\epsilon_1} + \frac{N_A}{\epsilon_2}\right\}\frac{w_n^2}{2} + \frac{eN_A}{\epsilon_o}\left\{\frac{1}{\epsilon_2} - \frac{1}{\epsilon_1}\right\} w_n w_p \quad \ldots 2\text{-}31$$

The potential distribution in the base region is

$$\Psi_2(x) = +\frac{eN_A}{\epsilon_2\epsilon_o}\frac{x^2}{2} - \frac{eN_A}{\epsilon_2\epsilon_o}(w_n+w_p)x$$
$$+ \frac{e}{\epsilon_o}\left\{\frac{N_D}{\epsilon_1} + \frac{N_A}{\epsilon_2}\right\}\frac{w_n^2}{2} + \frac{eN_A}{\epsilon_o}\left\{\frac{1}{\epsilon_2} - \frac{1}{\epsilon_1}\right\} w_n w_p \quad \ldots 2\text{-}32$$

The boundary condition 'b' gives

$$\frac{\phi_p - \phi_m}{e} = \frac{eN_A}{\epsilon_2 \epsilon_o} \frac{(w_n+w_p)^2}{2} - \frac{eN_A}{\epsilon_2 \epsilon_o} (w_n+w_p)^2$$

$$+ \frac{e}{\epsilon_o}\left\{\frac{N_D}{\epsilon_1} + \frac{N_A}{\epsilon_2}\right\}\frac{w_n^2}{2} + \frac{eN_A}{\epsilon_o}\left\{\frac{1}{\epsilon_2} - \frac{1}{\epsilon_1}\right\} w_n w_p$$

$$\frac{(\phi_p-\phi_m)}{e} = -\frac{eN_A}{\epsilon_2 \epsilon_o}\frac{(w_n+w_p)^2}{2} + \frac{e}{\epsilon_o}\left\{\frac{N_D}{\epsilon_1} + \frac{N_A}{\epsilon_2}\right\}\frac{w_n^2}{2}$$

$$+ \frac{eN_A}{\epsilon_o}\left\{\frac{1}{\epsilon_2} - \frac{1}{\epsilon_1}\right\} w_n w_p$$

By solving the above equation, the relation between w_n and w_p is got as

$$w_p = -\frac{\epsilon_2}{\epsilon_1} w_n + \left\{\frac{\epsilon_2^2}{\epsilon_1^2} w_n^2 + \frac{\epsilon_2}{\epsilon_1}\frac{N_D}{N_A} w_n^2 + \frac{2\epsilon_2 \epsilon_o}{eN_A} + \frac{\phi_p - \phi_m}{e}\right\}^{1/2} \quad \ldots \text{ 2-33}$$

At the maximum potential,

$$\frac{d\psi_1}{dx} = 0$$

so,

$$-\frac{eN_D}{\epsilon_1 \epsilon_o} \cdot x_m + \frac{eN_D w_n - eN_A w_p}{\epsilon_1 \epsilon_o} = 0$$

$$x_m = w_n - \frac{N_A}{N_D} w_p \qquad .. \qquad 2\text{-}34$$

At this distance (x_m), the maximum potential occurs. This implies that the maximum potential would occur in the thin layer inserted in between the metal and the base semiconductor. Hence the maximum potential

$$V_m = -\frac{eN_D}{\epsilon_1 \epsilon_o} \frac{\left\{ w_n - \frac{N_A}{N_D} w_p \right\}^2}{2} + \frac{e(N_D w_n - N_A w_p)}{\epsilon_1 \epsilon_o} \; w_n - \frac{N_A}{N_D} w_p$$

$$= -\frac{e}{\epsilon_1 \epsilon_o} \frac{\left(N_D w_n - N_A w_p\right)^2}{2N_D} + \frac{e}{\epsilon_1 \epsilon_o} \frac{(N_D w_n - N_A w_p)^2}{N_D}$$

or,

$$V_m = \frac{e}{\epsilon_1 \epsilon_o} \cdot \frac{(N_D w_n - N_A w_p)^2}{2N_D} \qquad .. \qquad 2\text{-}35$$

Hence the effective barrier height is

$$(\phi_B) = E_{g_2} + \chi_2 - \phi_m + eV_m \qquad .. \qquad 2\text{-}36$$

In similar way to homojunction, the photogenerated current in these type cells has been calculated by assuming the region $x = 0$ to $x = x_m$ as dead layer.

Here, the photogenerated current can be divided into three terms (1) photocurrent from the depletion region of top layer (2) photocurrent from the depletion region of base layer and (3) photocurrent from the remaining part of the base layer.

The rate of electron-hole pair generation in the top layer is

$$g\,(x) = \alpha_1 N \;\exp\,(-\alpha_1 x)$$

Hence the photocurrent in the top layer can be written as

$$J_{dr_1} = eN\left\{\exp\,(\alpha_1\, x_m) - \exp\,\left(-\alpha_1\,(w_n - x_m)\right)\right\} \quad .. \; 2\text{-}37$$

and the rate of electron hole pair generation in the base layer is

$$g(x') = \alpha_2 N \;\exp\left\{-\alpha_1\,(w_n - x_m)\right\}\;\exp\,(-\alpha_2 x') \quad .. \; 2\text{-}38$$

Hence the photocurrent from the depletion region as well as from the base region is obtained as

$$J_{dr_2} = eN \;\exp\left\{-\alpha_1\,(w_n - x_m)\right\}\;[1 - \exp\,(-\alpha_2 w_p)] \quad .. \; 2\text{-}39$$

and

$$J_{diff.} = \frac{eN\,\alpha_2 L_n}{1+\alpha_2 L_n}\;\exp\left\{-\alpha_1 (w_n - x_m)\right\}\exp\,(-\alpha_2 w_p) \quad .. \; 2\text{-}40$$

Hence the total photocurrent at a wave length λ is

$$J_1(\lambda) = eN\left[\exp(-\alpha_1 x_m) - \frac{\exp\{-\alpha_1(w_n - x_m)\}\exp(-\alpha_2 w_p)}{1+\alpha_2 L_n}\right] \quad \ldots 2\text{-}41$$

Thus the total photogenerated current under illumination can be calculated using the equation 2-20 and the results obtained are shown in Tables 4 and 5.

Results and Discussion

The values for various constants used are given as, for CdS, $\epsilon_s = 6.7$, $\chi_s = 4.55$ ev and $E_g = 2.4$ ev, for Cu_2S, $\epsilon_s = 9.0$, $\chi_s = 4.3$ ev and $E_g = 1.2$ ev, for ZnSe, $\epsilon_s = 9.1$, $\chi_s = 4.07$ ev and $E_g = 2.67$ ev and for GaAs, same as used in homojunction cells.

By varying the values of N_A, N_D and w_n (or w_p), the corresponding values of w_p (or w_n) have been calculated for M-n-p o M-p-n heterostructures with the help of the equations 2-33, 2-34, 2-35 and 2-36 and corresponding barrier height was obtained. These values are shown in the Table 4 and 5. The absorption coefficient $\alpha(\lambda)$ values for CdS, Cu_2S and ZnSe have been taken from Bube[51] and Thomas[52].

Table 4

Au/p-Cu_2S/n-CdS (hetero) Schottky barrier solar cell calculated under AM0 illumination.

N_D $\times 10^{16}$ cm^{-3}	w_p $\times 10^{-6}$cm	N_A $\times 10^{17}$ cm^{-3}	w_n $\times 10^{-5}$cm	x_m $\times 10^{-6}$cm	$(\phi_{Bn})_{max}$ ev	J_{sc} mA/cm^2	V_{oc} volt	P_{max} mW/cm^2	η %
0.5	2	7.46	3.19	1.781	0.888	30.71	0.463	11.25	8.33
1.0	2	8.12	2.28	1.710	0.890	30.79	0.464	11.34	8.4
5.0	2	10.8	1.04	1.510	0.898	30.96	0.473	11.63	8.6
10.0	2	12.6	0.74	1.410	0.901	30.76	0.476	11.64	8.62
50.0	2	19.4	0.32	1.160	0.914	30.89	0.488	12.07	8.94
100.0	2	23.6	0.25	1.06	0.919	29.00	0.492	11.42	8.46
0.5	4	1.96	3.090	3.212	0.853	26.81	0.424	8.51	6.3
1.0	4	2.26	2.20	3.02	0.857	28.35	0.429	9.50	7.03
5.0	4	3.37	0.988	2.53	0.867	27.81	0.439	9.57	7.09
10.0	4	4.1	0.688	2.325	0.873	27.75	0.445	9.70	7.19
50.0	4	6.54	0.276	1.889	0.884	28.24	0.456	10.17	7.53
100.0	4	7.89	0.178	1.740	0.890	26.12	0.460	9.51	7.04

contd....

Table 4 (contd.)

0.5	8	0.576	2.950	5.44	0.821	17.49	0.381	5.07	3.75
1.0	8	0.698	2.083	5.01	0.826	18.08	0.387	5.35	3.96
5.0	8	1.12	0.884	4.08	0.839	18.93	0.400	5.84	4.32
10.0	8	1.39	0.591	3.734	0.844	18.48	0.405	5.78	4.28
50.0	8	2.09	0.204	3.127	0.854	18.67	0.416	6.04	4.47
100.0	8	2.375	0.119	2.96	0.858	15.39	0.414	4.94	3.66
0.5	10	0.397	2.887	6.366	0.811	15.97	0.369	4.45	3.3
1.0	10	0.487	2.075	5.840	0.817	16.70	0.375	4.76	3.52
5.0	10	0.796	0.836	4.74	0.827	17.77	0.389	5.29	3.91
10.0	10	0.97	0.548	4.35	0.835	17.44	0.394	5.27	3.90
50.0	10	1.404	0.177	3.71	0.844	17.71	0.404	5.52	4.08
100.0	10	1.56	0.101	3.55	0.847	14.63	0.402	4.53	3.35

Table 5

Al/n-ZnSe/p-GaAs (hetero) Schottky barrier solar cell calculated under AMO illumination

N_A $\times10^{16}cm^{-3}$	w_n $\times10^{-6}$ cm	N_D $\times10^{17}cm^{-3}$	w_p $\times10^{-5}cm$	x_m $\times10^{-6}cm$	$(\phi_{Bn})_{max}$ ev	J_{sc} mA/cm^2	V_{oc} volt	P_{max} mW/cm^2	η %
0.5	2	14.76	5.45	1.81	1.422	36.63	1.001	32.34	23.95
1.0	2	15.85	3.88	1.75	1.425	36.60	1.003	32.38	23.98
5.0	2	20.10	1.75	1.56	1.430	36.47	1.009	32.48	24.05
10.0	2	23.1	1.23	1.46	1.433	36.27	1.012	32.40	24.00
50.0	2	34.0	0.53	1.22	1.442	36.05	1.020	32.52	24.08
100.0	2	40.9	0.36	1.11	1.447	35.52	1.025	32.19	23.84
0.5	6	1.98	5.26	4.67	1.369	35.53	0.946	29.49	21.84
1.0	6	2.28	3.72	4.37	1.372	34.84	0.950	29.02	21.49
5.0	6	3.38	1.60	3.63	1.382	34.73	0.959	29.26	21.67
10.0	6	4.08	1.09	3.325	1.387	34.77	0.965	29.47	21.82
50.0	6	6.17	0.403	2.74	1.399	34.24	0.975	29.38	21.76
100.0	6	7.14	0.25	2.55	1.402	33.01	0.978	28.42	21.05

contd....

Table 5 (contd.)

0.5	8	1.22	5.18	5.87	1.355	34.95	0.933	28.53	21.13
1.0	8	1.43	3.64	5.45	1.360	33.95	0.936	27.88	20.61
5.0	8	2.17	1.53	4.47	1.370	33.78	0.947	28.05	20.77
10.0	8	2.62	1.022	4.09	1.375	33.87	0.952	28.24	20.91
50.0	8	3.84	0.357	3.42	1.386	33.05	0.962	27.34	20.69
100.0	8	4.32	0.206	3.24	1.389	31.39	0.964	26.88	19.91
0.5	12	0.628	5.034	7.995	1.338	31.82	0.913	25.38	18.8
1.0	12	0.752	3.49	7.354	1.343	31.39	0.918	25.18	18.65
5.0	12	1.16	1.394	5.998	1.355	29.77	0.928	24.16	17.89
10.0	12	1.38	0.896	5.525	1.359	27.83	0.931	22.68	16.8
50.0	12	1.89	0.274	4.78	1.367	25.61	0.937	21.01	15.56
100.0	12	2.05	0.151	3.92	1.369	22.08	0.935	18.07	13.38
0.5	16	0.399	4.885	9.88	1.327	29.65	0.900	23.2	17.18
0.1	16	0.482	3.346	9.05	1.333	28.47	0.906	22.90	16.96
5.0	16	0.739	1.268	9.41	1.342	26.60	0.913	21.22	15.71
10.0	16	0.864	0.788	6.84	1.317	29.09	0.914	19.24	14.25
50.0	16	1.10	0.219	6.13	1.353	21.33	0.918	17.11	12.67
100.0	16	1.17	0.118	5.97	1.355	17.52	0.914	13.90	10.29

As it has been seen in the case of homojunctions, the effective barrier height $(\phi_{Bn})_{max.}$ increases as the thickness of the intermediate layer (i.e. either 'p' or 'n' layer) increases upto a certain thickness and it attains a maximum which is less than the band gap of the semiconductor.

In case of n-CdS/p-Cu_2S/Au configuration , the $(\phi_{Bn})_{max.}$ and the corresponding $(w_p)_{opt.}$ values for different N_A and N_D concentrations are shown in Fig. 2-16 and for p-GaAs/n-ZnSe/Al in Fig. 2-17. It is clear from the above graphs that the effective barrier height (ϕ_{Bn}) increases with the decrease in the thickness of the intermediate layer. However the $(\phi_{Bn})_{max.}$ remains constant at a given concentration of the intermediate layer which is parallel to the earlier observations in case of the homo-junction M-p-n configurations. Thus, in order to obtain the maximum effective barrier height one can select the donor and acceptor concentrations by choosing appropriate thickness of the intermediate layer from the N_A-N_D contours.

The characteristics of the photovoltaic solar cell have been computed by using the expressions 2-41, 2-21 and 2-16 after seeing the behaviour of $(\phi_{Bn})_{max.}$ and these values are also given in Tables 4 and 5. Figure 2-18 shows the maximum power (P_{max}) delivered by the solar cell (n-CdS/p-Cu_2S/Au) as a function of the dopant concentration in the base

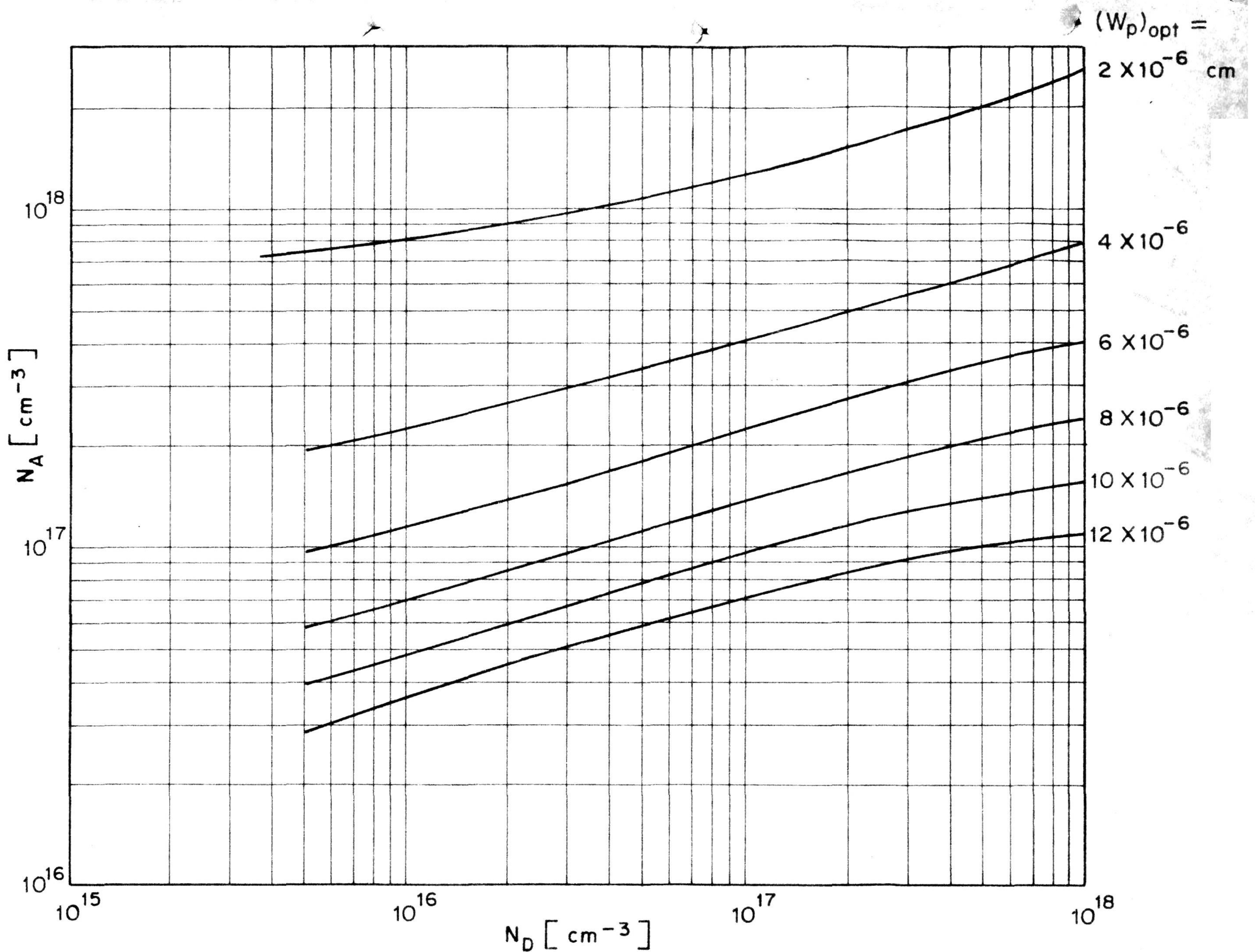

FIG. 2·16. $(W_P)_{opt}$ AS A FUNCTION OF DONOR AND ACEPTOR DENSITIES (N_D AND N_A) IN n-Cds/P·Cu_2S/METAL

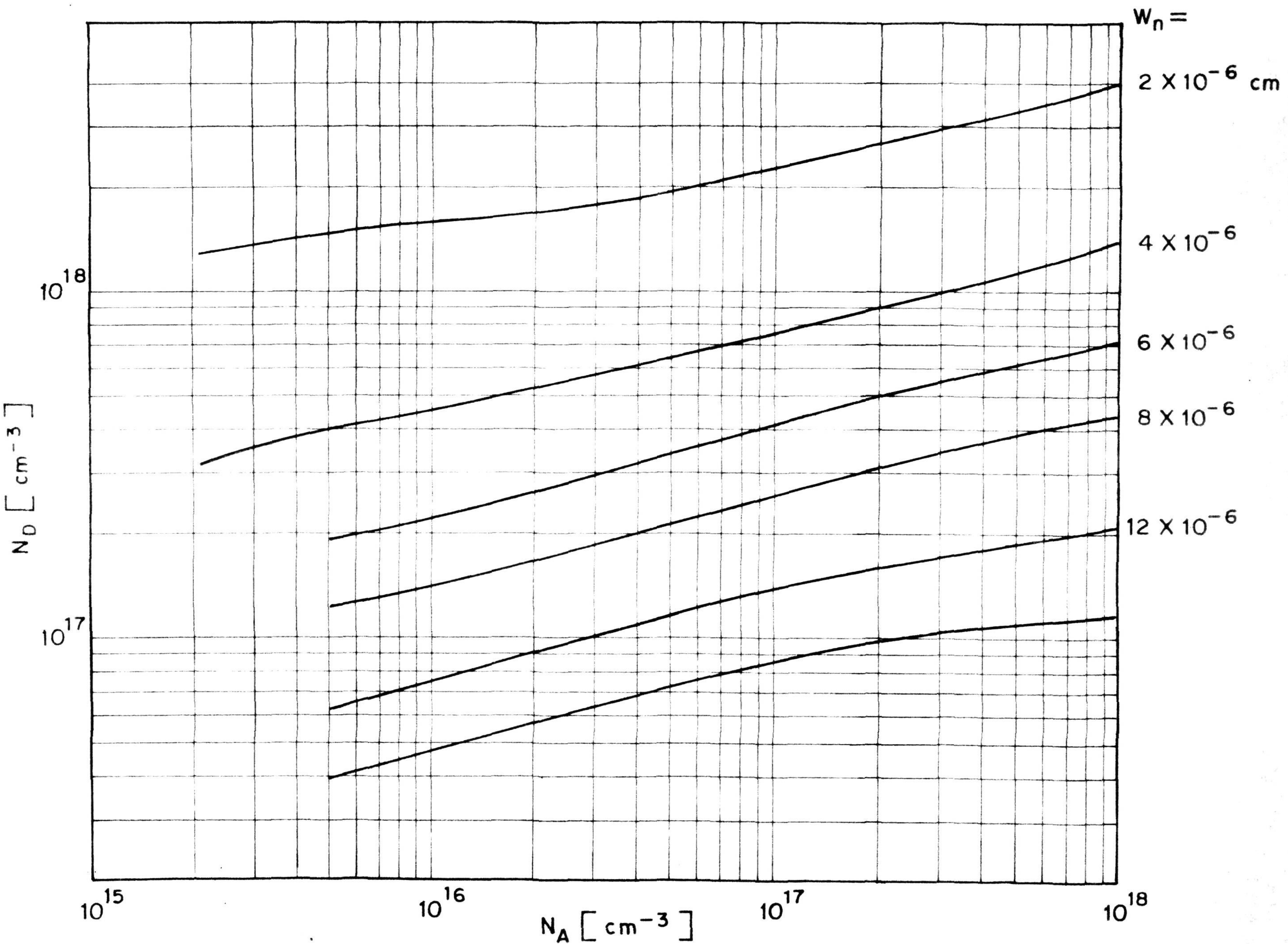

FIG. 2·17. $(W_n)_{opt}$ AS A FUNCTION OF ACEPTOR AND DONOR DENSITIES (N_A AND N_D) IN pGaAs/n-ZnSe/METAL (ALUMINIUM)

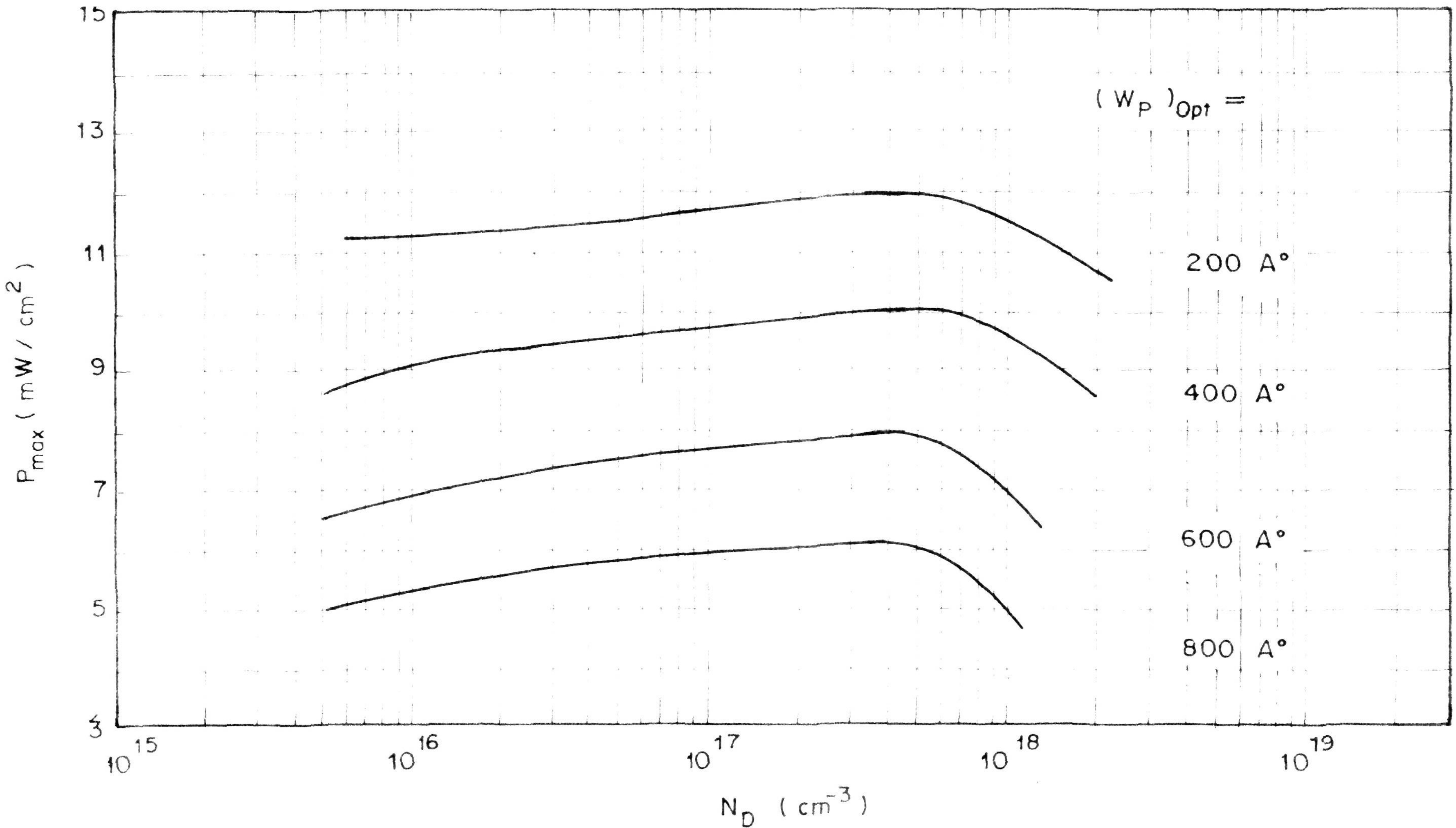

FIG. 2·18. MAXIMUM POWER OUTPUT AS A FUNCTION OF DONOR DENSITY AT DIFFERENT $(W_P)_{Opt}$ FOR n-CdS / p-Cu_2S / Au CELL

semiconductor. As is seen, for a given thickness of the intermediate layer, the $P_{max.}$ increases with the concentration of the base layer and remains constant in the range of $5x10^{16}$-$5x10^{17}$ cm^{-3} beyond which it decreases slowly. The same kind of behaviour is observed in case of p-GaAs/n-ZnSe/Al and is shown in Fig. 2-19.

Thus it has been shown theoretically that these configurations have a good prospect of delivering maximum power output by choosing the appropriate values of N_D, N_A and the intermediate layer thickness.

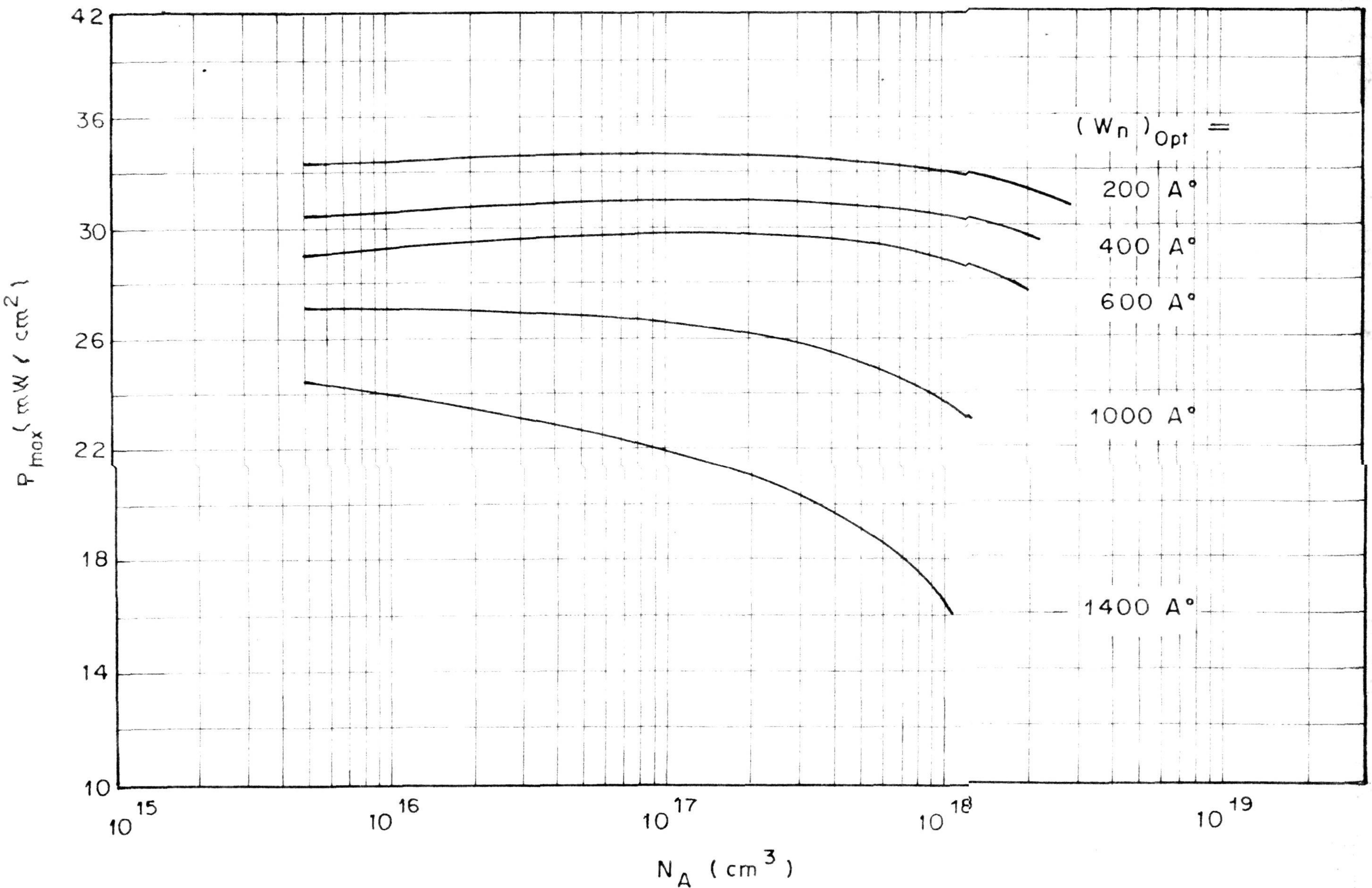

FIG. 2·19. MAXIMUM POWER OUTPUT AS A FUNCTION OF ACCEPTOR DENSITY AT DIFFENT $(W_n)_{Opt}$ FOR p-GaAs / n-ZnSe / Al CELL

References

1. W.A. Anderson and A.E. Delahoy, Proc.IEEE, 60, 1457 (1972).
2. W.A. Anderson and A.E. Delahoy, Proc. 8th IECEC, 326-330, (1973).
3. R.J. Stirn and Y.C.M. Yeh, Appl.Phys.Lett., 27, 95 (1975).
4. W.A. Anderson, A.E. Delahoy and R.A. Milano, J.Appl.Phys., 45, 3913 (1974).
5. M.A. Green, Appl.Phys.Lett., 27, 287 (1975).
6. W.A. Anderson and A.E. Delahoy, Proc. IEEE, 63, 206 (1975).
7. M. Wolf, Energy Conv., 11, 63 (1971).
8. P. Rappaport and J.J. Wysocki, Acta Electron, 5, 364 (1961).
9. J.A. Baicker and B.W. Faughnam, J.Appl.Phys., 33, 3271 (1962).
10. J. Lindmayer and J.F. Allison, COMSAT.Tech.Rev., 3, 1 (1973).
11. M.S. Bae,and R.V.D'Aiello, Appl.Phys.Lett., 31, 285 (1977)
12. D.L. Pulfrey and R.F. McOuat, Appl.Phys.Lett., 24, 167 (1974).
13. B. Pellegrini, J.Phys.D.Appl.Phys., 9, 55 (1976).
14. W.A. Anderson, A.E. Delahoy and R.A. Milano, J.Appl.Phys., 45, 3913 (1974).
15. J.G. Fassum, Solid State Electron., 19, 269 (1976).
16. S.J. Fonash, J.Appl.Phys., 46, 1286 (1975).
17. S.J. Fonash, Thin Solid Films, 36, 387 (1976).
18. H.C. Card and E.S. Yang, Appl.Phys.Lett., 29, 51 (1976).
19. S.J. Fonash, J.Appl.Phys., 47, 3597 (1976).
20. S.J. Fonash, Proc. 11th IEEE Photo.Spec.Conf., p.376 (1975).

21. H.C. Card and E.H. Rhoderick, J.Phys.D., 4, 1589 (1971).

22. E. Fabre, Appl.Phys.Lett., 29, 607 (1976).

23. R.J. Stirn and Y.C.M. Yeh, Appl.Phys.Lett., 27, 95 (1975).

24. E.J.E. Charlson and J.C. Lieu, J.Appl.Phys., 46, 3982 (1975).

25. D.R. Lillington and W.G. Townsend, Appl.Phys.Lett., 28, 97 (1976).

26. M.A. Green and R.B. Godfrey, Appl.Phys.Lett., 29, 610 (1976).

27. S. Shevenock, S. Fonash and J. Geneczko, International Electron.Devices, 1975 Meeting, Washington, D.C., p.211 (Unpublished).

28. H.K. Henisch, Rectifying Semiconductor Contacts, (Oxford Claredon Press, 1957).

29. J.M. Shannon, Appl.Phys.Lett., 24, 369 (1974).

30. J.M. Shannon, Appl.Phys.Lett., 25, 75 (1974).

31. J.M. Shannon, Appl. Solid State Electron, 19, 537 (1976).

32. Y.P. Pai, H.C. Lin, M. Peckarar and R.L. Kocher, Proc. IEDM, 40 (1976).

33. A. Vander Ziel, Solid State Electron., 20, 269 (1977).

34. S.S. Li, Solid State Electron., 21, 435 (1978).

35. G.S.R. Krishna Murthy and A.P.B. Sinha, Pramāna, 13, 39 (1979).

36. S.M. Sze, Physics of Semiconductor Devices, (John-Wiley and Sons, New York, 1969).

37. R.J. Handy, Solid State Electron., 10, 765 (1967).

38. H.J. Hovel, Semiconductors and Semimetals, Vol.11, 'Solar cells', (Academic Press, New York, 1975).

39. H.F. Wolf, Silicon Semiconductor Data, (Pergamon Press, Oxford, 1969).

40. J.J. Loferski, Proc. IEEE 11, 63 (1971).

41. M.P. Thekaekara, Opt.Spectra, 6, 32 (1972).

42. L.W. James and R.L. Moon, Appl.Phys.Lett., 26, 467 (1975).

43. L.W. James and R.L. Moon, 11th IEEE.Photovoltaic Spec. Conf., p.402 (IEEE, New York, May 1975).

44. H.J. Hovel and J.M. Woodall, Appl.Phys.Lett., 26, 467 (1975).

45. A.G. Milnes and D.L. Feucht, Heterojunctions and Metal-semiconductor Junctions (Academic Press, 1972).

46. B. Agusta, A. Lopez and R.L. Anderson, IEEE.Trans.Electron.Devices, ED-11, 533 (1964).

47. J.P. Donnelly and A.G. Milnes, Int.J.Electronics, 20, 295 (1966).

48. R.L. Anderson, IBM.J.Res.Develop., 4, 283 (1960).

49. R.L. Anderson, Proc.Int.Conf.Semicond., Prague, (Czech.Acad.Sci., 1960), p.563.

50. R.L. Anderson, Solid State Electron., 5, 341 (1962).

51. R.H. Bube, Photoconductivity of Solids, (John-Wiley and Sons, New York, 1960).

52. D.G. Thomas, II-VI Semiconducting Compounds, (W.A. Benjamin, Inc., New York, 1967).

CHAPTER III

THEORETICAL PERFORMANCE OF BACK-ILLUMINATED THIN FILM MIS SCHOTTKY BARRIER SOLAR CELLS

3.1 Introduction

In the Schottky cells that have been discussed in the last chapter, light first falls on the metal surface and then proceeds to the semiconductor through the Schottky junction[1-10]. Such cells are known as front wall cells. Under suitable conditions it is possible to improve the performance of the Schottky cells by allowing light to fall in the reverse direction i.e. first on the semiconductor through the back electrode. Such cells are known as 'back wall cells'[11,12].

As discussed in the last chapter, Schottky barrier (SB) solar cells have a number of advantages over their p-n junction counterparts[13,14]. Potentially they have lower cost of fabrication, lower series resistance, greater blue response and higher radiation resistance[15-17]. However, relatively less attention has been paid so far to the analysis and development of these cells[18-22]. The main reason is perhaps the fact that the fabrication of the present day SB cells are generally front-wall type, having a rectifying metallic contact at the front and an ohmic contact at the back, the fabrication of which is rather difficult. The front metallic film has to provide a good contact to the external circuit, a good optical matching for maximum transmission of the incident solar radiations[23-25].

and a high potential barrier with the semiconductor. The simultaneous satisfaction of all these criteria requires sophisticated control techniques, raising the cost of the front wall SB cells. This difficulty may be partly eliminated in case of back-wall SB cell which has an ohmic contact at the front surface and a rectifying metallic contact at the back[26]. The chief advantage of this type of cell would be that no optical matching is required for the metallic contact, which can now be made sufficiently thick and selected properly for providing a large potential barrier with the semiconductor. Further, this type of back wall SB cell would be easily amenable to any subsequent heat treatment, which is sometimes found helpful for enhancing the potential barrier through the controlled growth of an oxide layer at the metal-semiconductor interface (MIS)[27-33]. However, the maximum conversion efficiency of a back wall SB cell is potentially lower than that of a front wall one. In the front-wall cells both volume and surface recombination losses are negligible since most of the carriers are generated in the depletion region while this is not so for the back-wall cells. The presence of an interfacial layer at the junction, however. can lead to fairly high efficiencies (η) [27-33]. Furthermore, light is absorbed directly after penetrating through the window and is not partially lost in other semiconducting layers (collector and junction) as is the case in the back-wall cells. Nevertheless the ease of fabrication and other

possible advantages of back wall MIS SB cell warrants a deeper investigation.

In case of the back wall cell, light penetrates through collector and junction before it is absorbed in the emitter. This requires a very thin collector layer if made of the same basic material or preferably, a wider band gap collector, acting as window for most of the spectrum of the impinging light.

Collector doping (to provide sufficient conductivity) and thickness need to be optimized to minimize optical and series resistance losses.

Consider a n-type semiconductor coupled with a metal having an interfacial insulator layer of thickness δ. Several recent experimental[27-33] as well as theoretical papers indicate that the addition of such an interfacial layer improves solar cell performances. A Schottky diode retains its essential characteristics even when a thin insulator layer is introduced, provided that the thickness of the layer does not exceed about 10 Å or so.

For the MIS solar cell under illumination, the open-circuit voltage V_{oc} is given by[34]

$$V_{oc} = \frac{nkT}{e}\left\{\ln \frac{J_{sc}}{J_o} + \chi^{1/2}\,\delta\right\} \quad \cdots \quad 3\text{-}1$$

where $J_o = A^* T^2 \exp\left(-\frac{e\phi_B}{kT}\right)$

The barrier height, ϕ_B is given by[5]

$$\phi_B = \frac{1}{n}(\phi_B - \chi_s) + (1 - \frac{1}{n})\phi_o \qquad .. \quad 3\text{-}2$$

where $n = 1 + \frac{e\delta D_s}{\epsilon_1 \epsilon_o}$

In a recent paper, Basu and Saha[26] have studied the possible performance of back wall SB cells. They have assumed that the effect of tunnelling through the barrier is negligible and that the generation-recombination in the depletion region may be ignored, consequently J_o turns out to be quite large and V_{oc} too low leading to comparatively low values of η . In a subsequent paper[35], calculations have been made for both Si and GaAs cells and the variation of V_{oc} and η studied as a function of the thickness of the interfacial layer δ. It is concluded that efficiencies of 15% and 7% may be reached for the GaAs and Si cells with ϕ_B = 0.8 and 0.7 ev respectively in presence of a suitable interfacial layer.

Similarly Soukup and Akers[36] have done calculations for GaAs thin film MIS back wall cells and compared the performance with that of bulk single crystal cells. Here again, the effect of depletion region has not been considered.

3.2 Back illuminated solar cell

The purpose of the present investigation is to examine critically the possible performance of the back wall thin film MIS Schottky barrier solar cell in a mere general way without making the above-mentioned assumptions[37].

In order to compare the performance of the back illuminated solar cell with the front illuminated one, it is assumed that both these cells have identical properties. Earlier calculations have been made on certain assumptions which do not hold in actual practice, such as treating the surface recombination velocity as zero or neglecting the presence of a depletion region in the semiconductor at the semiconductor-insulator interface.

The schematic diagram of a back wall illuminated MIS Schottky barrier solar cell has been shown in Fig. 3-1. As the Schottky metal is sufficiently thick, it can be assumed to be totally reflective to the photons. This cell consists of two regions, designated as region 1 and the depletion region, $d-w_n < x < d$ as region 2 near the interface between the semiconductor and the insulator. Here d is thickness of the cell and w_n is the width of the depletion region.

It is assumed that the incident radiation is absorbed uniformly throughout the regions 1 and 2 and as the

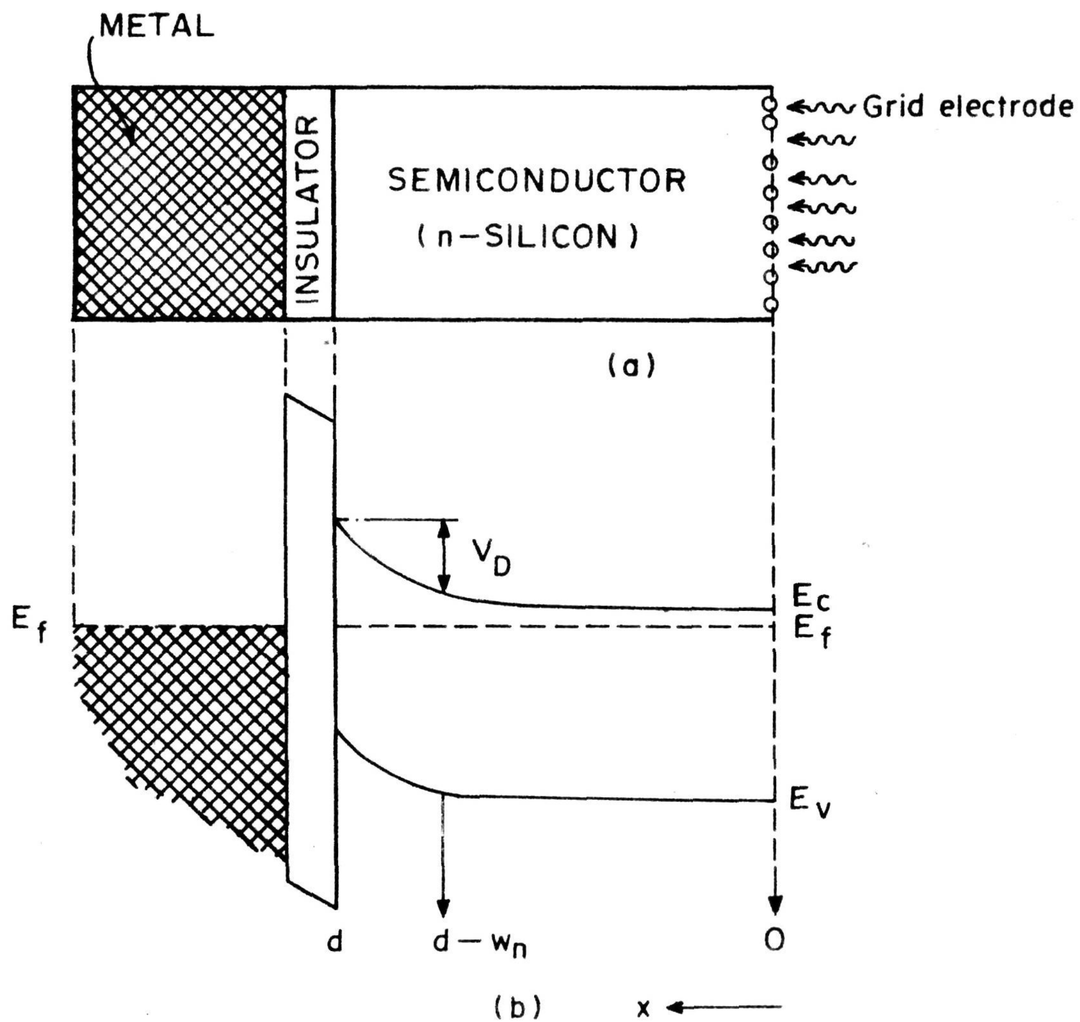

FIG. 3.1.

BACK-ILLUMINATED MIS SCHOTTKY BARRIER SOLARCELL

(a) CROSS-SECTIONAL VIEW OF THE CELL

(b) ENERGY DIAGRAM

semiconductor-insulator interface is reflective, the optical hole-electron generation rate consists of two terms[38], (i) $\alpha N \exp(-\alpha x)$ and (ii) $\alpha N \exp\{(2d-x)(-\alpha)\}$ where α and N are functions of λ. Therefore, the electron-hole pair generation rate,

$$g(x, \lambda) = \alpha N \left[\exp(-\alpha x) + \exp\{(2d-x)(-\alpha)\}\right] \quad .. \; 3\text{-}3$$

Then the steady state continuity equation is,

$$\frac{d^2\Delta p}{dx^2} - \frac{\Delta p}{L_p^2} + \frac{g(x,\lambda)}{D_p} = 0 \quad .. \; 3\text{-}4$$

In order to solve this equation, the boundary conditions under short-circuit conditions are,

$\Delta p(0) = P_s$ where P_s is given by

$$J_p(0) = -e\, S_p\, P_s, \quad .. \; 3\text{-}5$$

S_p being the surface recombination velocity and

$\Delta p(d-w_n) = 0$ where the width of depletion region

$$w_n = \left\{\frac{2\,\epsilon\epsilon_o\,(V_D-V)}{eN_D}\right\}^{1/2}$$

N_D is the density of donor states and V_D is the built-in potentia

The general equation for the hole current density

$$J_p(x) = -e\, D_p \frac{(d\Delta p)}{dx} \quad .. \; 3\text{-}6$$

<u>Current density due to diffusion</u>

In region 1, the photogenerated minority carriers diffuse towards the junction giving rise to the photo-current. Thus, the continuity equation for holes is[39]

$$\frac{d^2\Delta p}{dx^2} - \frac{\Delta p}{L_p^2} + \frac{\alpha N}{D_p}\left[\exp(-\alpha x) + \exp(-\alpha)(d-x)\right] = 0$$

i.e.

$$\frac{d^2\Delta p}{dx^2} - \frac{\Delta p}{L_p^2} + \frac{2\alpha N}{D_p}\left[\exp(-\alpha d)\cosh\alpha(x-d)\right] = 0 \quad .. \; 3\text{-}7$$

The general solution of this equation is obtained as

$$\Delta p = Ae^{-(x-d)/L_p} + B\, e^{(x-d)/L_p}$$

$$+ \frac{2\alpha N}{D_p\left(-\alpha^2 + \frac{1}{L_p^2}\right)} \exp(-\alpha d) \cdot \cosh\alpha(x-d) \quad .. \; 3\text{-}8$$

According to the first boundary condition,

$$\Delta p(0) = P_s$$

$$= Ae^{d/L_p} + Be^{-d/L_p} + \frac{2\alpha N\, e^{-\alpha d} \cosh\alpha d}{D_p\left(-\alpha^2 + \frac{1}{L_p^2}\right)} \quad .. \; 3\text{-}9$$

By differentiating the expression for the number of carriers with respect to x

$$\frac{d(\Delta p)}{dx} = -\frac{1}{L_p} A \; e^{-(x-d)/L_p} + \frac{1}{L_p} B \; e^{(x-d)/L_p}$$

$$+ \frac{2\alpha^2 N \; e^{-\alpha d}}{D_p\left(-\alpha^2 + \frac{1}{L_p^2}\right)} \sinh \alpha \; (x-d)$$

$$\left.\frac{d(\Delta p)}{dx}\right|_{x=0} = -\frac{1}{L_p} A \; e^{d/L_p} + \frac{1}{L_p} Be^{-d/L_p}$$

$$- \frac{2\alpha^2 Ne^{-\alpha d}}{D_p\left(-\alpha^2 + \frac{1}{L_p^2}\right)} \sinh (\alpha d) \qquad .. \quad 3\text{-}10$$

According to the second boundary condition

$$J_p(0) = -e \; S_p \; P_s$$

$$= -e \; D_p \left.\frac{d\Delta p}{dx}\right|_{x=0}$$

Therefore,

$$P_s = \frac{D_p}{S_p} \left.\frac{d\Delta p}{dx}\right|_{x=0} = \Delta p(0)$$

Hence the condition would be

$$A\left(e^{d/L_p} + \frac{e^{d/L_p}\; D_p}{L_p S_p}\right) + Be^{-d/L_p}\left(1 - \frac{D_p}{S_p L_p}\right)$$

$$+ \frac{2N\alpha\; e^{-\alpha d}}{D_p\left(-\alpha^2 + \frac{1}{L_p^2}\right)} \left[\cosh \alpha d + \frac{\alpha\; D_p}{S_p} \sinh (\alpha d)\right] = 0 \qquad .. \; 3\text{-}$$

Also, we know that $\Delta p\,(d - w_n) = 0$

which gives

$$Ae^{+w_n/L_p} + Be^{-w_n/L_p} + \frac{2\alpha N e^{-\alpha d}}{D_p\left(-\alpha^2 + \frac{1}{L_p^2}\right)} \cosh (\alpha w_n) = 0 \qquad .. \; 3\text{-}12$$

From the equations 3-11 and 3-12 the two constants A and B can be found out. By multiplying equation 3-11 by e^{w_n/L_p} and equation 3-12 by $e^{d/L_p}\left(1 + \frac{D_p}{L_p S_p}\right)$ and substracting, it gives

$$Be^{-(d-w_n)/L_p}\left[1 - \frac{D_p}{S_p L_p}\right] - Be^{(d-w_n)/L_p}\left[1 + \frac{D_p}{S_p L_p}\right]$$

$$+ \frac{2\alpha N}{D_p\left(-\alpha^2 + \frac{1}{L_p^2}\right)} e^{-\alpha d} \cdot e^{w_n/L_p} \left[\cosh \alpha d + \frac{\alpha D_p}{S_p} \sinh \alpha d\right]$$

$$- \frac{2\alpha N}{D_p\left(-\alpha^2 + \frac{1}{L_p^2}\right)} e^{-\alpha d} \cdot e^{d/L_p} \cosh \alpha w_n \left[1 + \frac{D_p}{L_p S_p}\right] = 0$$

Therefore,

$$B = \frac{\alpha N e^{-\alpha d}}{D_p\left(-\alpha^2 + \frac{1}{L_p^2}\right)}$$

$$\frac{e^{w_n/L_p}\left\{\cosh \alpha d + \frac{\alpha D_p}{S_p}\sinh(\alpha d)\right\} - e^{d/L_p}\cosh \alpha w_n\left(1 + \frac{D_p}{L_pS_p}\right)}{\sinh\frac{d-w_n}{L_p} + \frac{D_p}{L_pS_p}\cosh\frac{d-w_n}{L_p}} \qquad .. \quad 3\text{-}13$$

Then

$$A = -\ B\ e^{-2w_n/L_p} + \frac{2\alpha N\ e^{-\alpha d}\ e^{-w_n/L_p}\ \cosh(\alpha w_n)}{D_p\left(-\alpha^2 + \frac{1}{L_p^2}\right)} \qquad .. \quad 3\text{-}14$$

The diffusion current at the junction can thus be written as

$$J_{diff.}\ (x = d-w_n)$$

$$= -e\ D_p \left.\frac{d\Delta p}{dx}\right|_{x = d-w_n}$$

$$J_{diff.} = -e\ D_p\left[-\frac{A}{L_p}\ e^{w_n/L_p} + \frac{B}{L_p}\ e^{-w_n/L_p} - \frac{2\alpha^2 N e^{-\alpha d}}{D_p\left(-\alpha^2 + \frac{1}{L_p^2}\right)}\ \sinh\ \alpha w_n\right]$$

i.e.

$$J_{diff.} = e\, D_p \left[\frac{e^{w_n/L_p}}{L_p}\ Be^{-2w_n/L_p} + \frac{1}{L_p}\, e^{+w_n/L_p} \cdot \frac{2\alpha N\, e^{-\alpha d}\, e^{-w_n/L_p}}{D_p\left(-\alpha^2 + \frac{1}{L_p^2}\right)} \cosh \alpha w_n + \frac{B}{L_p}\, e^{-w_n/L_p} - \frac{2\alpha^2 N\, e^{-\alpha d}}{D_p\left(-\alpha^2 + \frac{1}{L_p^2}\right)} \sinh \alpha w_n \right]$$

Therefore,

$$J_{diff.} = -e\, D_p \left[\frac{2B}{L_p}\, e^{-w_n/L_p} + \frac{2\alpha N\, e^{-\alpha d}}{D_p L_p\left(-\alpha^2 + \frac{1}{L_p^2}\right)} \cosh \alpha w_n - \frac{2\alpha^2 N\, e^{-\alpha d}}{D_p\left(-\alpha^2 + \frac{1}{L_p^2}\right)} \sinh\ (\alpha w_n) \right] \quad .. \quad 3\text{-}15$$

Thus the hole-current from base region is found out.

In the depletion region (region 2), the photocurrent is due to the generation of electron-hole pairs and is equal to

$$J_{dr} = eN \left[\int_{d-w_n}^{d} \alpha \exp\ (-\alpha d)\ dx + \int_{d-w_n}^{d} \alpha \exp\ (2d-x)(-\alpha)\ dx \right]$$

$$J_{dr} = eN \Big[-\exp(-\alpha d) + \exp(-\alpha(d-w_n))$$

$$+ \exp(-\alpha d) - \exp(-\alpha(d+w_n)) \Big]$$

Therefore,

$$J_{dr} = eN \Big[\exp(-\alpha d) \Big\{ \exp(\alpha w_n) - \exp(-\alpha w_n) \Big\} \Big]$$

$$= 2eN \exp(-\alpha d) \sinh \alpha w_n \qquad .. \; 3\text{-}16.$$

Thus the total photogenerated current at a given time is the sum of the diffusion current and the current due to the generation of electron-hole pairs in the depletion region.

$$J_1(\lambda) = J_{diff.} + J_{dr}$$

Thus,

$$J_1(\lambda) = -e\, D_p \Big[\frac{2B}{L_p} \exp \frac{(-w_n)}{L_p} + \frac{2\alpha N \exp(-\alpha d) \cosh \alpha w_n - 2N \exp(-\alpha d) \sinh(\alpha w_n)}{D_p (1 - \alpha^2 L_p^{\,2})} \Big] \qquad .. \; 3\text{-}17$$

The total short-circuit current density can be obtained by integrating the above equation over the entire wave length of energy greater than the band gap of the semiconductor. Thus the short-circuit current

$$J_{sc} = \int_{0.3\mu}^{hc/E_g} \left[1 - r(\lambda)\right] J_1 (\lambda)\, d\lambda \qquad .. \quad 3\text{-}18$$

where $r(\lambda)$ is the loss term which includes reflection from the surface and absorption of photons in the metal contact grid.

3.3 Results and conclusions

When the performance of a cell is examined, the short circuit current as well as the open circuit voltage V_{oc} are to be considered. V_{oc} can be calculated from equation 3-1. As we are comparing the performance of the back wall cell with a corresponding front wall solar cell, where there is no difference, except in the direction of the illumination, it is reasonable to expect that the barrier height remains the same in the two cases, if the oxide thickness is kept constant and thus there is no change in J_o.

Before calculating the efficiency of the cell, the short circuit current has been calculated as a function of the thickness of the base semiconductor 'd' at the different donor concentrations i.e. for different diffusion lengths.

In order to do these computations we have considered gold as the Schottky metal with n-Si as base material in this MIS configuration with a given oxide thickness. All these calculations have been carried under AMO illumination by using the data for silicon[40] as given in chapter 2.

The calculated photogenerated current at a given concentration is given in Table 1. Fig. 3-2 shows the variation of J_{sc} as a function of the thickness of the cell. These back wall cells have an optimum thickness to get the maximum photocurrent. At the same time, from the graph, it is clear that this optimum value is always less than the diffusion length of the minority carriers, L_p.

As our main intention is to see the effect of surface recombination velocity on the efficiency of the cell which is essentially the same as seeing its effect on the photogenerated current. The photocurrent has been calculated as functions of surface recombination velocity at different values of the cell thickness for a given donor concentration. The results are given in Table 2.

Fig. 3-3 shows the effect of surface recombination velocity on the J_{sc} of the back illuminated Si Schottky barrier solar cell, wherein variations of J_{sc} with the thickness of the semiconductor have been plotted with S_p as a parameter.

Fig. 3-4 shows the variation of J_{sc} as a function of surface recombination velocity at different values of w for a given donor concentration. From Figs. 3-3 and 3-4, it is clear that the photocurrent decreases rapidly in the range of 10^2 to 10^3 cm/sec, a range which occurs in most

Table 1

Au/SiO_2/Si back-illuminated solar cell calculated under AMO illumination

Surface recombination velocity, $S_p = 10^2$ cm/sec.									
Cell thickness	Base concentration $N_D = 10^{15}$ cm^{-3}			$N_D = 10^{17}$ cm^{-3}			$N_D = 10^{18}$ cm^{-3}		
x10^{-4} 'd' cm	J_{sc} mA/cm^2	V_{oc} volt	$J_{sc} \cdot V_{oc}$ mW/cm^2	J_{sc} mA/cm^2	V_{oc} volt	$J_{sc} \cdot V_{oc}$ mW/cm^2	J_{sc} mA/cm^2	V_{oc} volt	$J_{sc} \cdot V_{oc}$ mW/cm^2
1	19.94	0.577	11.513	19.92	0.577	11.501	19.90	0.577	11.49
5	34.27	0.592	20.308	33.72	0.592	19.97	32.91	0.591	19.46
10	38.95	0.596	23.23	36.62	0.594	21.77	33.46	0.592	19.80
15	40.87	0.597	24.42	35.68	0.593	21.18	29.69	0.588	17.47
20	41.77	0.598	24.49	33.09	0.592	19.57	24.77	0.583	14.44
25	42.15	0.598	25.23	29.78	0.588	17.53	20.01	0.577	11.55
30	42.22	0.598	25.26	26.27	0.585	15.37	15.92	0.570	9.07
40	41.70	0.598	24.94	19.72	0.577	11.37	9.96	0.557	5.55

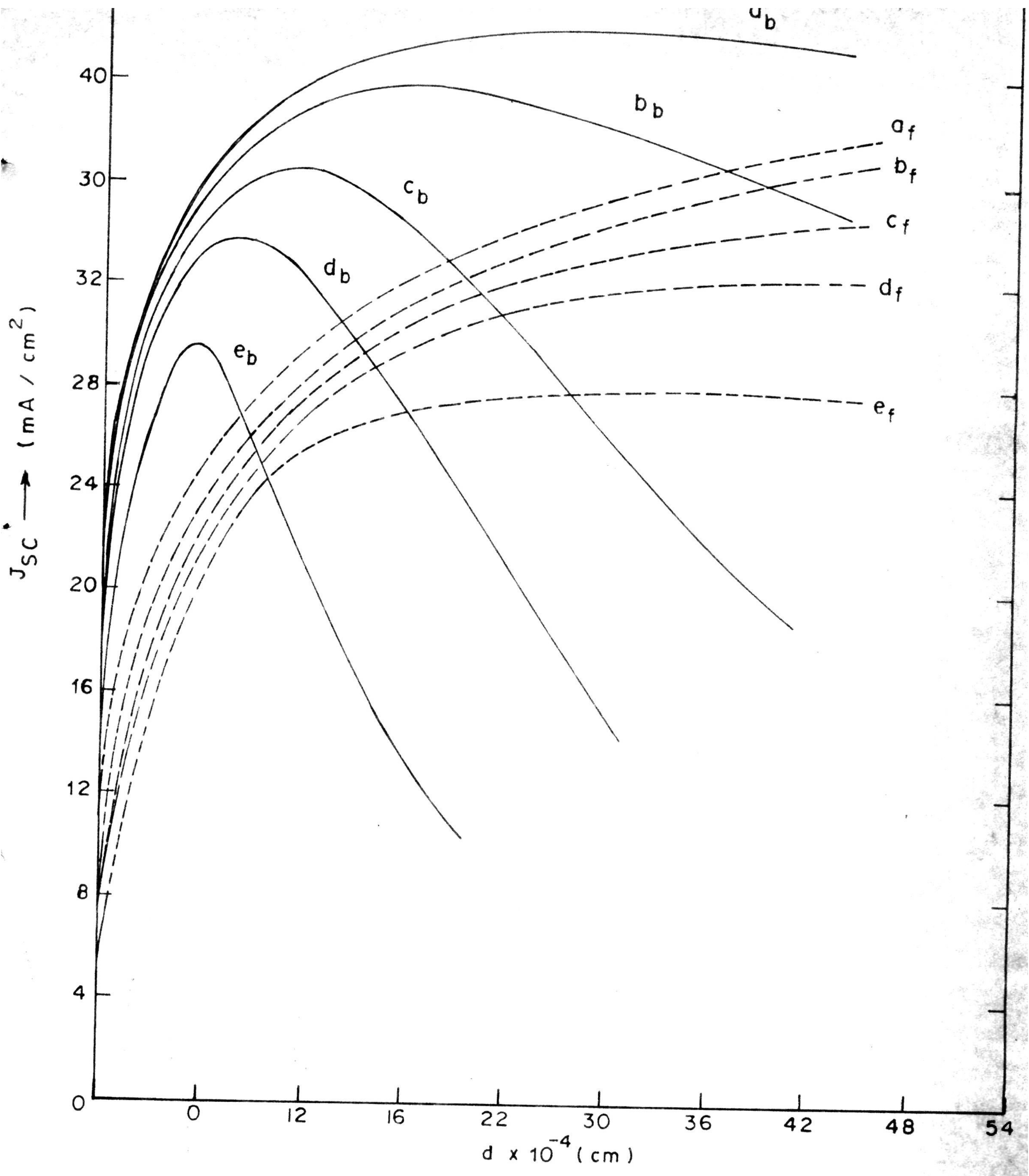

FIG. 3.2. J_{SC} AS A FUNCTION OF THE SEMICONDUCTOR THICKNESS, 'd' AT $N_D = 10^{15}, 10^{16}, 10^{17}, 10^{18}$ AND 10^{19} FOR 'a' 'b' 'c' 'd' AND 'e' RESPECTIVELY. THE SUBSCRIPTS 'b' AND 'f' REFER TO BACK AND FRONT ILLUMINATION RESPECTIVELY ($S_P = 10^2$ cm / S)

Table 2

$Au/SiO_2/Si$ back-illuminated solar cell calculated under AMO illumination

Base concentration, $N_D = 10^{15}$ cm^{-3}									
Surface recombination velocity	Thickness of the cell $d = 1x10^{-4}$ cm			Thickness of the cell 5×10^{-4} cm			Thickness of the cell $10x10^{-4}$ cm		
S_p	J_{sc}	V_{oc}	$J_{sc} \cdot V_{oc}$	J_{sc}	V_{oc}	$J_{sc} \cdot V_{oc}$	J_{sc}	V_{oc}	$J_{sc} \cdot V_{oc}$
cm/sec.	mA/cm^2	volt	mW/cm^2	mA/cm^2	volt	mW/cm^2	mA/cm^2	volt	mW/cm^2
0	19.94	0.577	11.513	34.34	0.592	20.352	39.16	0.596	23.35
10^1	19.94	0.577	11.513	34.33	0.592	20.34	39.14	0.596	23.34
10^2	19.94	0.577	11.513	34.27	0.592	20.308	38.95	0.596	23.23
10^3	19.94	0.576	11.512	33.66	0.592	19.92	37.26	0.595	22.16
10^4	19.92	0.576	11.501	29.08	0.587	17.09	27.54	0.586	16.14
10^5	19.76	0.575	11.404	18.48	0.575	10.62	15.43	0.569	8.79
10^6	18.98	0.575	10.92	14.42	0.568	8.22	12.67	0.564	7.15

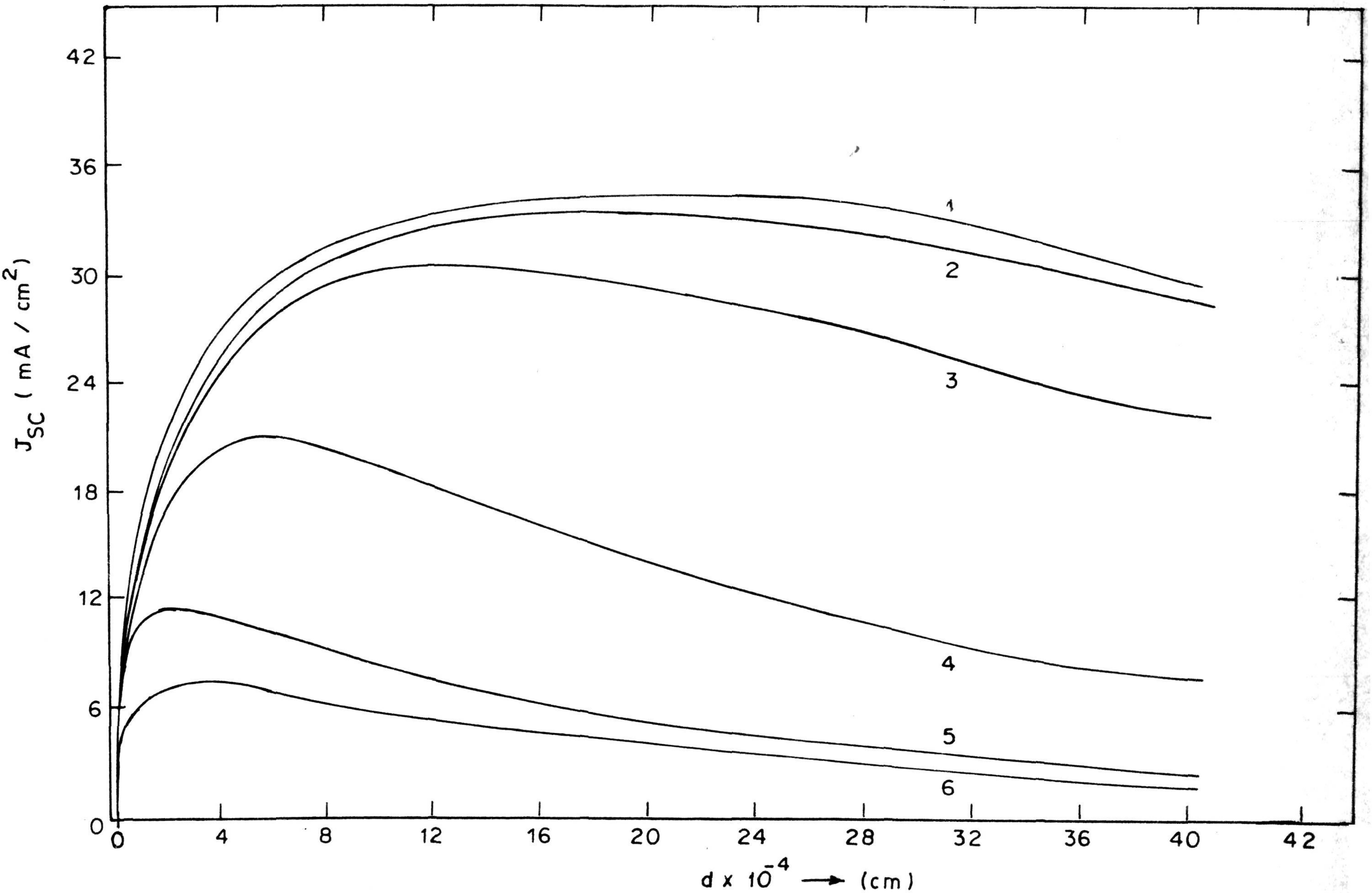

FIG. 3.3. J_{SC} AS A FUNCTION OF THICKNESS 'd' FOR THE BACK ILLUMINATED MIS CELL AT $N_D = 10^{16}$ cm^{-3} AND $S_P = 0, 10^2, 10^3, 10^4$ AND 10^6 cm S^{-1} FOR 1, 2, 3, 4, 5 AND 6 RESPECTIVELY

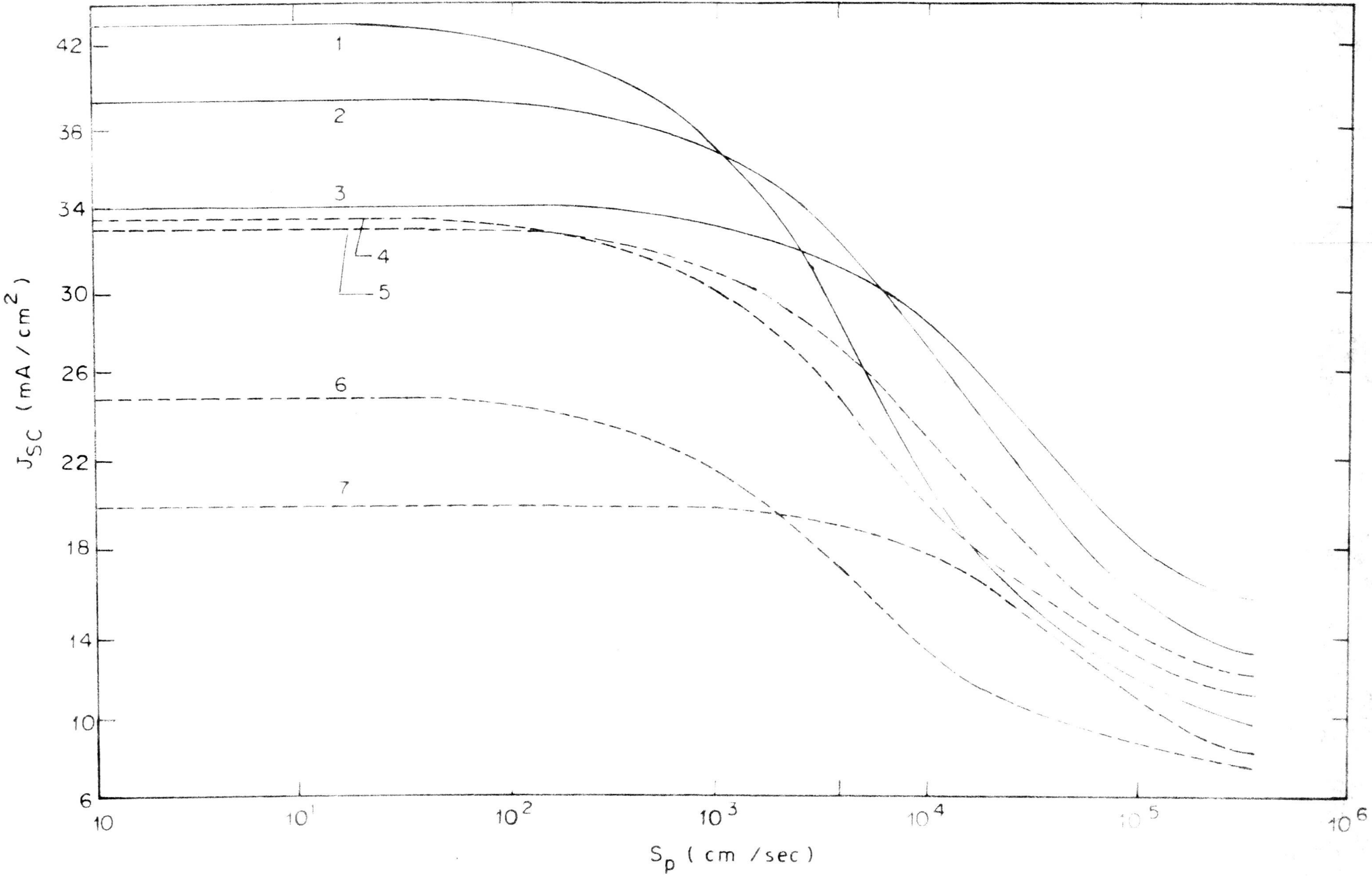

FIG. 3-4. J_{SC} AS A FUNCTION OF S_p FOR DIFFERENT VALUES OF 'd' AND N_D

--------- $N_D = 10^{18}\ cm^{-3}$ ——— $N_D = 10^{15}\ cm^{-3}$

(1) d = 25 (2) 10 (3) 5 (4) 10 (5) 5 (6) 20 (7) 1 μm

practical cases. Beyond $S_p > 10^3$ cm/sec, the photocurrent is quite small and so is the efficiency.

It is relevant to compare the photo response of the back wall thin film MIS solar cells with that of the front wall thin film MIS solar cells.

The two major contributions to the spectral response and to the photocurrent come from the depletion region and from the bulk (the base of solar cell). It is assumed that the high field in the depletion region sweeps carriers out before they recombine, leading to a current J_{dr} for a monochromatic light given by[36]

$$J_{dr} = eN\,[1 - \exp(-\alpha w_n)] \qquad \text{.. 3-19}$$

when the thickness of the base material is w, the photocurrent due to holes collected from the n-Si base material is

$$J_p = \frac{eN\alpha L_p}{(\alpha^2 L_p^2 - 1)} \exp(-\alpha w_n) \times$$

$$\left[\alpha L_p - \frac{\cosh d-w_n - \exp\left\{2\,(-\alpha)\,(d-w_n)\right\}}{\sinh \dfrac{d-w_n}{L_p}} \right]$$

Thus the total photocurrent for the front wall illuminated solar cell has been calculated. As the barrier height remains same in both the situations, the saturation current

is same. After substituting the values for J_{sc} and J_o in equation 3-1, the open-circuit voltage can be obtained and hence the efficiency. These values are tabulated in Table 3.

In order to facilitate comparison, J_{sc} has been shown in Fig. 3-2 as a function of the semiconductor thickness over a range of donor concentrations for both the front and back-wall illuminated Schottky barrier solar cells.

As the back contact is assumed to be ohmic, and sufficiently thick for front wall cells, the surface recombination velocity at the back is considered to be infinite.

Even though for bulk crystals, the short-circuit current is higher for the front-illuminated cells, for thin film MIS cells, the back-illuminated ones are better upto a certain value of the cell thickness. In order to find this thickness, the variation of the power output has been calculated as a function of cell thickness in both cases. The fill-factor has been taken as unity in both cases. The results are shown in Fig. 3-5. In Fig. 3-6, R, given by

$$R = \frac{(J_{sc}\ V_{oc})^{back}}{(J_{sc}\ V_{oc})^{front}}$$

is plotted as a function of the cell thickness, d and the donor concentration N_D. From this figure it is clear that

Table 3

$Au/SiO_2/Si$ front-illuminated solar cell ~~under~~ calculated under AMO illumination

Thickness of the cell	Base concentration $N_D = 10^{15}$ cm^{-3}			Base concentration $N_D = 10^{16}$ cm^{-3}			Base concentration $N_D = 10^{18}$ cm^{-3}		
d	J_{sc}	V_{oc}	$J_{sc} \cdot V_{oc}$	J_{sc}	V_{oc}	$J_{sc} \cdot V_{oc}$	J_{sc}	V_{oc}	$J_{sc} \cdot V_{oc}$
$cm \times 10^{-4}$	mA/cm^2	volt	mW/cm^2	mA/cm^2	volt	mW/cm^2	mA/cm^2	volt	mW/cm^2
1	16.53	0.572	9.45	11.93	0.563	6.71	8.94	0.554	4.96
5	23.77	0.582	13.84	21.50	0.579	12.46	20.11	0.577	11.61
10	28.27	0.587	16.60	26.79	0.585	15.69	25.61	0.584	14.97
15	31.03	0.590	18.30	29.89	0.588	17.60	28.47	0.587	16.72
20	32.96	0.591	19.50	31.98	0.590	18.89	30.14	0.589	17.75
25	34.39	0.593	20.38	33.51	0.592	19.84	31.15	0.590	18.38
30	35.53	0.594	21.09	34.66	0.593	20.55	31.77	0.590	18.76
40	37.19	0.595	22.12	36.31	0.594	21.58	32.39	0.591	19.14

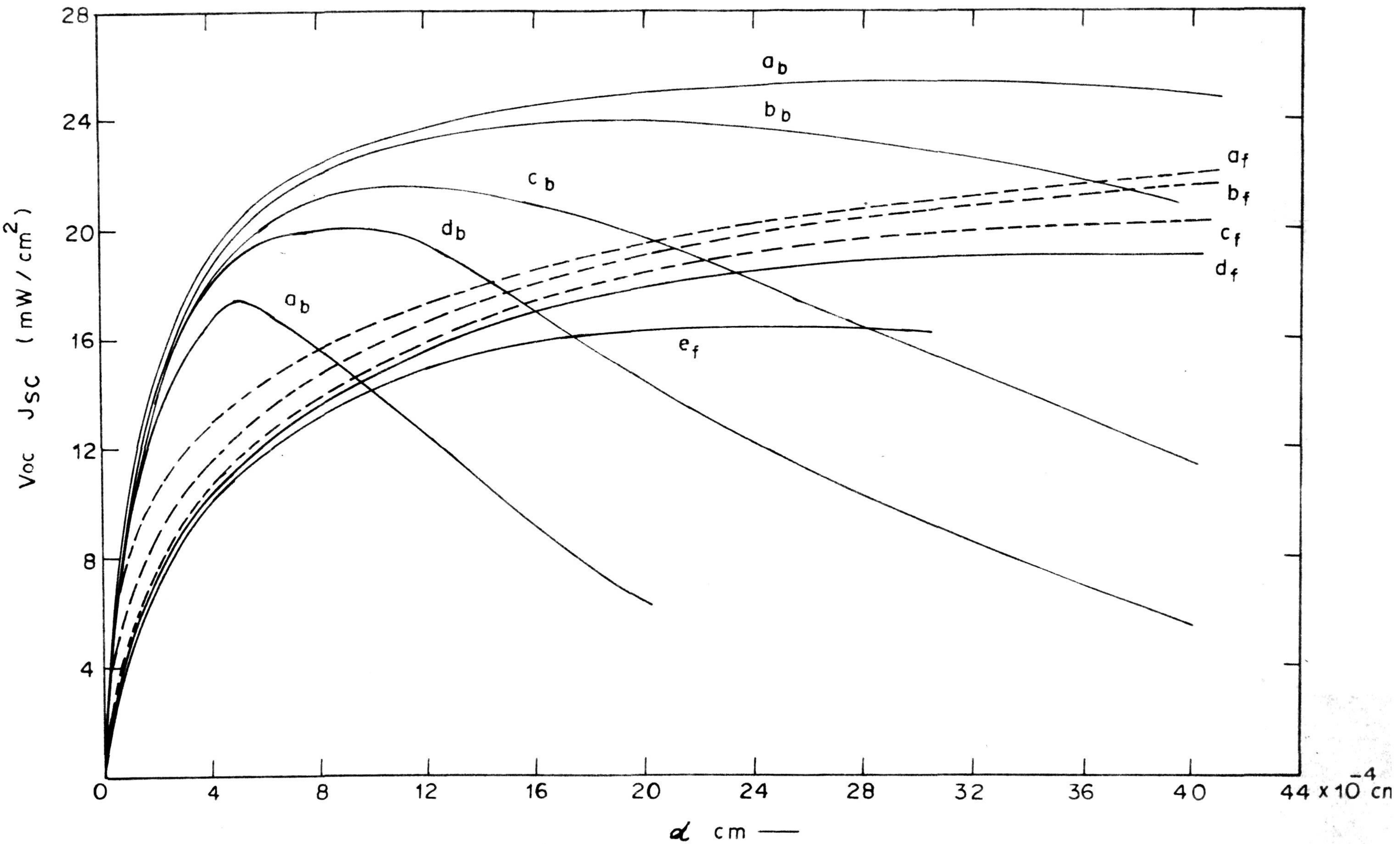

FIG. 3.5. Voc J_{SC} AS A FUNCTION OF THE SEMICONDUCTOR THICKNESS (d) AT DONOR CONCENTRATIONS, $N_D = 10^{15}$, 10^{16}, 10^{17}, 10^{18} AND 10^{19} cm^{-3} FOR 'a' 'b' 'c' 'd' AND 'e' RESPECTIVELY. THE SUBSCRIPTS 'b' AND 'f' REFER TO BACK AND FRONT ILLUMINATION ($S_P = 10^2$ cm / S)

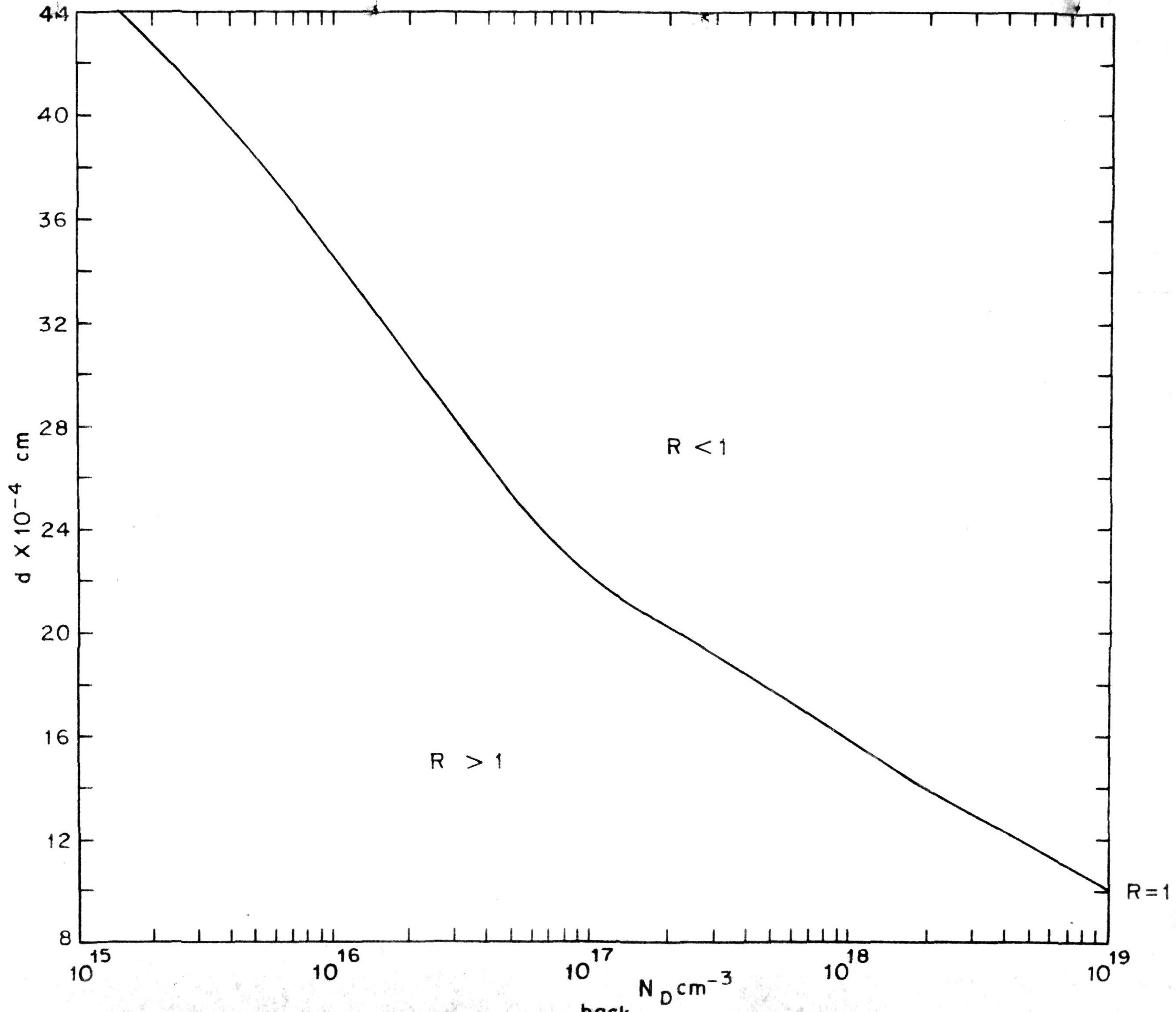

FIG. 3.6. THE RATIO $R = \frac{(J_{SC} V_{OC})^{back}}{(J_{SC} V_{OC})^{front}}$ AS A FUNCTION OF d AND N_D

for thin film MIS Schottky barrier solar cells, the short-circuit current is higher for the back wall solar cell as compared to the front illuminated one. Even if we consider the bulk single crystal MIS Schottky barrier solar cells the back wall cells gives better performance in cases of lower donor concentration.

From this calculation it is clear that for thin film MIS solar cell, back wall configuration is indeed better even efficiency-wise, in addition to the fabrication advantages discussed earlier.

References

1. S.J. Fonash, J.Appl.Phys., 46, 1286 (1975).

2. S.J. Fonash, J.Appl.Phys., 47, 3597 (1976).

3. W.A. Anderson, S.M. Vernon, A.E. Delahoy, J.K. Kim and P. Mathe, J.Vac.Sci.Technol., 13, 1158 (1976).

4. M.A. Green and R.B. Godfrey, Jap.J.Appl.Phys., 17, 295 (1978).

5. H.C. Card and E.H. Rhoderick, J.Phys., D4, 1589 (1971).

6. J.P. Ponpon and P. Siffert, J.Appl.Phys., 47, 3248(1976).

7. M.A. Green and P. Siffert, Appl.Phys.Lett., 29, 610 (1976).

8. S. Kar, IEEE Int.Electron.Dev.Mtg. Washintong D.C., Tech.Digest, p. 79 (1976).

9. R.Singh and J. Shewchun, Appl.Phys.Lett., 28, 512 (1976).

10. J.T. Lue and Y.D. Hong, Solid State Electronics, 21, 1213 (1978).

11. H.I. Moss, RCA Rev., 22, 29 (1961).

12. A.E. Carlson, L.R. Shiozawa and J.D. Finegan, U.S. Patent No.2,820,841 (1958).

13. H.K. Henisch, Rectifying Semiconductor Contacts, (Oxford at the Claredon Press, Oxford, 1957).

14. D.L. Pulfrey, Photovoltaic Power Generation (Van Nostrand Reinhold, New York, 1978,)Chapters 1 and 6.

15. W.A. Anderson, A.E. Delahoy and R.A. Milano, Appl.Opt., 15, 1621 (1976).

16. E. Fabre, J.Michel and Y. Bandet, in Proc. 12 IEEE Photo.Spec.Conf., p.904 (1976).

17. M.A. Green, J.Appl.Phys., 47, 547 (1976).

18. R.J. Stirn and Y.C.M. Yeh, 10th IEEE Photovoltaic Specialists Conference, 1973 (IEEE, New York, 1973).

19. W.A. Anderson and A.E. Delahoy, Proc. IEEE, 60, 1457 (1972).

20. D.L. Pulfrey and R.F. McOuat, Appl.Phys.Lett., 24, 167 (1974).

21. R.J. Stirn and Y.C.M. Yeh, 27, 95 (1975). Appl. Phys. Lett.

22. E.J. Charlson, J.C. Lieu, J.Appl.Phys., 46, 3982 (1975).

23. R.F. McOuat and D.L. Pulfrey, J.Appl.Phys., 47, 2113 (1976).

24. H.J. Hovel, J.Appl.Phys., 47, 4968 (1976).

25. Y.C.M. Yeh, F.P. Ernest and R.J. Stirn, J.Appl.Phys., 47, 4107 (1976).

26. P. Basu and H. Saha, Phys.Stat.Sol. (a), 37, 625 (1976).

27. W.A. Anderson, S.M. Vernon, P. Mathe and B. Lalevic, Solid State Electron., 19, 973 (1976).

28. W.A. Anderson, A.E. Delahoy, J.S. Kim, S.H. Hyland and S.K. Dey, Appl.Phys.Lett., 33, 588 (1978).

29. L.C. Olsen, Solid State Electronics, 20, 741 (1977).

30. R.B. Godfrey and M.A. Green, Appl.Phys.Lett., 33, 637 (1978).

31. E. Fabre, Appl.Phys.Lett., 29, 607 (1976).

32. S.J. Fonash, Thin Solid Films, 36, 1, (1976).

33. D.R. Lillington and W.G. Townsend, Appl.Phys.Lett., 28, 97 (1976).

34. H.C. Card, Solid State Electronics, 20, 971 (1977).

35. K. Bhattacharya, P. Basu and H. Saha, Phys.Stat.Sol., (a), 41, 317 (1977).

36. R.J. Soukup and L.A. Akers, J.Appl.Phys., 49, 4031 (1978).

37. G.S.R. Krishna Murthy, V.V. Kapadia, V.J. Rao and A.P.B. Sinha, Phys.Stat.Sol. (a) 57, 691 (1980).

38. R.J. Soukup, J.Appl.Phys., 47, 555 (1976).

39. H.J. Hovel, Semiconductors and Semimetals, Vol.11, Solar Cells (Edited by R.K. Willardson and A.C. Beer, Academic Press, 1975).

40. H.F. Wolf, Silicon Semiconductor Data (Pergamon Press, Oxford, 1969).

CHAPTER IV

THEORETICAL CALCULATIONS ON THE PERFORMANCE OF AMORPHOUS-Si/LOW GRADE SINGLE CRYSTAL Si SOLAR CELLS

4.1 Introduction

At present one of the materials being studied more extensively in solid state research is the hydrogenerated amorphous silicon[1-8]. The attraction lies chiefly in the fact that large area thin film solar cells can possibly be made from this material relatively cheaply as compared to the conventional single crystal cells. Since silicon for solar cell does not require as good a protection and as stringent a purity control as for the other semiconductor devices, polycrystalline or amorphous thin films of silicon become acceptable materials for solar cells. In particular the amorphous Si offer many other advantages. Its optical absorption coefficient has been measured[9-11] and the data show that the radiation with $\lambda > 0.7 \mu m$ is absorbed almost completely in a film of ~ 1 μm thickness[10]. Furthermore amorphous silicon has a band gap of 1.5 - 1.7 ev which is closer to the optimum than the band gap of the crystalline silicon (1.1 ev)[1,12,13].

Discharge produced a-Si was first studied by Chittick[1] et al. Later Spear and his coworkers at the University of Dundee announced in 1975 that amorphous silicon (a-Si), when produced by means of a r-f glow discharge decomposition of silane (SiH_4), could easily be doped by admitting phosphine (PH_3) or diborane to the gas producing samples of n-type

or p-type a-Si respectively[3,14,6]. This was a very significant advance over the previous methods of producing a-Si by vacuum evaporation[15,16,17] or sputtering[18,19] in argon in which doping was not achieved upon incorporation of appropriate impurities. The broken bonds introduced in large densities (~ 10^{19} cm^{-3}) in a-Si gave rise to electron states lying deep within the forbidden energy gap which trapped any excess carriers introduced by the dopant atoms[20,21]. Indeed these defect states controlled to a very large extent much of the electronic behaviour of such films. These difficulties were obviated to a large extent in the case of hydrogenated a-Si as obtained by Spear and his coworkers by glow discharge.

In spite of this promising progress, several problems still remain with the glow discharge produced a-Si,
(i) The properties seem to be a sensitive function of the conditions of deposition. For example, the hydrogen content and hence the allied properties vary with small changes in the substrate temperature, gas pressure, r-f power, etc.[22a]
(ii) There are several photo-induced changes, such as metastable decrease in conductivity after optical illumination[22].
(iii) The doping efficiency is relatively low in that only ~ 30% of the impurity atoms act as donors or acceptors[23] (i.e. ~ 70% of the impurity atoms bond according to their normal valence and are not forced into tetrahedral environments

on substituting for Si atoms) and the fermi level can be moved only to within ~ 0.2 ev from the conduction or valence band edge[3]. (iv) The minority carrier life time is small[9,24].

However, the a-Si alloys produced from a mixture of silicon tetrafluoride and hydrogen containing both fluorine and hydrogen are reported to be markedly superior to those produced by the glow discharge decomposition of silane[25-27]. Doping efficiencies are large, photo structural changes are absent and the deposition conditions only weakly affect the properties of these a-Si-F-H alloys.

The theoretical estimates of the limiting efficiency of p-n and Schottky cells based on amorphous silicon have ranged from 8 to 15%[10]. The factor which is most significant in reducing the efficiency in comparison with single crystal cells is the short diffusion length of the charge carriers[27,28] Electrons and holes excited within only about one micron of the junction contribute to the photogenerated current. In a crystalline semiconductor, the active layer may be as much as 0.5 mm thick.

So far, by using a-Si produced by the r-f glow discharge, Schottky barriers with the efficiency upto 5% only has been reported[29-35]. Furthermore, these have been made on small areas only and large area cells show a

considerable degradation in the efficiency. Also a p-n homojunction in amorphous silicon has not been a success yet[6,10]. The chief difficulty appears to be in establishing a good junction in thin film amorphous Si by sequential deposition. In order to overcome this difficulty, we examined the prospects of a junction between bulk crystalline Si and thin film amorphous Si of the opposite type. This would in effect be a heterojunction. Since most of the light absorption would take place in the top amorphous layer, all the advantages of the thin film amorphous Si material would be retained. Furthermore the active layer being the amorphous material, the base material need not be of high purity single crystal, and at the same the difficulty of making a junction within the amorphous material would be overcome.

An efficient thin film solar cell requires[36-39] (i) absorption of a large fraction of the incident solar-radiation,(ii) an efficient collection of both photo-generated holes and electrons, (iii) a junction with built-in potential of the order of 1 volt and (iv) a low internal series resistance.

All these features can be achieved in this proposed configuration. The photovoltaic behaviour of such a configuration is examined theoretically in the following pages.

The effect of lower carrier mobility in the base material on the overall efficiency is looked into more specifically in view of its relevance to the proposal of using a low grade base material.

4.2 J-V characteristics under illumination

By taking a low grade single crystal silicon of (say) p-type as a substrate on which an amorphous layer of silicon of n-type is deposited, the system becomes a p/n hetero-junction. The schematic diagram is shown in Fig. 4-1.

It being a heterojunction type, the theory[40] discussed in chapter 2 is applicable. Let us assume that E_{g_1}, χ_1, ϵ_1 and E_{g_2}, χ_2, ϵ_2 are energy gap, electron affinity and dielectric constant of amorphous and crystalline silicon respectively.

As is known,

$$\Delta E_c = \chi_2 - \chi_1 \qquad \ldots 4\text{-}1$$

$$\Delta E_v = (E_{g_1} - E_{g_2}) - \Delta E_c \qquad \ldots 4\text{-}2$$

The electron affinity and dielectric constant are assumed to be the same for the amorphous and single crystal silicon. Hence

$$\Delta E_c = 0, \quad \Delta E_v = E_{g_1} - E_{g_2} - 0$$

Therefore,

$$\Delta E_v = E_{g_1} - E_{g_2}$$

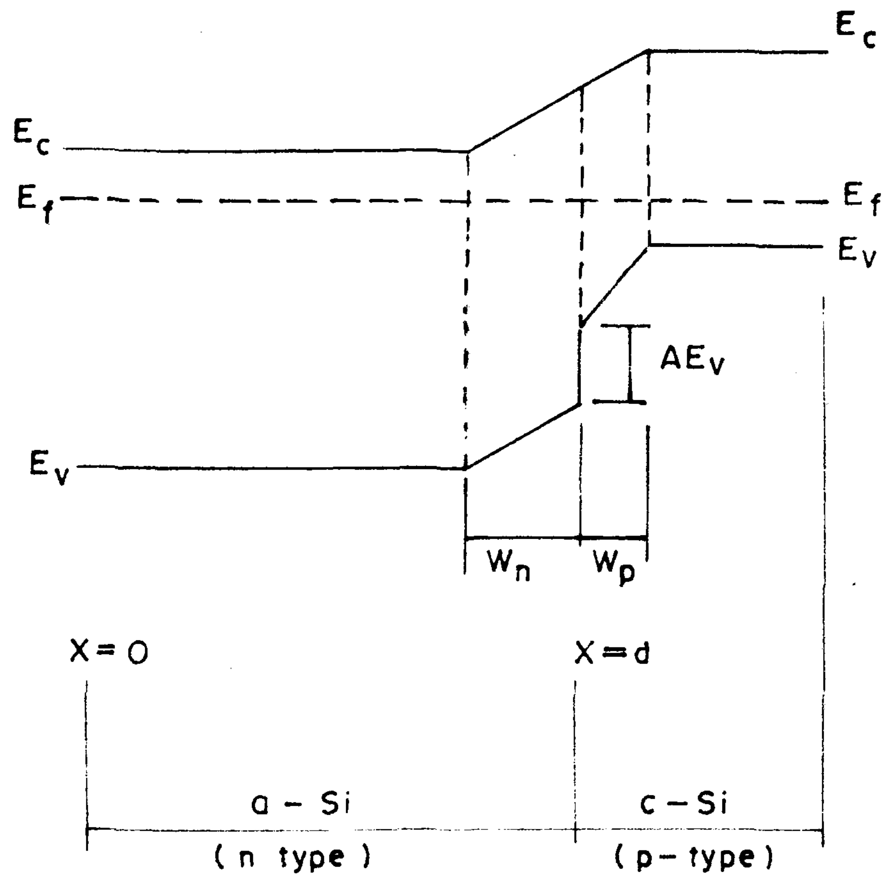

FIG. 4·1 . SCHEMATIC DIAGRAM OF A n-a-Si / p-c-Si HETEROJUNCTION

As a-Si has high absorption coefficient, the base layer is of less importance, unlike single crystal solar cell. When light is incident on the surface of amorphous silicon, the generation rate of electron-hole pair, is given ~~by~~ as

$$g(\lambda, x) = \alpha(x) \; N(\lambda) \; \exp(-\alpha_1 x) \qquad .. \; 4\text{-}3$$

where $N(\lambda)$ is number of photons incident at wave length λ and α_1 is absorption coefficient of the amorphous silicon. If 'd' is the thickness of the amorphous silicon, the generation rate of electron hole pair in the base silicon is

$$g(\lambda, x') = \alpha_2 N \exp(-\alpha_1 d) \; \exp(-\alpha_2 x') \qquad .. \; 4\text{-}4$$

where $x' = 0$ at the junction (interface of amorphous and single crystal silicon).

Photocurrent in amorphous silicon

The width of the depletion regions in a-Si and crystalline Si are w_n and w_p respectively. As we have already discussed, the photogenerated current is the sum of the current due to the depletion region and the base region[41,42].

The photocurrent due to generation of carriers in the depletion region is

$$J_{P_1} = \int_{d-w_n}^{d} e\alpha_1 \, N \exp(-\alpha_1 x) \, dx$$

$$J_{P_1} = eN \exp(-\alpha_1 d)\,[\exp(\alpha_1 w_n) - 1]$$

$$= eN \exp(-\alpha_1(d-w_n))\,[1 - \exp(-\alpha_1 w_n)] \quad .. \quad 4\text{-}5$$

Outside the depletion region, the equation for diffusion of minority carriers under steady state is

$$\frac{d\Delta p}{dt} = g(\lambda, x) - \frac{\Delta p}{\tau_p} + D_p \frac{d^2 \Delta p}{dx^2} = 0 \quad .. \quad 4\text{-}6$$

The boundary conditions are

$$\text{when} \quad x = d - w_n, \quad \Delta p = 0$$

$$x = 0, \quad D_p \frac{d\Delta p}{dx} = S_p \Delta p$$

where S_p is the surface recombination velocity. The general solution of this equation is

$$\Delta p = A \sinh x/L_p + B \cosh x/L_p - \frac{\alpha N \tau_p}{(\alpha_1^2 L_p^2 - 1)} \exp(-\alpha x) \quad .. \quad 4\text{-}7$$

The boundary condition

$$\frac{d\Delta p}{dx} = \frac{S_p}{D_p} \Delta p \quad \text{at } x = 0 \quad \text{gives}$$

$$\left[\frac{A}{L_p} + \frac{\alpha N \tau_p}{(\alpha^2 L_p^2 - 1)} \alpha\right] = \frac{S_p}{D_p}\left[B - \frac{\alpha N \tau_p}{(\alpha^2 L_p^2 - 1)}\right]$$

and $\Delta p = 0$ at $x = d - w_n$ gives

$$A \sinh \frac{d-w_n}{L_p} + B \cosh \frac{d-w_n}{L_p} - \frac{\alpha N \tau_p}{\alpha^2 L_p^2 - 1} \exp\left\{(d-w_n)(-\alpha_1)\right\} = 0$$

Hence

$$B = \frac{\alpha_1 N \tau_p}{\alpha_1^2 L_p^2 - 1}$$

$$\times \frac{\left(\frac{S_p L_p}{D_p} + \alpha_1 L_p\right) \sinh \frac{d-w_n}{L_p} + \exp\left(-\alpha_1 (d-w_n)\right)}{\frac{S_p L_p}{D_p} \sinh \frac{d-w_n}{L_p} + \cosh \frac{d-w_n}{L_p}}$$

and

$$A = \frac{\alpha_1 N \tau_p}{\alpha_1^2 L_p^2 - 1}$$

$$\times \frac{\exp \frac{d-w_n}{L_p} \cdot \frac{S_p L_p}{D_p} - \left(\frac{S_p L_p}{D_p} + \alpha_1 L_p\right) \cosh \frac{d-w_n}{L_p}}{\frac{S_p L_p}{D_p} \sinh \frac{d-w_n}{L_p} + \cosh \frac{d-w_n}{L_p}}$$

Thus the carrier concentration would be

$$\Delta p = \frac{\alpha_1 N \tau_p}{\alpha_1^2 L_p^2 - 1}$$

$$\left[\frac{\left(\frac{S_p L_p}{D_p} + \alpha_1 L_p\right) \sinh \frac{d-w_n-x}{L_p} + \exp\left(-\alpha_1(d-w_n)\right)\left(\frac{S_p L_p}{D_p} \sinh \frac{x}{L_p} + \cosh \right.}{\frac{S_p L_p}{D_p} \sinh \frac{d-w_n}{L_p} + \cosh \frac{d-w_n}{L_p}} - \exp(-\alpha_1 x) \right] \quad .. \; 4\text{-}8$$

The hole current density at the junction edge is

$$J_{p_2} = -e \; D_p \left. \frac{d\Delta p}{dx} \right|_{x = d-w_n}$$

Th. 6645

Therefore,

$$J_{p_2} = \frac{eN \alpha_1 L_p}{\alpha_1^2 L_p^2 - 1}$$

$$\left[\frac{\left(\frac{S_p L_p}{D_p} + \alpha_1 L_p\right) - \exp\left(-\alpha_1(d-w_n)\right)\left(\frac{S_p L_p}{D_p} \cosh \frac{d-w_n}{L_p} + \sinh \frac{d-w_n}{L_p}\right)}{\frac{S_p L_p}{D_p} \sinh \frac{d-w_n}{L_p} + \cosh \frac{d-w_n}{L_p}} - \alpha_1 L_p \exp\left(-\alpha_1(d-w_n)\right) \right] \quad .. \; 4\text{-}9$$

Thus the photocurrent that would be collected from the top layer is the sum of J_{P_1} and J_{P_2}.

Photocurrent in base layer

The surface recombination velocity at the back is infinite as the contact is ohmic. Here also, the photocurrent from the depletion region is

$$J_{n_1} = \int_0^{w_p} e\alpha_2 N \exp(-\alpha_1 d) \exp(-\alpha_2 x') \, dx'$$

$$J_{n_1} = eN \exp(-\alpha_1 d) \left[1-\exp(-\alpha_2 w_p)\right] \qquad .. \text{ 4-10}$$

In the base region, outside the depletion region, the steady state equation for electron is

$$\frac{d\Delta n}{dt} = g(x', \lambda) - \frac{\Delta n}{\tau_n} - D_n \frac{d^2 \Delta n}{dx^2} = 0$$

The general solution can be written as

$$\Delta n = A \exp\left(x'/L_n\right) + B \exp(-x'/L_n)$$

$$- \frac{\alpha N \tau_n}{\alpha_n^2 L_n^2 - 1} \exp(-\alpha_2 x') \exp(-\alpha_1 d)$$

The boundary conditions are

$$\text{at } x' = w_p, \quad \Delta n = 0 \quad \text{and } x' \to \infty, \ \Delta n = 0$$

Thus the constants would be

$$A = 0$$

$$B = \frac{\alpha_2 N \tau_n}{1-\alpha_2^2 L_n^2} \exp(-\alpha_1 d) \exp(-\alpha_2 w_p) \exp \frac{(w_p)}{L_n}$$

The electron density is

$$\Delta n(x') = \frac{\alpha_2 N \tau_n}{1-\alpha_2^2 L_n^2} \exp(-\alpha_1 d)$$

$$\times \left\{ \exp(-\alpha_2 x') - \exp(-\alpha_2 w_p) \exp \frac{w_p}{L_n} \exp - \frac{x'}{L_n} \right\} \qquad .. \; 4\text{-}11$$

The diffusion current in the base layer is[42]

$$J_{n_2} = eD_n \left. \frac{d\Delta n}{dx'} \right|_{x'=w_p}$$

Therefore,

$$J_{n_2} = \frac{e\alpha_2 L_n}{1+\alpha_2 L_n} \exp(-\alpha_1 d) \exp(-\alpha_2 w_p) \qquad .. \; 4\text{-}12$$

The total photocurrent generated in the base layer is the sum of J_{n_1} and J_{n_2}. Hence

$$J_n = eN \exp(-\alpha_1 d) \left[1 - \frac{\exp(-\alpha_2 w_p)}{1+ \alpha_2 L_n} \right] \qquad .. \; 4\text{-}13$$

The total photocurrent at a given wave length

$$J_1 (\lambda) = J_{P_1} + J_{P_2} + J_n \quad .. \quad 4\text{-}14$$

Thus the total photogenerated current under AMO illumination can be obtained by integrating the above equation over the entire AMO illumination[43].

The dark current in heterojunction cells is mainly due to the injection of minority carriers from each side of the junction into the other, and the recombination of holes and electrons in the space charge region.

As the base layer thickness of the crystalline silicon is assumed to be large as compared to the thickness of the a-Si layer, the dark current from the base layer

$$J_{o_1} = \frac{e\, n_i^2}{L_n} \times \frac{D_n}{N_A} \quad .. \quad 4\text{-}15$$

and that from the top layer, i.e. from the amorphous silicon layer

$$J_{o_2} = \frac{e\, n_i^2}{L_p} \times \frac{D_p}{N_D}$$

$$\times \quad \frac{\frac{S_p L_p}{D_p} \cosh \frac{d-w_n}{L_p} + \sinh \frac{d-w_n}{L_p}}{\frac{S_p L_p}{D_p} \sinh \frac{d-w_n}{L_p} + \cosh \frac{d-w_n}{L_p}} \quad .. \quad 4\text{-}16$$

Thus the total dark current in the system is

$$J_o = J_{o_1} + J_{o_2}$$

Hence, the open circuit voltage can be obtained by using the relation

$$V_{oc} = \frac{kT}{e} \ln \left\{ \frac{J_{sc}}{J_o} + 1 \right\} \qquad .. \quad 4\text{-}17$$

4.3 Results and Discussion

(i) Effect of variation in the thickness of top amorphous layer

As mentioned earlier, the mobility of the carriers in a-Si is low and for the purpose of calculations we have considered the mobilities of holes in this layer in the range of 0.1 - 10 cm^2/volt-sec. Computations have been made for J_{sc} and V_{oc} as a function of the thickness of the a-Si layer at a given mobility in the base layer. Figs. 4-2 and 4-3 show these plots. It is clear from the graph that both J_{sc} and V_{oc} increases and attains a maximum with the thickness of the a-Si layer. Both J_{sc} and V_{oc} appear to be reasonable where the thickness of a-Si is of the order of 0.1 μ. These values are given in Table 1. All the subsequent calculations have been made by considering the thickness of a-Si layer as 0.1μ .

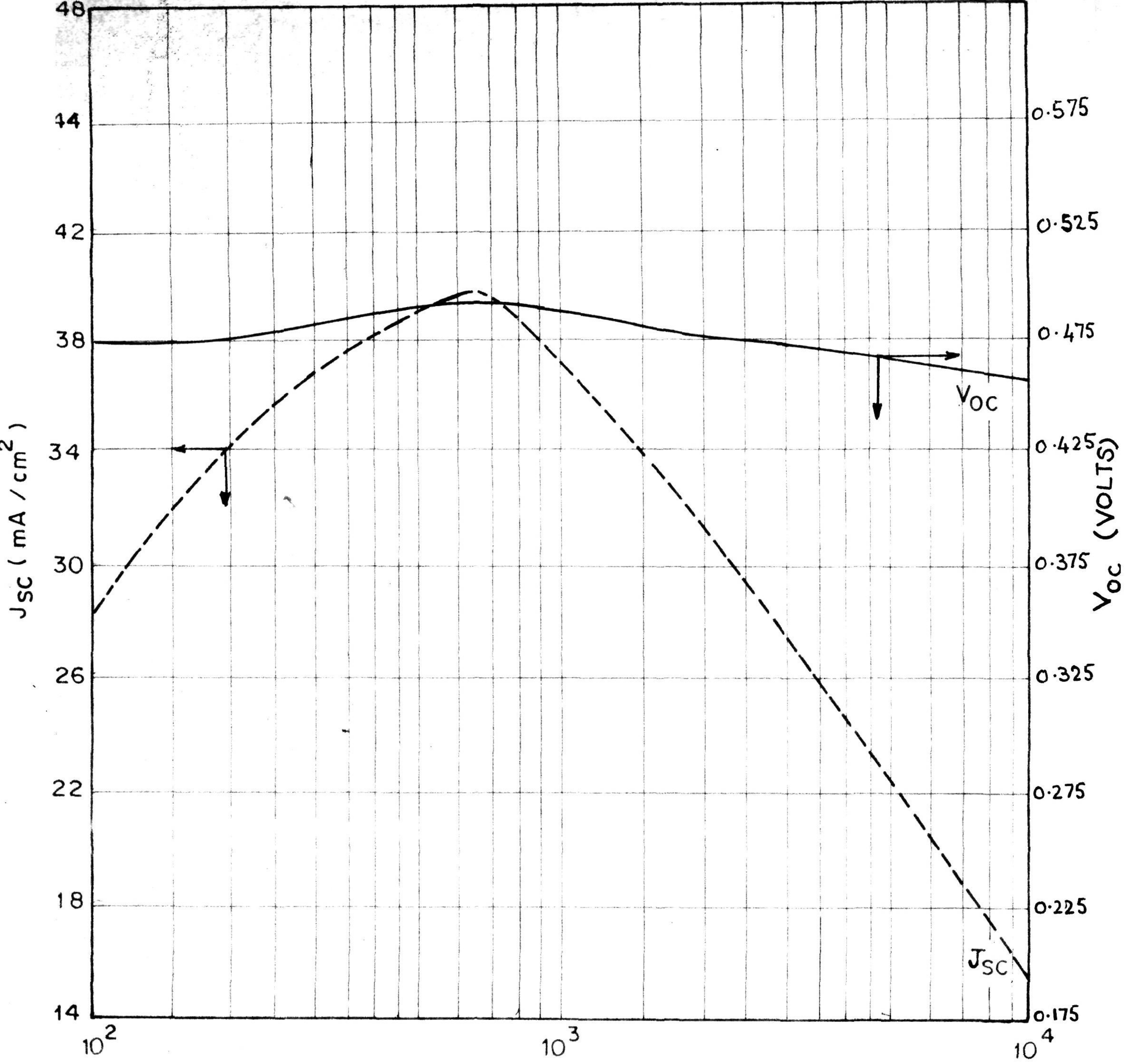

FIG. 4·2. J_{SC} AND V_{OC} AS A FUNCTION OF THICKNESS OF AMORPHOUS SILICON LAYER

μ_p IN a-Si = 5 cm^2 / VOLT-SEC

μ_n IN c-Si = 1200 cm^2 / VOLT-SEC

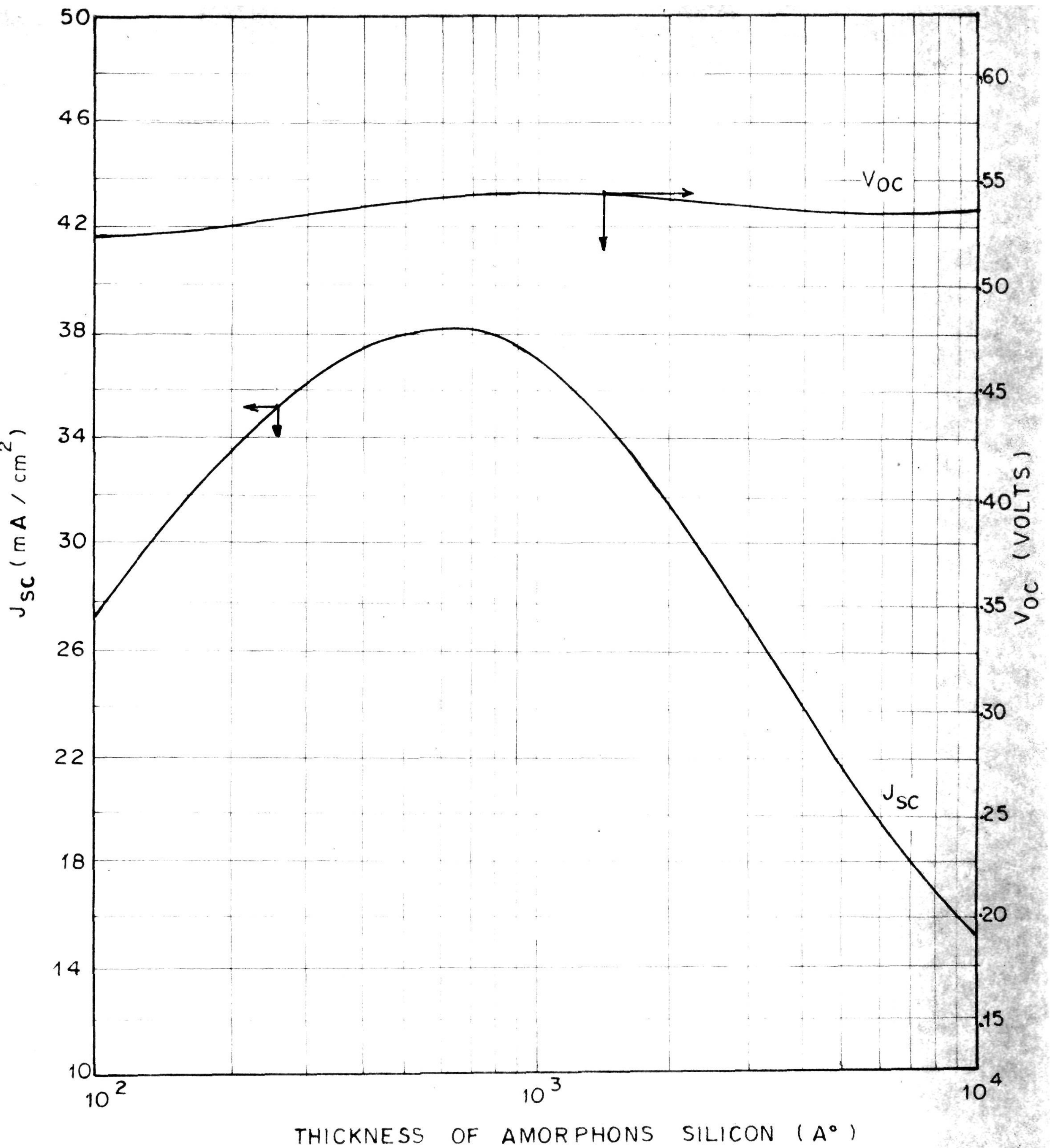

FIG. 4·3. J_{SC} AND V_{OC} AS A FUNCTION OF THICKNESS OF AMORPHOUS SILICON LAYER

μ_n (IN a-Si) – 5 cm^2 / VOLT-SEC

μ_p (IN C-Si) – 900 cm^2 / VOLT-SEC

Table 1

Amorphous layer thickness	Carrier mobility in a-Si layer = 5 cm^2/volt-sec.					
	Carrier mobility in C-Si = 1200 cm^2/volt-sec.			900 cm^2/volt-sec.		
$x10^{-6}$cm	J_{sc} mA/cm^2	V_{oc} volt	$J_{sc} \cdot V_{oc}$ mW/cm^2	J_{sc} mA/cm^2	V_{oc} volt	$J_{sc} \cdot V_{oc}$ mW/cm^2
1	29.18	0.473	13.83	27.46	0.520	14.28
2	35.50	0.479	17.02	33.80	0.527	17.87
4	39.65	0.482	19.14	38.09	0.534	20.36
6	39.77	0.482	19.24	38.29	0.537	20.58
8	38.78	0.482	18.72	37.36	0.539	20.15
10	37.44	0.482	18.07	36.14	0.540	19.53
20	31.59	0.478	15.10	30.43	0.542	16.51
40	24.44	0.472	11.54	23.49	0.542	12.74
100	15.74	0.461	7.28	15.09	0.537	8.11

(ii) Effect of variations in the carrier mobility in the base layer

Calculations have been made for the photogenerated current, J_{sc} and V_{oc} as a function of the mobility of the base single crystal Si and the results have been shown graphically in Figs. 4-4 and 4-5 and also tabulated in Table 2. The α-Si layer thickness has been kept fixed at the optimum value 0.1μ as derived above. The α layer mobility is also kept fixed for each graph. From the figure one can see that J_{sc} decreases as the mobility of the carriers decreases, whereas V_{oc} increases slightly with the decrease of mobility. However, the product of J_{sc} and V_{oc} remains more or less constant up to a certain value of the mobility below which it starts decreasing. The increase in V_{oc} can be accounted as due to the decrease in J_o as is expected. The product of J_{sc} and V_{oc} is constant down to the mobility of 800-500 cm^2/volt sec. below which it decreases slowly. However, a mobility of 300 cm^2/volt sec. which is likely to be encounted in a low grade material envisaged here is also acceptable as is seen from the graph.

(iii) Effect of variations in the mobility of the amorphous layer.

By keeping the thickness of α-Si layer and the mobility of the base layer fixed at 0.1μ and 300 cm^2/volt -sec, the

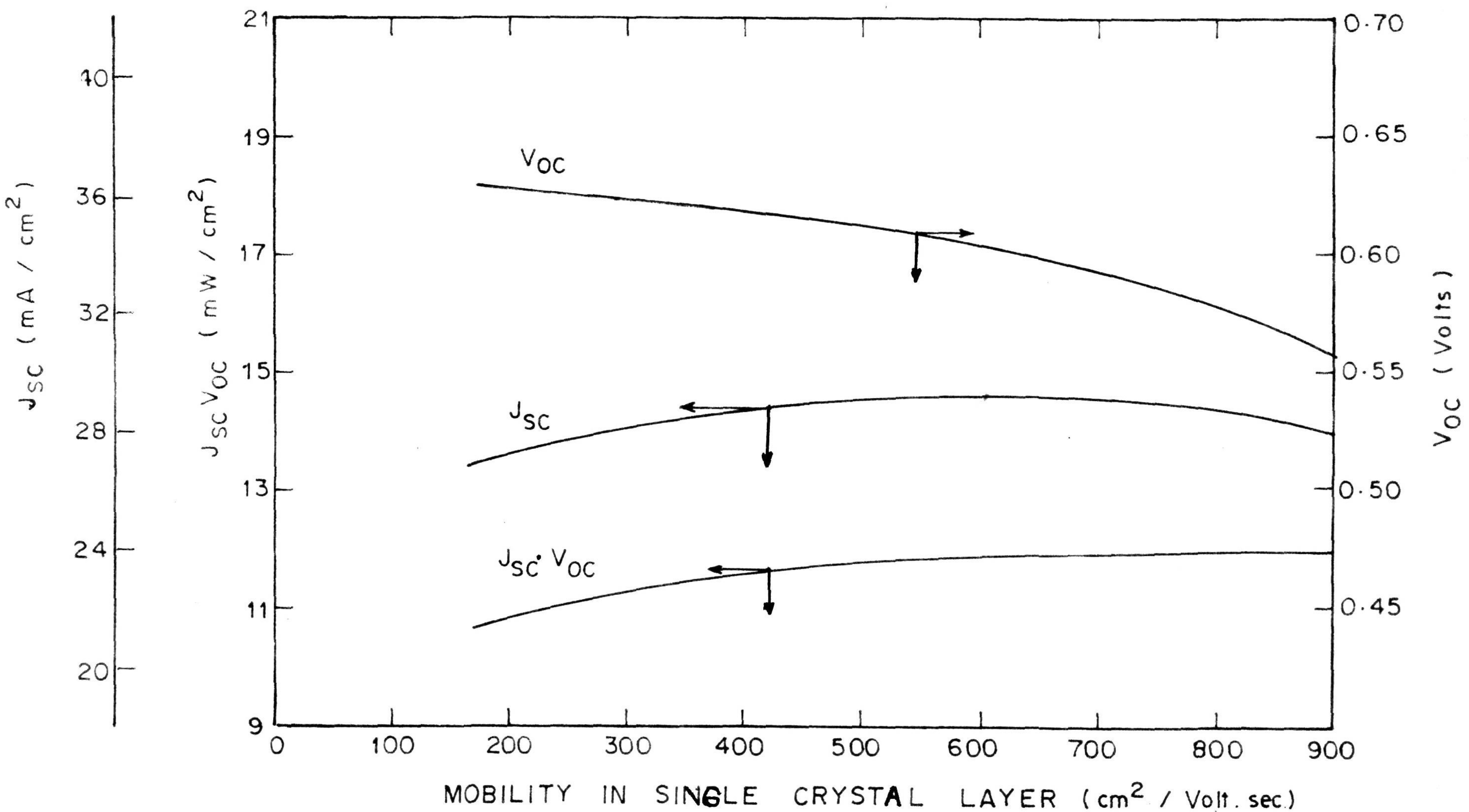

FIG. 4·4 . J_{SC} , V_{OC} & $J_{SC} \cdot V_{OC}$ AS A FUNCTION OF CARRIER MOBILITY IN CRYSTALINE SILICON (THICKNESS OF a – Si = 0·1 μ
μp (a- Si) = 0·1 cm / volt – sec)

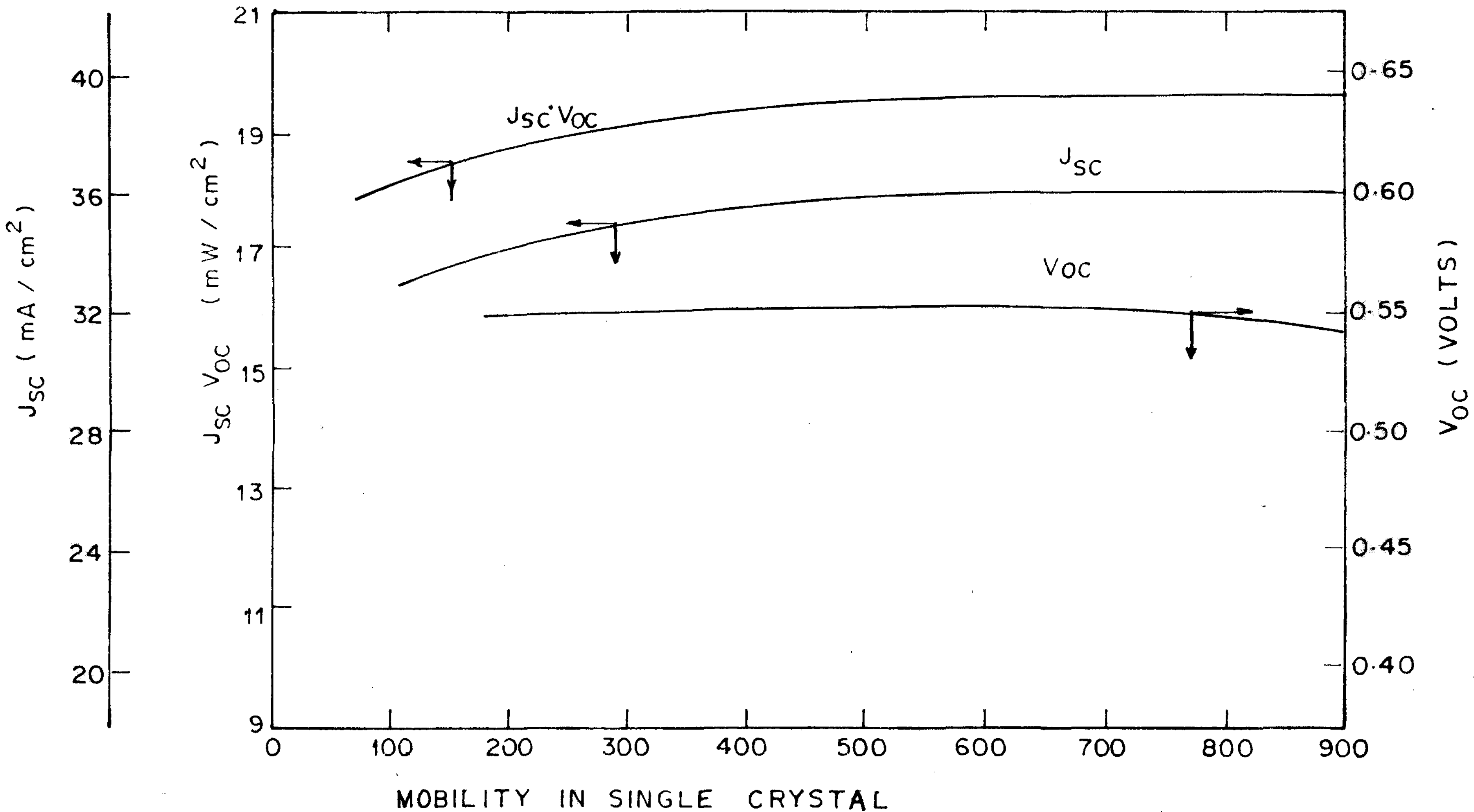

FIG. 4·5. J_{SC}, V_{OC} & $J_{SC} \cdot V_{OC}$ AS A FUCTION OF CARRIER MOBILITY IN CRYSTALINE SILICON (THICKNESS OF a−Si = 0·1 μ
μ_P (a−Si) = 5 cm^2 / VOLT − SEC)

Table -2

Carrier Mobility in base layer	Thickness of a-Si 'd' = 0.1					
	Carrier mobility in a-Si = 2 cm^2/volt-sec.			Carrier mobility of a-Si = 5 cm^2/volt-sec.		
	J_{sc} mA/cm^2	V_{oc} volts	$J_{sc} \cdot V_{oc}$ mW/cm^2	J_{sc} mA/cm^2	V_{oc} Volts	$J_{sc} \cdot V_{oc}$ mW/cm^2
900	31.93	0.561	17.93	36.14	0.540	19.53
500	31.43	0.608	19.12	35.63	0.550	19.61
300	30.42	0.608	18.50	34.62	0.549	19.03
180	29.75	0.610	18.15	33.95	0.549	18.65

effect of mobility of the charge carriers in a-Si on the performance of solar cell has been examined. These values are represented graphically in Fig. 4-6 and also given in Table 3. From the graph, it is clear that the J_{sc} increases whereas V_{oc} decreases with the increase in the mobility of the carriers. However, the product of J_{sc} and V_{oc} remains constant in the mobility region of 2-5 cm^2/volt sec.

From the analysis the suggested optimum values are

α layer thickness	..	~ 0.1 μ
base layer mobility	..	400-200 cm^2/volt -sec.
α layer mobility	..	2-5 cm^2/volt-sec.

Under these conditions the expected efficiency should be of the order of 10%.

From the above discussion, it is clear that n/p heterojunction made with a-Si over low grade crystalline Si would have the advantage of ease of fabrication over the conventional amorphous homojunction, without any significant sacrifice in efficiency. Furthermore, the low grade crystalline silicon itself acts as a substrate which avoids the consideration of any other substrate material.

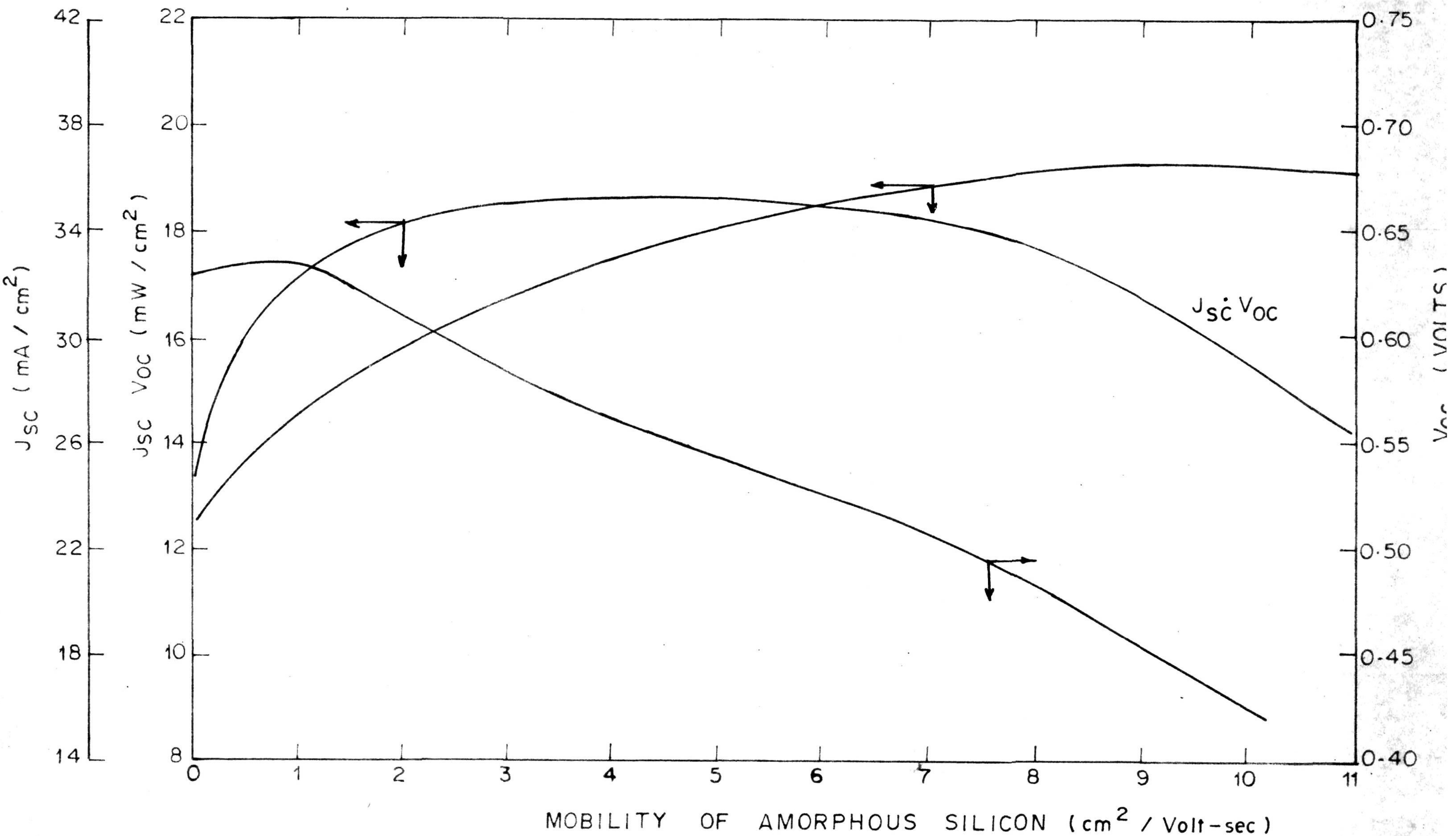

FIG. 4·6. J_{SC}, V_{OC} AND $J_{SC} \cdot V_{OC}$ AS A FUNCTION OF CARRIER MOBILITY IN AMORPHOUS SILICON (THICKNESS OF a-Si = 0·1 μ CARRIER MOBILITY IN C-Si = 180 cm^2/ VOLT-SEC)

Table 3

Carrier mobility in a-Si layer	Thickness of a-Si 'd' = o.1 Carrier mobility in -Si = 180 cm^2/volt-sec.		
cm^2/volt-sec	J_{sc} mA/cm^2	V_{oc} volt	$J_{sc} \cdot V_{oc}$ mW/cm^2
0.1	21.71	0.630	13.71
0.5	25.43	0.632	16.09
1.0	27.07	0.632	17.11
2.0	29.75	0.610	18.15
5.0	33.95	0.549	18.65
8.0	36.45	0.483	17.62
10.0	36.45	0.423	15.45

References

1. R.C. Chittick, J.H. Alexander and H.F. Sterling, J.Electrochem.Soc., 116, 77 (1969).

2. M.V. Coleman and D.J.D. Thomas, Phys.Stat.Solidi, 24, K111 (1967).

3. W.E. Spear and P.G. LeComber, Solid State Communication, 17, 1193 (1975).

4. S.R. Elliott, Nature 277, 85 (1979).

5. Z.S. Jan and R.H. Bube, J.Electro.Mater, 8, 47,(1979).

6. W.E. Spear, P.G. LeComber, S. Kinmond and M.H. Broadsky, Appl.Phys.Lett., 28, 105 (1976).

7. J.C. Knights, Phil.Mag., 34, 663 (1976).

8(a) D.I. Jones, P.G. LeComber and W.E. Spear, Phil.Mag., 36, 541 (1977).

(b) D. Weaire, N. Higgins, P. Moorie and I. Marshall, Phil.Mag., B40, 243 (1979).

9. R.L. Toveland, W.E. Spear and A.Al-Sharboty, J.Non.Cryst.Solids, 13, 55 (1973/74).

10. D.E. Carlson and C.R. Wronski, Appl.Phys.Lett., 28, 671 (1976).

11. R.C. Chittick, J.Non.Cryst.Solids, 3, 255 (1970).

12. C.R. Wronski, D.E. Carlson, R.E. Daniel and A.R. Triano, Technical Digest of the 1976 IEEE International Electron Devices Meeting, (Washington, D.C., 1976) p.75.

13. P.G. LeComber, A. Madan and W.E. Spear, J.Non.Cryst.Solid, 11, 219 (1972).

14. W.E. Spear and P.G. LeComber, Phil.Mag., 33, 935 (1976).

15. P.A. Walley, Thin Solid Films, 1, 327 (1968).

16. P.A. Walley, Thin Solid Films, 2, 327 (1968).

17. M.H. Brodsky, R.S. Title, K. Weiser and G.D. Pettil, Phys.Rev. B1, 2632 (1970).

18. J.J. Hauser, Phys.Rev. B8, 607 (1973).

19. J.J. Hauser, Phys.Rev., B8, 3817 (1973).

20. W.E. Spear, Amorphous and Liquid Semiconductors, edited by J. Stuke and B. Brenig (Taylor and Francis, London, 1974).

21. J.J. Hauser, Solid State Communication, 19, 1049 (1976).

22(a) J.F. Graczyk, Phys.Stat.Sol.(a) 55, 231 (1979).

22. D.L. Staebler and C.R. Wronski, Appl.Phys.Lett., 31, 292 (1977).

23. M.A. Paesler, D.A. Anderson, E.C. Frreman, G. Moddel and W. Paul, Phys.Rev.Lett., 41, 1492 (1978).

24a. D.E. Carlson and C.R. Wronski, J.Electron.Mater, 6, 95 (1977).

24b. J.M. Marshall and D. Allan, Phil.Mag., B40, 71 (1979).

25. S.R. Ovshinsky and A. Madan, Nature, 276, 482 (1978).

26. S.R. Ovshinsky and D. Adler, Contemp.Phys., 19, 109 (1978).

27. P.G. LeComber and W.E. Spear, Phy.Rev.Lett., 25, 509 (1970).

28. P.G. LeComber and W.E. Spear, J.Non.Cryst.Solids, 8-10, 727 (1972).

29. C.R. Wronski, D.E. Carlson and R.E. Daniel, Appl.Phys.Lett., 29, 602 (1976).

30. D.E. Carlson, IEEE Trans.Elect.Dev. ED-24, 449 (1977).

31. C.R. Wronski, IEEE Trans.Elect.Dev., ED-24, 351 (1977).

32. J.I.B. Wilson and P.Robinson, Solid State Electronics, 21, 489 (1978).

33. D.E. Carlson, J.I. Pankove, C.R. Wronski, and P.J. Zanzucchi, Thin Solid Films, 45, 43 (1977).

34. P. Viktrovitch, D. Jouse, A. Chenevas-Paul and L.View-Rochas, Rev. De.Phys.Appl., 14, 201 (1979).

35. D.E. Carlson and C.R. Wronski, 18th Annual Electronic Materials Conference, Salt Lake City, Utah, June 23-25 (1976).

36. J.J. Loferski, J.Appl.Phys., 27, 777 (1956).

37. W. Shockley and H.J. Queisser, J.Appl.Phys., 32, 510 (1961).

38. M. Wolf and H. Rauschenbach, Adv.Energy.Conv., 3, 455 (1963).

39. C.E. Backus, Solar Cells (IEEE Press, 1976).

40. A.G. Milnes and D.L. Feucht, Heterojunctions and Metal-semiconductor Junctions, (Academic Press, New York, 1972).

41. J.P. Donnelly and A.G. Milnes, Int.J.Electronics, 20, 295 (1966).

42. H.J. Hovel "Semiconductors and Semi-metals", Vol.11, Solar Cells (Edited by R.K. Willardson and A.C. Beer, Academic Press, New York, 1975).

43. M.P. Thekaekara, Opt.Spectra, 6, 32 (1972).

The thesis presents some theoretical calculations on the performance of photovoltaic solar cells. The first chapter gives the general principles of photovoltaic solar cells. The second chapter deals with a theoretical study of metal-p-n-Schottky barrier solar cells, a new configuration suggested in the literature to improve the performance of the Schottky barrier photovoltaic solar cell. Shannon has proposed this model in which an oppositely doped layer is present in between the metal and semiconductor (metal-p-n). The theory of m-p-n structure was first presented by S.S. Li. This theory has been modified in this thesis and it is found that the maximum effective barrier height depends upon the donor or acceptor concentration in the intermediate layer. This conclusion is of significance in optimizing the solar cell parameters. By taking examples of silicon and gallium arsenide semiconductors, the photovoltaic performance has been calculated with gold as the Schottky metal. The behaviour of the barrier height is investigated as a function of carrier densities in the n and p regions and as a function of the p layer thickness. The photovoltaic cell characteristics are worked out and conditions for maximum efficiency obtained. The results are given below together with the corresponding

calculatted values of the barrier height, power output under AMO and the resultant efficiency.

Material	Acceptor density	Donor density	Thickness of 'p' layer	Barrier height	Power output	Efficiency
Semi-conductor	N_A cm^{-3}	N_D cm^{-3}	w_p cm	$(\phi_{Bn})max.$ ev	P mW/cm^2	η %
Si	$7.8x10^{17}$	$2x10^{15}$	$2x10^{-6}$	1.02	26.25	19.5
GaAs	$2.44x10^{18}$	$1x10^{16}$	$2x10^{-6}$	1.424	24.40	18.1

Another new type of configuration i.e. Metal-p-n (hetero) Schottky has been investigated theoretically on similar lines. Out of various possibilities, the following two, which appear more important from practical point of view, have been chosen for detailed calculations: (1) Metal-n(large)-p(small) and (2) Metal-p(small)-n(large). Numerical results of the barrier height and efficiency have been obtained by taking the examples of n-CdS/p-Cu_2S/Au and p-GaAs/n-ZnSe/Al.

Configuration	Acceptor density	Donor density	Thickness of 'p' or 'n' layer	Barrier height	Power output	Efficiency
	N_A	N_D	w_p/w_n	$(\Phi B_n)_{max.}$	P	η
	cm^{-3}	cm^{-3}	cm	ev	mW/cm^2	%
n-CdS/p-Cu_2S/Au	1.74×10^{18}	5×10^{17}	2×10^{-6}	0.914	12.07	8.95
p-GaAs/n-ZnSe/Al	5×10^{17}	3.4×10^{18}	2×10^{-6}	1.442	32.52	24.08

The third chapter consists of some theoretical calculations on back-wall illuminated MIS Schottky barrier solar cells. The treatment takes into account the role of surface recombination velocity and the presence of a depletion region in the semiconductor. Computations for J_{sc} have been made for back-illuminated n-Si/SiO_2/Au Schottky barrier solar cells for different values of thickness of the cell with various surface recombination velocities. Thus the drift current in the base layer is given as

$$J_{p(diff.)} = eD_p \left[\frac{2B}{L_p} \exp - \frac{w_n}{L_p} + \frac{2\alpha N \exp(-\alpha d) \cosh(\alpha w_n)}{D_p L_p \left(\frac{1}{L_p^2} - \alpha^2 \right)} - \frac{2\alpha^2 N \exp(-\alpha d) \sinh(\alpha w_n)}{D_p \left(\frac{1}{L_p^2} - \alpha^2 \right)} \right]$$

where

$$B = \frac{\alpha N \exp(-\alpha d)}{D_p \left(\frac{1}{L_p^2} - \alpha^2 \right)}$$

$$\frac{\exp \frac{w_n}{L_p} \left(\cosh \alpha d + \alpha D_p \sinh \alpha d \right) - \exp \frac{d}{L_p} \cosh \alpha w_n \left(1 + \frac{D_p}{L_p S_p} \right)}{\sinh \frac{d - w_n}{L_p} + \frac{D_p}{L_p S_p} \cosh \frac{d - w_n}{L_p}}$$

and the photocurrent due to the generation of electron-hole pair in the depletion region

$$J_{dr} = 2eN \exp(-\alpha d) \sinh(\alpha w_n)$$

The total short-circuit current (J_{sc}) is obtained after integrating the sum of J_p and J_{dr} over the entire spectral wave length. The available parameters such as cell thickness, surface recombination velocity, dopant concentration are varied and the effect on J_{sc} studied and the results compared with that for front-walled cells. It has been shown that for a given donor concentration the back-illuminated solar cells give higher short-circuit photocurrent upto a certain value of thickness beyond which front-wall illumination cells are better. When the dopant concentration is low, the back-walled cells are better even for thicker cells.

In the last chapter, a theory deriving an equation for the photogenerated current in a p-n junction of amorphous silicon over a low grade crystalline silicon is presented. Amorphous silicon prepared by glow discharge is free from grain boundaries. Furthermore, because of its high absorption coefficient, and an energy gap close to optimum, it holds great promise in the fabrication of solar cell, even though it may have slightly lower life-time of the minority carriers.

Computations have been made for J_{sc} and V_{oc} as a function of the thickness of the a-Si layer at a given mobility in the base layer. The calculations show that at, a thickness of the order of 0.1μ, the efficiency of the device is maximum. By taking this optimum thickness, the effect of carrier mobility in base material has been examined. Even if the carrier mobility is very low (~ 200 cm^2/volt-sec.) this configuration has a reasonably good photoresponse. Thus after optimizing the thickness of a-Si layer the effect of carrier mobility in a-Si over photoresponse has been seen. As the mobility increases, the efficiency would increase, but it remains more or less constant in the region of 2-5 cm^2/volt-sec. beyond which it starts decreasing.

Mobility of minority carriers in a-Si	Thickness of a-Si	Mobility of minority carriers in base material (cm^2/volt-sec.)					
		1200			900		
cm^2/(volt sec.)	cm	V_{oc}	J_{sc}	$J_{sc} \cdot V_{oc}$	V_{oc}	J_{sc}	$J_{sc} \cdot V_{oc}$
		volt	mA/cm^2	mW/cm^2	volt	mA/cm^2	mW/cm^2
5	0.08	0.482	38.78	18.72	0.539	37.36	20.50
5	0.1	0.482	37.44	18.07	0.541	36.14	20.15
5	0.2	0.478	31.59	15.10	0.542	30.43	19.53

Thus one could get good efficiency with amorphous silicon p-n junction, if the thickness of the amorphous silicon is properly chosen.